A CONVECTIVE HEAT TRANSFER MODEL FOR SIMULATION OF ROOMS WITH ATTACHED WALL JETS

By

WEIXIU KONG

Bachelor of Science
Shenyang Architectural and Civil Engineering Institute
Shenyang, China
1994

Master of Science
Tianjin University
Tianjin, China
1997

Submitted to the Faculty of the
Graduate College of the
Oklahoma State University
in partial fulfillment of
the requirements for
the degree of
DOCTOR OF PHILOSOPHY
May, 2006

A CONVECTIVE HEAT TRANSFER MODEL FOR SIMULATION OF ROOMS WITH ATTACHED WALL JETS

Dissertation Approved:

Dr. Daniel E. Fisher
Dissertation Adviser

Dr. Jeffrey D. Spitler

Dr. Afshin J. Ghajar

Dr. Arland H. Johannes

Dr. A. Gordon Emslie

Dean of the Graduate College

Acknowledgement

I would like to thank first my advisor, Dr. Daniel Fisher, for his inspiration, guidance, support, and encouragement throughout the course of my studies. His positive attitude affected me not only in my work but also in other areas of my life.

I would like to extend my gratitude to the members of my thesis committee, Dr. Jeffrey Spitler, Dr. Afshin Ghajar, and Dr. Arland Johannes, for their committed service and support. Valuable insights from each of them have improved this study significantly.

I wish to express my warmest appreciation and love to my husband, Guohuan Wang. I could not have accomplished my goal without his encouragement, love, and support. The coming of our baby son, Daniel, has brought me great joy. Seeing him grow gave me a new level of energy and hope.

Without a doubt, my family members have been the largest supporters throughout my academic career. I would like to thank my parents, Dequan Kong and Guixia Cui, and my sisters, Weiling, Weidong, and Weichao for their continuous love and words of encouragement.

I would like to acknowledge the undergraduate students who directly worked on this project: Ben Alexander, Mike Forsberg, Joseph Pruitt, Adam Shupe, Nathan Weber, and Joshua Bruce. Their help made it possible to complete this project. I am also very thankful for the help and friendship of my colleagues at the Building and Environmental Thermal Systems Research Group in Oklahoma State University. Here are a few names: Zheng Deng, Dongyi Xiao, Xiaobing Liu, and Calvin Iu.

TABLE OF CONTENTS

LIST OF TABLES

LIST OF FIGURES

Chapter 1: Introduction

A convection model is an approximate description of the convection coefficient based on available surface and flow parameters. An internal convection model for building simulations describes the convection heat transfer occurring on the inside surfaces of buildings. Building simulations have been developed in detail in order to meet the needs of new energy standards and energy conscious design methods, which require more accurate cooling/heating load calculations. Recently, nodal and zonal air models, which lie between the simplicity of the well mixed zone model and the complexity of a CFD model, have been developed and implemented in building simulation packages. However, the convection heat transfer models that were developed based on the well mixed air assumption are still used with the new air models. Although multiple air nodes are used to model air distribution in the space, a single reference air node must be used to model surface convection. The single node convection models compromise the increased accuracy obtained from the room air simulation. A new convection model that will select the appropriate reference node for the air models is needed to correctly evaluate convective heat transfer for nodal and zonal air models.

All convection models are approximate, and the amount of detail involved depends on the purpose of the model. The details of available convection models range from single values to complex correlations. The simplest convection model is found in the BLAST (Building Load Analysis and System Thermodynamics) program, a building simulation package released in 1977. The convection coefficient is a specified constant based only on the surface position. A BLAST surface is considered horizontal if its tilt is within 22.5° of the horizontal direction, or vertical if its tilt is within 22.5° of the vertical direction. All other surfaces are considered to be tilted surfaces. Convection heat transfer on internal surfaces is assumed to be purely natural convection. For horizontal and tilted surfaces, the convection coefficient is reduced or enhanced depending on heat flow direction. If the heat flow is upward, the air tends to circulate and enhance the convection. On the contrary, if the heat flow is downward, the air tends to stratify and reduce the convection. Altogether, the BLAST model has five constant convection coefficients. The EnergyPlus building simulation package, a DOE sponsored energy calculation program, has a number of convection models, including the simple BLAST model. A detailed natural convection model includes three correlations that relate the convection coefficient to surface orientation and the surface-zone air temperature difference. Of these three correlations, one is used for vertical surfaces or for cases which there is no temperature difference, one is used for enhanced convection on tilted surfaces, and one for reduced convection on tilted surfaces. Horizontal surfaces are modeled as tilted surfaces with a tilt angle of zero. The correlations were originally developed for flat plate convection heat transfer and referenced in the ASHRAE Handbook of Fundamentals (1993). The forced convection model, which was based on room outlet temperature, was developed for the ceiling diffuser room configuration (Fisher 1997). It was reformulated from the published correlations to use the outlet temperature instead of the inlet temperature as the reference temperature. Three equations, correlating the convection coefficient to room ventilative flow rate (in Air Change per Hour, ACH), are included for ceiling, floor and walls.

Among currently available building simulation packages, the research version of the Environmental System Performance simulation program, ESP-r (Clarke 1974) has the most complete selection of convection models. Three natural convection models, two forced convection models, and one mixed convection model are included. The three natural convection models are: the Alamdari and Hammond (1983) model for isolated surfaces, the Khalifa (1990) model and Awbi and Hatton (1999) model for surfaces in confined spaces. The Alamdari and Hammond model includes correlations for vertical surfaces and for horizontal surfaces with both enhanced and reduced convection heat transfer. The Khalifa model has ten correlations for cold walls, windows, and ceilings under different heating configurations. The Awbi and Hatton model includes two correlations for heated walls and floors developed in a test room. The two forced convection models are the Fisher (1997) model for the radial ceiling jet and Fisher and Pedersen (1995) model for the free horizontal jet. Both models have correlations for walls, ceilings and floors in isothermal rooms. The mixed convection model was introduced by Beausoleil-Morrison (2000) applying Churchill and Usagi's "blending" approach (1972) to Alamdari and Hammond's natural convection model and Fisher's forced convection model. The mixed convection model has correlations for walls with both assisting and opposing buoyancy effect on mechanically driven flows and correlations for ceiling and floor with both enhanced and reduced convection heat transfer.

When applying these convection models, well-stirred zone air is assumed for all building simulations. The zone air is treated as a single node, representing the mean air temperature of zone, zone outlet air temperature, and the zone thermostat set point temperature. In addition, a single convection flow regime is assumed in both BLAST and EnergyPlus. Interior convection is assumed to be pure natural convection in BLAST irrespective of the ventilative flow rate. EnergyPlus assumes that forced convection occurs on all interior surfaces for ventilative flow rates greater than 3 ACH, otherwise, natural convection is assumed. ESP-r compares the magnitude of the convection coefficient predicted by forced and natural convection correlations for each surface. If the natural convection coefficient is much greater than the forced convection coefficient, buoyancy driven flow is assumed to be dominant. Mechanically driven flow is assumed to be dominant if the forced convection coefficient is larger. If natural and forced convection coefficients are of the same order of magnitude, the mixed convection flow regime is assumed.

For modern air distribution systems, the well-stirred zone assumption is increasingly invalid. One of the newest systems, the Under Floor Air Distribution (UFAD) system, tends to provide a comfort environment only in the occupied region and saves energy by not conditioning the unoccupied region. The well-stirred assumption is not applicable to this system. Cold Air Distribution (CAD) systems may also result in non-uniform space temperatures, and displacement ventilation systems are designed specifically to thermally stratify the zone air.

The single regime assumption is also invalid for many air distribution systems. For CAD systems, strong forced convection occurs on the surfaces where cold air jet attaches, while mixed or natural convection may occur on other surfaces. Even for conventional air distribution systems, multiple convection flow regimes may occur in a single room or on a single surface depending on how the airflow is organized. Although

ESP-r considers multiple flow regimes in a room, the zone air temperature from the well-stirred assumption is still used to evaluate the convection coefficient.

In summary, modern room air management systems require detailed airflow solutions in building simulations. Convection models should consider near wall airflow characteristics and determine convection flow regimes on individual surfaces. Room airflow characteristics are now considered in both ESP-r with a coupled CFD simulation and in the ASHRAE Air Toolkit with different types of room air models. However, the detailed airflow information is currently condensed into one parameter--zone air temperature--for all convection models. This compromise is a result of the limitations of current convection models, which correlate the convection coefficient to global zone air parameters rather than near wall local air parameters.

This thesis develops a new convection model for building simulations with multi-node zone air models. The new convection model addresses both the well stirred assumption and the single flow regime assumption. Chapter two gives detailed information on the heat balance model, the air model, and the convection model and how they are connected. Chapter three defines the new convection model and discusses the objectives of this research. Chapter four reviews previously developed convection models. Natural, forced, and mixed convection models are reviewed. Chapter five describes the experimental methods and the facility for developing the proposed convection model. Chapter six introduces a general method to find nondimensional parameters for room convection models. Room airflow is characterized with this research goal, i.e. to find new convection correlations and convection flow regime definitions. Chapter seven develops convection correlations based on parameters obtained from the analysis of Chapter six and experimental data from this and previous research. Chapter eight presents experimental results to validate and extend convection models developed in Chapter seven. Chapter nine summarizes results and conclusions obtained up to this point and gives future plans for this research.

Chapter 2: Convection Models in Building Energy/Load Calculations

All modern building simulation programs are based on the so-called heat balance model. The heat balance (HB) model for building simulations include: the outside heat balance, the wall conduction process, the inside heat balance, and the air heat balance. Figure 2.1 shows the detailed heat transfer processes of HB method for the opaque surfaces in one zone. A zone is an individual calculation unit in a building simulation. It may include one or more rooms.

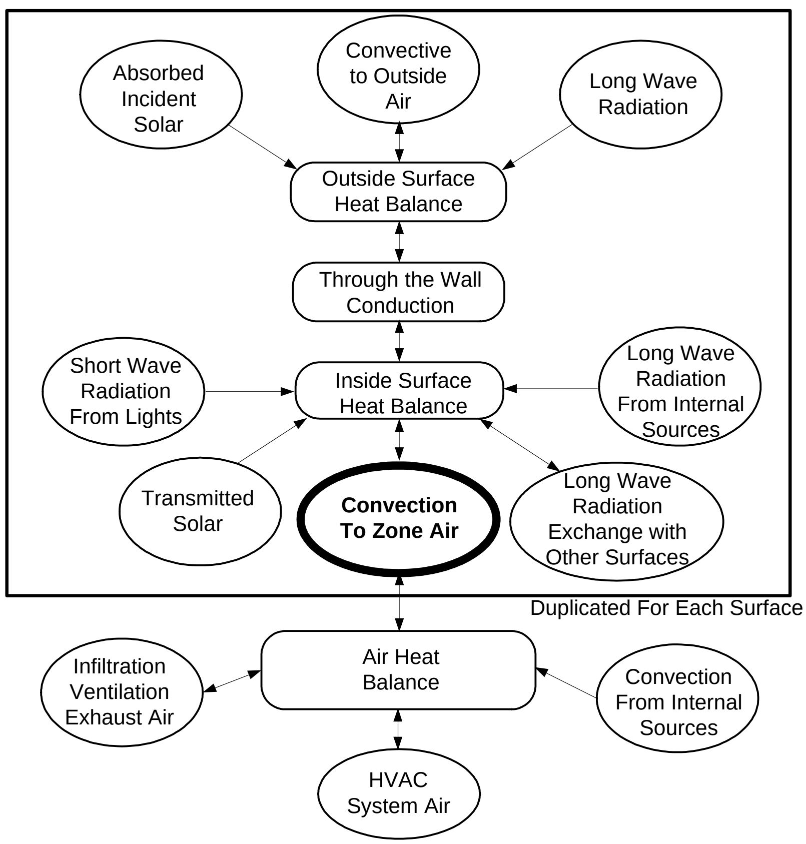

Figure 2.1 Schematic of Heat Balance Processes in a Zone (Pedersen, 2001)

The inside surface convection heat transfer connects the inside surface heat balance and the air heat balance. This chapter will describe in detail heat transfer processes in building simulations. The introduction of nodal and zonal air models in room air simulation and the corresponding requirement for convection models will be discussed. With the ASHRAE Air Toolkit as an example, the relationship between the convection model and of the various types of air models will be demonstrated.

2.1 Heat Balances

2.1.1 Outside Heat Balance

The outside surface heat balance is comprised of four heat transfer processes: short wave radiation, including direct, reflected, and diffuser sunlight, long wave radiation from the environment, convection heat transfer from outside air, and conduction heat transfer into the wall. These heat transfer components are shown schematically in Figure 2.2. T_{so} is the outside surface temperature. The rate of heat transfer per unit area perpendicular to the direction of transfer is defined as heat flux and denoted as q''. The subscripts on q'' correspond to the heat transfer modes.

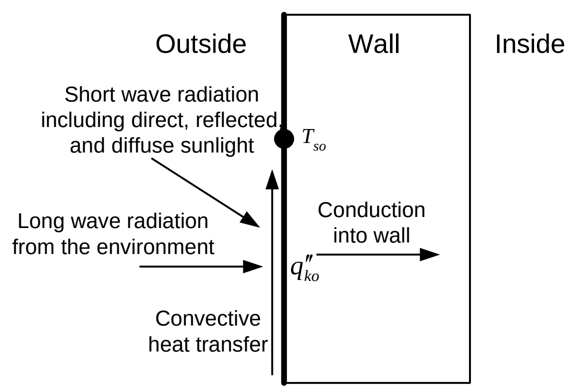

Figure 2.2 Outside Surface Heat Transfer Components

The outside heat balance is expressed by the following equation:

$$q''_{\alpha sol} + q''_{LWR} + q''_{conv} - q''_{ko} = 0 \tag{2.1}$$

where:

$q''_{\alpha sol}$ = absorbed direct and diffuse solar (short wavelength) radiant heat flux, W/m^2

q''_{LWR} = net thermal (long wavelength) radiant flux from the air and the surroundings, W/m^2

q''_{ko} = conductive heat flux into the wall, W/m^2

q''_{conv} = convective heat transfer to the outside air, W/m^2

The heat transfer processes are modeled individually in the ASHRAE Air Toolkit with an iterative solution procedure to ensure convergence of the de-coupled models. The short wave radiation model, $q''_{\alpha sol}$, uses the procedures given in the ASHRAE Handbook of Fundamentals to calculate the direct, diffuse, and ground reflected solar radiation. The long wave radiation model, q''_{LWR}, calculates the net long wave radiant heat transfer from the sky and the ground to the surface. Model inputs include the surface absorptance and temperature, sky and ground temperature, and sky and ground view factors. The outside surface convection, q''_{conv}, is calculated using convection coefficients predicted from several optional models along with the outside surface-air temperature difference. The conduction heat flux into the wall, q''_{ko}, is generally calculated using the Conduction Transfer Function (CTF) method, which considers both surface temperature and heat flux histories as discussed in the following section.

2.1.2 Wall Conduction Process

The wall conduction process is shown schematically in Figure 2.3. T_{si} and T_{so} are the surface temperatures on the inside and outside of the wall, and q''_{ko} and q''_{ki} are the conduction heat fluxes at the inside and outside surface. These four terms are all functions of time and are incorporated with the heat balances on both sides of the wall element. A simultaneous solution technique is required for this process. The CTF formulation is generally selected for building simulation programs because of its computational efficiency.

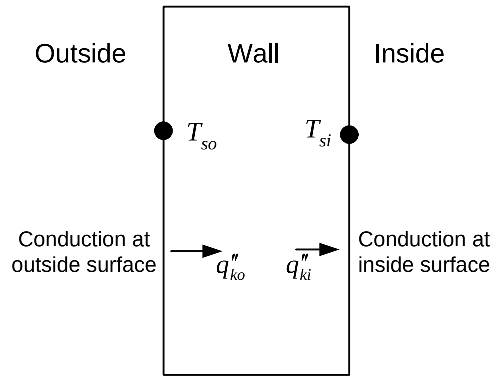

Figure 2.3 Wall Conduction Process

The CTF formulation relates the conductive heat flux to the current and past surface temperatures and the past heat fluxes. For the outside surface heat flux:

$$q''_{ko}(t) = -Y_0 T_{i,t} - \sum_{j=1}^{nz} Y_j T_{i,t-j\delta} + X_0 T_{o,t} + \sum_{j=1}^{nz} X_j T_{o,t-j\delta} + \sum_{j=1}^{nq} \Phi_j q''_{ko,t-j\delta} \tag{2.2}$$

and for the inside surface heat flux:

$$q''_{ki}(t) = -Z_0 T_{i,t} - \sum_{j=1}^{nz} Z_j T_{i,t-j\delta} + Y_0 T_{o,t} + \sum_{j=1}^{nz} Y_j T_{o,t-j\delta} + \sum_{j=1}^{nq} \Phi_j q''_{ki,t-j\delta} \tag{2.3}$$

where:

X_j = outside CTF, $j = 0,1,...nz$

Y_j = cross CTF, $j = 0,1,...nz$

Z_j = inside CTF, $j = 0,1,...nz$

Φ_j = flux CTF, $j = 0,1,...nq$

T_i = inside surface temperature

T_o = outside surface temperature

q''_{ko} = conduction heat flux on outside surface, W/m^2

q''_{ki} = conduction heat flux on inside surface, W/m^2

The subscript "t" indicates the current time and "$t - j\delta$" the time that occurred j time steps previously with a time step size of δ. The summation limits, nz and nq, depend on the wall construction and the scheme used for calculating the CTFs. The values of nz and nq are generally set to minimize the amount of computation.

2.1.3 Inside Heat Balance

The inside heat balance also includes four heat transfer components: conduction from the wall element, convection from the zone air, short wave radiation, and long wave radiation. Figure 2.4 schematically shows these four components. Here again, T_{si} is the inside surface temperature and q''_{ki} is the conduction at the inside surface.

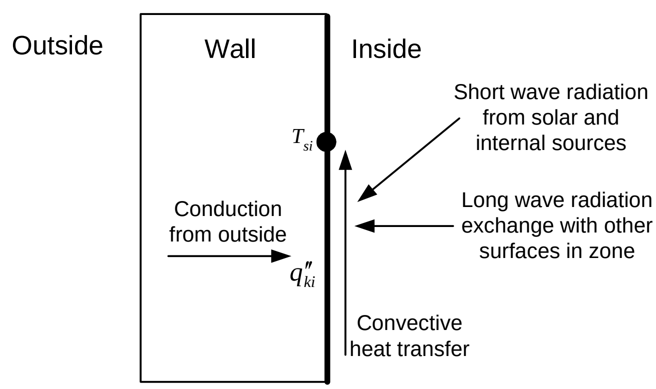

Figure 2.4 Inside Surface Heat Transfer Components

The inside surface heat balance for each element can be written as:

$$q''_{LWX} + q''_{SW} + q''_{LWS} + q''_{ki} + q''_{sol} + q''_{conv} = 0 \qquad (2.4)$$

where:

q''_{LWX} = net long wave radiation from zone surfaces, W/m^2

q''_{SW} = net shortwave radiation from lights, W/m^2

q''_{LWS} = long wave radiation from equipment in zone, W/m^2

q''_{ki} = conduction through the wall, W/m^2

q''_{sol} = transmitted solar radiation absorbed at the surface, W/m^2

q''_{conv} = convection to the zone air, W/m^2

The internal convection heat transfer from surface to zone air is the interest of this research. Two natural convection models and one forced (also used for mixed) convection model are included in the ASHRAE Air Toolkit and are summarized in Table 2.1.

Table 2.1 Internal Convection Models Included in ASHRAE Air Toolkit

Model type	Model	Applied surfaces
Simple Natural	$h_c = 1.25$	Horizontal surface, downward facing
	$h_c = 4.68$	Vertical surface
	$h_c = 4.37$	Horizontal surface, upward facing
Detailed Natural	$h_c = 1.31\lvert\Delta T\rvert^{\frac{1}{3}}$ *	Vertical surface
	$h_c = \dfrac{9.482\lvert\Delta T\rvert^{\frac{1}{3}}}{7.283-\lvert\cos\Sigma\rvert}$ **	Horizontal or tilted surface, enhanced convection
	$h_c = \dfrac{1.810\lvert\Delta T\rvert^{\frac{1}{3}}}{1.382+\lvert\cos\Sigma\rvert}$ **	Horizontal or tilted surface, reduced convection
Forced and Mixed	$h_c = 0.13ACH^{0.8}$	Floors (ceiling diffuser)
	$h_c = 0.49ACH^{0.8}$	Ceilings (ceiling diffuser)
	$h_c = 0.19ACH^{0.8}$	Walls (ceiling diffuser)

* ΔT = temperature difference between the surface and zone air

** Σ = the surface tilt angle

The internal convection heat transfer is calculated using Newton's law of cooling as follows:

$$q''_{conv} = h_c(T_s - T_a) \tag{2.5}$$

The reference temperature T_a is the zone air temperature following the well-stirred assumption. The forced and mixed convection model is based on the room outlet temperature.

2.1.4 Air Heat Balance

The zone air heat balance includes: convection from zone surfaces, transport of outside air directly into zone by infiltration and ventilation, and transport of the HVAC system air into the zone. The air heat balance is expressed as:

$$q_{conv} + q_{CE} + q_{IV} + q_{sys} = 0 \tag{2.6}$$

where:

q_{conv} = convective heat transfer rate from zone surfaces, W

q_{CE} = convective heat transfer rate from internal sources, W

q_{IV} = sensible heat transfer rate due to infiltration and direct zone ventilation, W

q_{sys} = heat transfer rate due to mechanical, HVAC system ventilation, W

The convective heat transfer rate from zone surfaces q_{conv} is the sum of all convective heat transfer terms from the inside surface heat balance:

$$q_{conv} = \sum_{i=1}^{nsurfaces} h_{c,i} A_i (T_{s,i} - T_a) \tag{2.7}$$

Convection coefficients on surfaces $h_{c,i}$ are selected from the available internal convection models listed in Table 2.1.

The convective heat transfer rate from internal sources, q_{CE} , is the companion part of the radiant contribution from internal sources, q''_{LWS} . It is added to the air heat balance to support the simple equipment model. The air that enters through infiltration and ventilation and through the HVAC system is assumed to mix with the zone air immediately. The air capacitance is neglected in calculating the heat transfer rate into the zone.

2.2 Air Models

The complexity of the air heat balance is determined by the air model that is used to describe the flow field in the zone. A number of air models supporting new systems as well as conventional systems have been developed in the last three decades. According to Chen and Griffith (2002), air models can be classified into four types based on their structure and complexity: mixing models, nodal models, zonal models, and CFD models. Figure 2.5 shows the four types of air models.

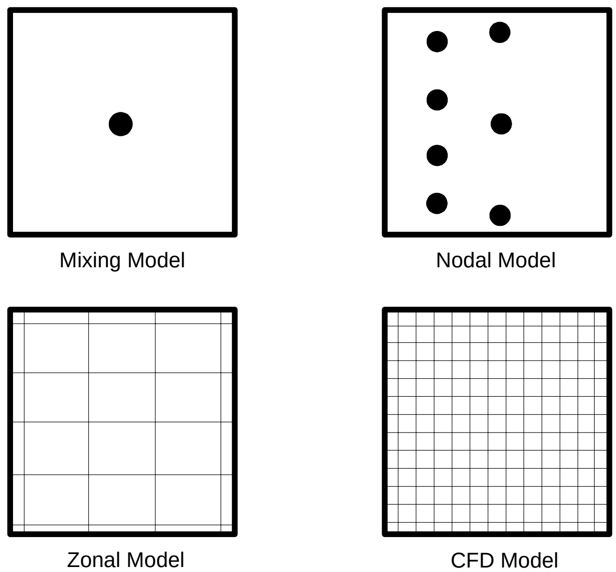

Figure 2.5 Room Air Model Classification (Chen and Griffith, 2002)

The mixing model is the traditional well-stirred zone model. A single air node represents the entire zone. Most building simulation programs still used a mixing model at this time.

Nodal models treat the zone air as an idealized network of nodes connected with flow paths. Nodal air models have been subcategorized into convective heating, displacement ventilation and natural ventilation models depending on the application. Subcategories can also be formed depending on the number of nodes (2-node, 5-node, etc) and the flow configurations (prescribed or modeled). For nodal models, the thermal zone is divided into several nodes and separate heat balances are formulated for each. Compared to CFD models, nodal air models have a smaller number of control volumes that do not have specific geometric boundaries.

Zonal models define the air grid geometrically, and each control volume has a well-defined boundary. Zonal models are distinguished from CFD models because they have much coarser grids and do not attempt to predict the flow field accurately but only attempt to solve for specific variables. Subcategories of zonal models are formed according to the variables that are solved for and include: temperature zonal models (Togari et al, 1993), pressure zonal models (Inard, 1996), POMA -**P**ressurized z**O**nal **M**odel with **A**ir diffuser (Lin, 1999), and momentum zonal model (Chen and Griffith, 2002). The mass transfer in the mass and energy conservation equations for temperature and pressure zonal models is calculated with temperature differences and pressure differences respectively. The momentum zonal model solves the steady state Euler equation for inviscid flow as well as the mass and energy conservation equations.

CFD models predict detailed airflow information in the whole flow field. Temperature and velocity distributions as well as surface heat flux and shear stresses can be obtained through CFD models.

2.3 Coupled Heat Balance and Air Models

Coupling the HB model with the air model introduces detailed air flow information into the building simulation so that new air management systems can be modeled more accurately. This strategy is especially useful for stratified room air. The ASHRAE Air Toolkit is a framework to incorporate available air models in the ASHRAE load toolkit. In this framework, each zone surface can be subdivided into at most four parts and each part is considered as an individual surface. The zone air details from the air model calculations are aggregated to conform to the surface resolution. Figure 2.6 schematically shows the HB model and the coupled HB and air model.

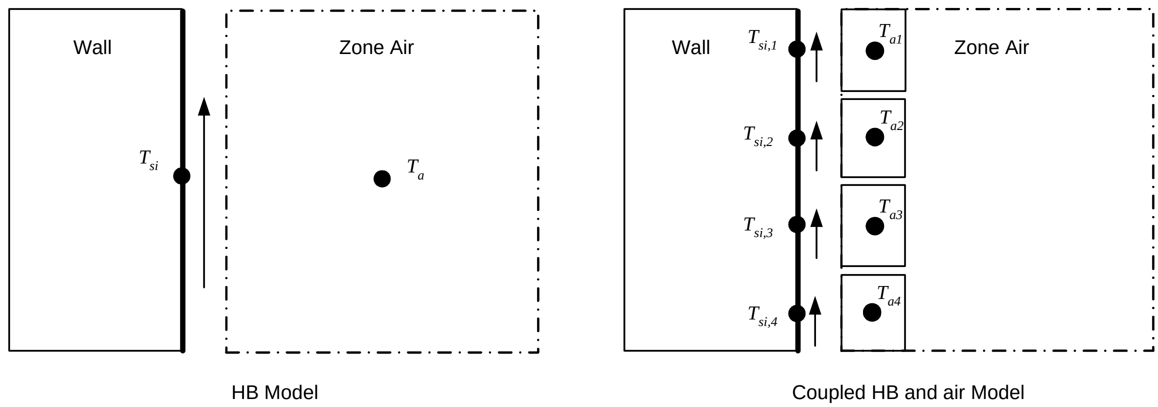

Figure 2.6 HB Coupled with Mixing Model (left) and Zonal Model (right)

The coupled HB and air model that is applied to the subdivided zone surfaces is identical to the HB model, which is applied to the entire surface. All the heat flux modeling procedures remain the same except the convection heat transfer from inside surfaces. Rather than a single value, the zone air temperature is represented by an array of values generated from the air model. The equations for generating the zone air temperature array are part of the air model and depend on which model is applied. The air temperature is also known as the reference temperature for convection heat transfer calculations. The reference temperature for classical heat transfer configurations is the 'far field' temperature, which is the temperature of the uniform flow field far from the boundary. In a room, especially a room that is not well mixed, uniform 'far field' conditions do not exist. The convection heat transfer calculation requires that the reference temperature should be outside the thermal boundary layer but not too far away. Although the distance from the air node, where the reference temperature is specified, to the surface is uniformly 0.1m in the ASHRAE Air Toolkit, determining the location of the air node is an important topic that will be discussed at length in Chapter 7.

The contribution of convection heat transfer rate from surfaces then becomes:

$$q_{conv} = \sum_{i=1}^{nsurfaces} h_{c,i} A_i (T_{si,i} - T_{ai}) \qquad (2.8)$$

Two coupling strategies are used: the T-Couple strategy and the DT-Couple strategy. The T-Couple method uses the air model results directly to calculate the inside surface convection heat transfer rate:

$$q_{conv_i} = h_{c,i} A_i (T_{s_{i,i}} - T_{a_i}) \tag{2.9}$$

The DT-Couple method is based on the equation:

$$\begin{aligned} q_{conv_i} &= h_{c,i} A_i\ (T_{s_i} - T_{RoomAir}) - h_{c,i} A_i (T_{a_i} - T_{RoomAir}) \\ &= h_{c,i} A_i (T_{s_i} - T_{RoomAir} - \Delta T_{a_i}) \end{aligned} \tag{2.10}$$

where:

$T_{RoomAir}$ = a reference air temperature (averaged, set point)

$\Delta T_{a_i} = T_{a_i} - T_{RoomAir}$

Subscript " i " denotes individual surfaces.

In the DT-Couple method, the air model results are not used directly, but are shifted by substituting the set point temperature T_{set} for room air temperature $T_{RoomAir}$. If the air model result for $T_{RoomAir}$ does not agree with the controlled condition, this deviation is applied to the distribution. After iteration, the actual shift is expected to be small. This DT-couple method is more stable and is a very important method if the air model has relative poor accuracy in terms of absolute temperature but still produces good information on the air temperature distribution.

The equations for the coupled HB and air model are solved by successive substitution. Figure 2.7 diagrams the implementation in a building simulation program. The heat balances are rearranged in terms of outside surface temperature, inside surface temperature, and system load. The innermost loop (i.e. the iteration loop) iterates at a single time step until a solution that satisfies all the relationships is reached. The toolkit calls the air models at the same frequency as the HB model.

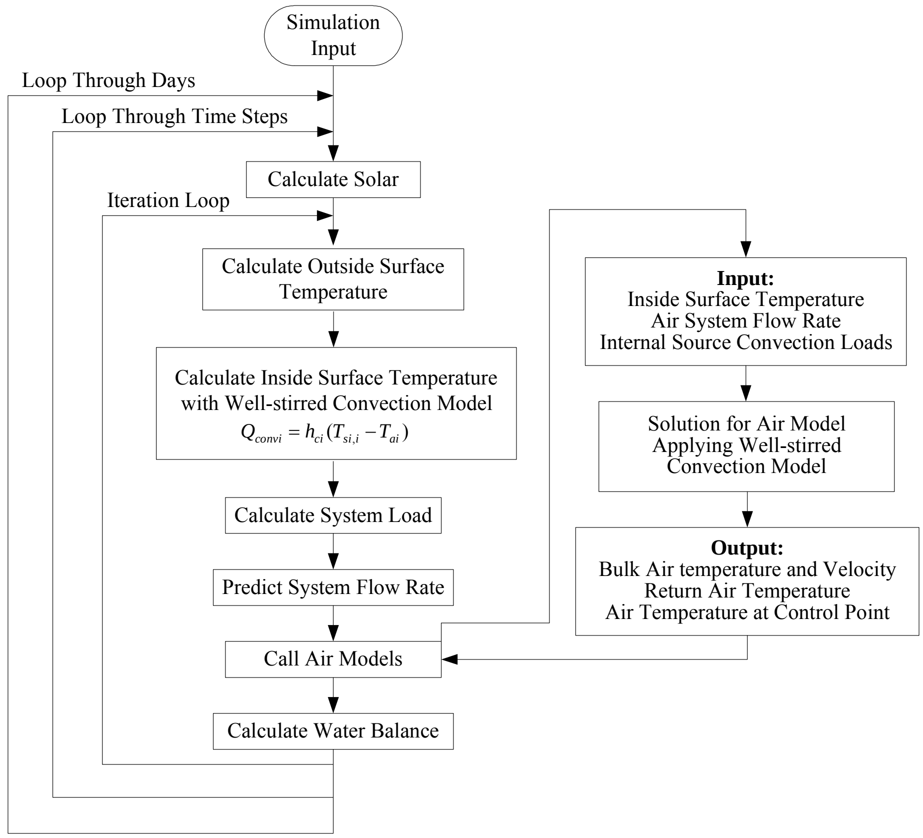

Figure 2.7 Coupled HB and Air Model (Left: HB Model, Right: Air Model)

The figure illustrates the current state of the art, with the well-stirred convection model implemented in both the heat balance and in the air model. For the non-uniform flow field, however, this implementation incorrectly predicts the surface convection. Basically, the problem is that the convection coefficient is predicted with "global variables" while the air models need convection coefficients predicted with "local variables". Global variables refer to those measured in terms of the room entity, such as room inlet temperature, inlet velocity, and the ventilative flow rate. Local variables refer to near wall parameters such as air temperatures and velocities.

Chapter 3: Problem Definitions and Research Scope

3.1 Convection Model Classification

Convection models that are related to global or room scale variables are here defined as "global variable based convection models". Comparatively, Convection models that are related to local variables are here defined as "local variable based convection models". Published convection models include both global and local models. Natural convection correlations of Alamdari and Hammond (1993), Awbi (1998), and Khalifa (1990) correlate convection coefficients to the near wall air temperature and surface dimensions such as hydraulic diameter or height. These correlations are typical local variable based convection models. The forced convection correlations of Fisher (1997), Fisher-Pedersen (1994), and Spitler (1990) correlate the convection coefficient to inlet/outlet temperature, ventilative flow rate, inlet air velocity, and room volume. These correlations are typical global variable based convection models.

There are some models that involve both global and local variables. For example, Awbi's (2000) mixed convection correlation includes global variables such as inlet nozzle velocity and width and local variables such as near wall air temperature. Beausoleil-Morrison's (2000) mixed convection model considers both ventilative flow rate and near wall air temperatures. Both are mixed convection models obtained from "blending" natural and forced convection correlations. These two models are categorized as global convection models since the forced convection part does not consider local conditions.

3.2 Prospective Convection Models

Local variable based convection models are required to correctly couple the HB and air models. However, a complete local convection model with natural, mixed, and forced convection correlations is not available at the present time and needs to be developed for this specific purpose. To develop this model, the following conditions are required:

1. The model should be developed for use in enclosures, not on free surfaces.
2. The model should clearly define a convection correlation for each flow regime.
3. The reference temperature and correlation parameters should be clearly defined and generally available in building simulation programs.

The first two requirements address the problem of the misapplication of convection models. Dascalaki et al. (1994) reviewed natural convection correlations and assessed their applicability to enclosure surfaces. Two groups of correlations were reviewed. The first group of correlations was developed for enclosure surfaces and the second group was developed for isolated horizontal and vertical surfaces. Dascalaki estimated that the free surface correlations could over-predict the heat transfer rate by 30-50% when applied to enclosures. This work demonstrated the importance of room scale configurations to obtain convection models that are applicable to building heat transfer processes.

Calay et al. (1998) experimentally examined the applicability of available natural convection correlations to a rectangular enclosure. The experimental results were compared with correlations from literature. The study concluded that convection correlations developed in enclosed spaces are much more suitable for building applications than the flat plate models recommended by ASHRAE and CIBSE (The Chartered Institution of Building Services Engineers). Calay pointed out that even though there were a large number of correlations available for energy/load calculations, many of them were not suitable for building applications.

Besides the configuration, the flow regime should be determined properly. An extreme example is the simple assumption in the BLAST simulation program that natural convection dominates under any circumstance. Spitler (1991) developed forced convection correlations for rooms with the ventilative flow rate ranging from 15ACH (Air Change per Hour) to 100ACH. Implementing the correlations into BLAST, Spitler found that the default BLAST model under predicted convection heat flux by up to 5 times at high ventilative flow rates.

Flow regime definition is required in dynamic building simulations in order to switch convection models according to instantaneous conditions. Beausoleil-Morrison (1999) analyzed the sensitivity of dynamic, whole-building simulation programs to internal surface convection models. One of the IEA (International Energy Agency) Annex 21 (Environmental Performance) Task 12 double-glazed test rooms was simulated. The internal surface convection coefficient was calculated with the Alamdari and Hammond model when the radiator was off and with the Khalifa and Marshall model when the radiator was on. Compared to the energy consumption predicted by the Alamdari and Hammond model alone, switching between models based on flow regime predicted 8% more energy consumption. This sensitivity is significant compared to the impact of other parameters, such as fabric characteristics (3.3%), room air leakage (2.7%), and sky models (4.7%).

The third of the three requirements listed above addresses the problem of developing room convection models using experimental data. A properly defined reference temperature and length scale is needed for a valid and widely applicable room convection model. However, no agreement has been reached on how to select these two parameters from the literature. In natural convection model development, Awbi and Hatton (1999) measured local air temperature at 100mm and 50mm from the surfaces of a room sized chamber and a small box respectively, and Khalifa and Marshall (1990) measured local air temperature 100mm from surfaces. In his forced convection model development, Fisher (1997) selected the room inlet air temperature and Spitler (1990) selected the room outlet temperature. Both Fisher and Spitler's selection were based on uncertainty analysis and convenience for engineering applications.

Length scale is another parameter that is not obvious for room airflow, and available studies are not in agreement on how to define it. Awbi and Hatton's natural convection model used the surface hydraulic diameter defined by the surface area and the perimeter as the length scale. Khalifa's natural convection model is dimensional and doesn't include a length scale. Kapoor and Jaluria (1991)'s mixed convection model used nozzle width (D) as the length scale for nondimensional numbers, Gr_D, Re_D, and Nu_D. The ratio of ceiling length to nozzle width (L/D) was also considered to have an effect on the surface convection heat transfer and was included in the correlations. Surface height was used in Alamdari and Hammond's (1983) natural convection model; overall length of the heated wall was used in Neiswanger's (1987) forced convection model, and nozzle width was used in Awbi's (2000) forced convection model. All of these length scales were used without theoretical analysis.

Clearly, the effect of length scale and reference temperature on model applicability and accuracy requires further investigation. A general method with a more solid theoretical background is desired to define reference temperature and length scale. The accessibility of the defined reference temperature and length scale in building simulation programs should also be considered.

3.3 Research Scope

The local convection model presented in the following chapters includes correlations in three flow regimes for the radial ceiling diffuser airflow configuration and smooth surface characteristics. A general method for local convection model development is presented, and the problems of flow regime, length scale, and reference temperature are specifically addressed.

Experiments with the radial ceiling diffuser room configuration are presented in Chapter 5. The purpose of these experiments is to characterize the room flow field for scaling parameters and to develop a set of local convection correlations. The airflow characterization and scale analysis is given in Chapter 6 and correlation development is discussed in Chapter 7.

The experimental data, which were obtained from the UIUC (University of Illinois - Urbana Champaign) test room (Spitler, 1990 and Fisher, 1995), are available for further analysis. The data sets have the detailed air temperature and velocity information that is needed for the local convection model. The data was used to validate the new local convection model as discussed in Chapter 7.

The new local convection model was implemented in ASHRAE Air Toolkit. Test cases simulated with both current and new convection models were compared with experimental data. The simulation work is presented in Chapter 8.

Chapter 4: Literature on Convection Model Development

Strictly speaking, whenever a temperature difference exists, buoyancy driven flow also exists. In practice, however, the buoyancy force is neglected when it is small compared to the momentum force. At the point where the buoyancy effect cannot be neglected, the upper bound of the mixed convection regime is defined. On the other side, where the buoyancy effect is significant but momentum forces are not small enough to be neglected, the lower bound of the mixed convection regime is defined. Various criteria defining the boundaries of the mixed convection regime have been suggested (Sparrow (1979) and Neiswanger (1987)). The flow driving forces not only determine the flow regime but also determine the correlation forms. This chapter will review how convection correlations have been developed and present convection correlations for different flow regimes.

4.1 Natural Convection Model

Natural convection models that are used in building simulation programs include correlations developed from both flat plate and enclosures. Most of the correlations were developed from experimental measurements.

Alamdari and Hammond (1983)

Alamdari and Hammond derived a two-part (laminar and turbulent) natural convection heat transfer correlation for building applications using Churchill and Usagi's (1972) mathematical model, $y = \left\{(Ax^p)^m + (Bx^q)^m\right\}^{\frac{1}{m}}$. In this application, Ax^p and Bx^q refer to correlations for buoyancy driven flow in laminar and turbulent regimes, "x" refers to Rayleigh number and "y" refers to the Nusselt number. So the blended form is:

$$Nu = \left\{(ARa^p)^m + (BRa^q)^m\right\}^{1/m} \qquad (4.1)$$

where:

Ra = Rayleigh number, $\frac{C_p \rho^2 g \beta \Delta T L^3}{k\mu}$

L = the characteristic length of heat transfer surface

A, B, p, q, m = empirical coefficients for buoyancy driven flow over vertical and horizontal surfaces

Correlations were developed for vertical surfaces and horizontal surfaces with both enhanced and reduced convection heat transfer. Experimental data from the literature for isolated surfaces were used to develop these correlations. In room applications where air properties can be assumed constant, the Rayleigh number is only related to the surface – air temperature difference. To make the correlations usable in building simulations, the dimensional form of the correlations were derived as shown in Table 4.1. The limitation of these correlations is that they were based on free surface data.

Khalifa and Marshall (1990)

Khalifa and Marshall (1990) investigated natural convection heat transfer on interior surfaces using a room sized test cell. A total of 142 experiments were performed to cover eight of the most widely used heating configurations including radiant floor, radiant wall, and radiator in windowless rooms and windowed rooms. The east wall of the test chamber was the test surface, which was maintained at a low temperature through a controlled cold space on the other side of the surface.

Convection heat transfer on the inside surface was balanced by radiation heat exchange with other surfaces and conduction heat transfer through the wall. The radiation was neglected in the calculation since the inside surfaces were coated with aluminum foil, which has a very low emissivity. The convection heat flux was balanced only with wall conduction:

$$q_{conv} = q_k$$

q_k was calculated from the measured inside-outside surface temperature difference, wall conductivity and thickness. Convection heat transfer coefficient h_c was calculated from q_{conv} and the temperature difference between the surface and air.

Khalifa and Marshall correlated the convection coefficient h_c to the surface-air temperature difference. A total of 10 correlations were finally obtained. The correlations for heated whole surfaces are given in Table 4.1. Khalifa and Marshall's correlations have been implemented in building simulation programs such as ESP-r.

Awbi and Hatton (1998)

Awbi and Hatton (1998) studied natural convection heat transfer in two-dimensional rooms using CFD technique. The room configurations included heated wall, heated floor and heated ceiling. Two kinds of CFD models were applied: a standard $k-\varepsilon$ model with "wall functions" and the low Reynolds number $k-\varepsilon$ model of Lam and Bremhorst (1981). For the standard $k-\varepsilon$ model, the first calculation grid was in the turbulent inner region, while for the low Reynolds number model, calculations were made in the viscous sublayer. The convection coefficients for the standard $k-\varepsilon$ model with the wall function and the low Reynolds number model were calculated by their respective equations as follows:

$$h = \frac{\rho u_\tau C_p}{T^+}\left(\frac{T_w - T_p}{T_w - T_{ref}}\right) \tag{4.2}$$

$$h = \frac{k}{y_p}\left(\frac{T_w - T_p}{T_w - T_{ref}}\right) \tag{4.3}$$

where:

T^+ = a dimensionless temperature

T_w = surface temperature

T_p = air temperature at the first grid

T_{ref} = reference temperature, such as bulk air temperature

y_p = distance of the first grid from the wall

The predicted convection coefficients were compared with experimental measurements from a room sized test chamber. The comparison showed that the low Reynolds number $k-\varepsilon$ model predicts the convection coefficient more accurately than the standard $k-\varepsilon$ model with the wall function. In addition, the convection coefficients predicted by the standard $k-\varepsilon$ model are extremely sensitive to the distance from the first grid to the surface. This distance is case sensitive, so the recommended distance to the first grid is not applicable to other configurations. For the low Reynolds number models, the first grid is required to be less than 1mm from the surface. Therefore, a very fine grid and more computer resources were needed to get accurate results. Awbi and Hatton concluded that it was more plausible to use experimentally determined convection correlations for room surface convection calculations.

Awbi and Hatton (1999)

Together with their numerical work, Awbi and Hatton experimentally investigated natural convection heat transfer from room surfaces. A room sized test chamber with interior dimensions of 2.78m x 2.78m x 2.3m and a small test chamber with internal dimensions of 1.05m x 1.01m x 1.05m located inside the bigger chamber against the cold wall as shown in Figure 4.1 were used in this research. The cold wall was maintained at a low temperature with the cold air in the adjacent compartment. To reduce radiation heat transfer, the heating plate was covered with polished aluminum plate. The heating plate was constructed from an electric heating element sandwiched between the aluminum plate and a 6mm plywood board.

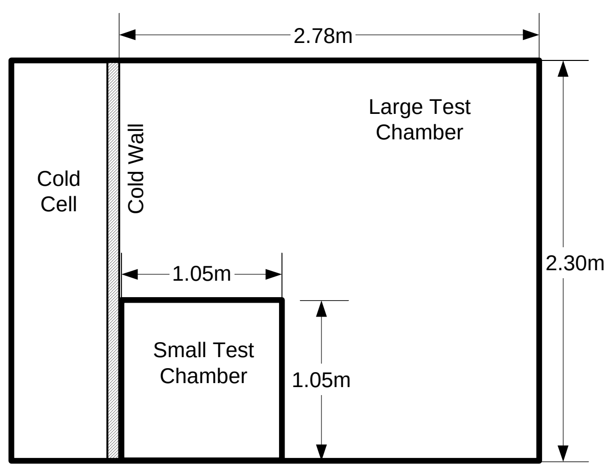

Figure 4.1 Test Chambers of Awbi's Experiment

Experimental configurations included a heated wall opposite to a cold wall, a heated wall adjacent to a cold wall, heated ceiling, heated floor, and heated plates mounted at different locations opposite to the cold wall and on the ceiling and the floor.

To calculate the rate of heat transfer to the chamber, the conduction heat loss from the heated wall was subtracted from the power input to the heating plate:

$$Q_{in} = P - \frac{kA}{L}(T_{in} - T_{out}) \tag{4.4}$$

where:

P = heating plate power input, W

Q_{in} = heat flux from heat panels to the inside room, W

T_{in} = inside surface temperature, ˚C

T_{out} = outside surface temperature, ˚C

A = surface area, m^2

L = surface thickness, m

k = surface conductivity, W/m-˚C

In calculating the convection coefficient, Awbi and Hatton subtracted the radiation heat flux from the total energy input:

$$Q_{conv} = Q_{in} - Q_{rad} \tag{4.5}$$

$$Q_{rad} = \frac{A\varepsilon[\sigma T_{in}^4 - q_j]}{1-\varepsilon} \tag{4.6}$$

where:

Q_{rad} = radiation heat flux, W

ε = surface emissivity

σ = Stefan-Boltzmann constant, W/m^{2}K^4

q_j = surface radiosity, W/m^2

The convection coefficient was obtained from:

$$h_c = \frac{Q_{conv}}{A(T_{in} - T_a)} \tag{4.7}$$

where:

T_a = air temperature, ˚C

The air temperature was measured 100 mm from the walls of the large chamber and 50 mm from the walls of small chamber. The air temperature was considered nearly uniform beyond this distance with the exception of the heated ceiling configuration. For this configuration, the air temperature was measured at the chamber center due to air temperature stratification in the room.

The experiments, performed with small heated plates, whole heated surfaces and large and small test chambers, introduced surface scale effects into the convection heat transfer coefficient. Starting from Bejan's (1995) laminar and turbulent natural convection correlations, and using Churchill and Usagi's (1972) "blending" approach, the following generalized form of the natural convection correlation was obtained:

$$h_c = \frac{c_1}{D^{c_2}}(\Delta T)^{c_3} \tag{4.8}$$

where:

D = surface hydraulic diameter

ΔT = surface and air temperature difference

c_1, c_2, c_3 = correlation constants

Table 4.1 summarizes the natural convection correlations obtained by different researchers. The common term in these correlations is the surface-air temperature difference, which reflects the buoyancy force that drives the natural convection flow.

Table 4.1 Natural Convection Correlations

Developer	Correlation	Nomenclature
Alamdari-Hammond	$h_c = \left[\left\{ a \left(\frac{\Delta T}{L} \right)^p \right\}^m + \left\{ b (\Delta T)^q \right\}^m \right]^{\frac{1}{m}}$	ΔT : Surface – air temperature difference L : Vertical surface height, H; horizontal surface hydraulic diameter, $L = 4A_s / P_s$, (A_s : surface area, P_s :perimeter)
Khalifa	$h = C_1 (\Delta T)^{C_2}$	ΔT : Surface-air (50mm from surface) temperature difference
Awbi	$h_c = \frac{c_1}{D^{c_2}} (\Delta T)^{c_3}$	D : Hydraulic diameter ΔT : Surface – air temperature difference

4.2 Forced Convection Model

In Spitler's (1990) summary of room convection literature, no forced convection heat transfer in rooms had been studied in terms of finding convection models for building simulation programs. Since 1990, only three studies have been completed and three convection models have been developed.

Spitler (1990)

Spitler investigated forced convection heat transfer in an office-sized test chamber of 15' x 9' x 9' with high ventilative flow rates ranging from 15ACH (Air Changes per Hour) to 100ACH. The test room was located inside a larger structure, which acted as a guard space to maintain a small temperature difference between the inside and outside of the test chamber. Fisher (1989) gave a detailed description of the experimental room. The test chamber consisted of 53 heated panels, which were individually controlled to maintain the panel surface temperature at the set point. Each of the 53 heated panels was instrumented with two thermocouples to measure the surface temperature. Experiments were conducted with a radial ceiling jet and a free horizontal jet.

The convection coefficient was calculated as follows:

$$h = \frac{q''_{conv}}{(T_s - T_{ref})} \tag{4.9}$$

where:

q''_{conv} = convective heat flux, W/m^2

T_s = surface temperature, ˚C

T_{ref} = reference temperature, ˚C

The convective heat flux was calculated as the measured total power input to the panel corrected for the radiation exchange. The room outlet temperature was selected as the reference temperature after investigating four options: outlet temperature, bulk air temperature, near wall air temperature, and air temperature as a function of height.

The convection coefficient was correlated to the jet momentum number in the form of:

$$h = C_1 + C_2 J^{0.5} \tag{4.10}$$

where:

J = jet momentum number defined as $J = \dfrac{VU_0}{gV_{room}}$

V = volumetric flow rate, m/s^3

U_0 = air velocity at diffuser, m/s

V_{room} = volume of the room, m^3

C_1 , C_2 = empirically derived constants, holding different values for different surfaces and for different diffuser configurations.

Fisher (1995)

Fisher (1995) studied convection heat transfer in rooms in the same office-sized test cell that was used by Spitler. The experimental room configurations included both radial ceiling jets and horizontal free jets. The ventilative flow rate of these experiments ranged from 3 ACH to 12 ACH. Fisher selected the inlet temperature as the reference temperature. The “enclosure Nusselt number” and “enclosure Reynolds number” were defined by the following equations:

$$Nu_e = \frac{h}{k}\sqrt[3]{V_{room}} \tag{4.11}$$

$$\mathrm{Re}_e = \frac{\dot{m}}{\rho \nu}\frac{1}{\sqrt[3]{V_{room}}} \tag{4.12}$$

where:

$\forall_{room}$ = room volume

ρ = air density

ν = air kinematic viscosity

$\dot{m}$ = ventilative mass flow rate

k = air conductivity

The convection correlations were derived with these two nondimensional numbers. For walls, floors and ceilings with both the radial ceiling jet and the horizontal free jet, the convection correlation form is:

$$Nu_e = c_1 + c_2 \mathrm{Re}_e^{0.8} \tag{4.13}$$

For ceilings with the horizontal free jet, the convection correlations are in the following form:

$$Nu_e = c_1 + c_2 \frac{\mathrm{Re}_e^{0.8}}{Ar} \tag{4.14}$$

These correlations have also been implemented in ESP-r.

Fisher and Pedersen (1997)

Fisher and Pedersen (1997) combined Spitler's data (15ACH - 100ACH) and Fisher's data (3ACH - 12ACH) for the radial ceiling diffuser to develop forced convection correlations that could be easily used in simulation programs in the form of $h = C(ACH)^{0.8}$.

The Fisher and Pedersen correlations show that the pure forced convection coefficient is only related to the ventilative flow rate for building air conditioning systems. The results are very close to the pure forced convection correlations for other simplified configurations, in which the convection coefficient is only related to the fluid velocity or its non-dimensional form the Reynolds number, for example, $Nu_x = 0.0296 \mathrm{Re}_x^{4/5} \mathrm{Pr}^{1/3}$ for turbulent boundary layer flow over a flat plate.

The forced convection correlations are summarized in Table 4.2.

Table 4.2 Forced Convection Correlations

Developer	Correlation	Nomenclature
Spitler *(Sidewall and ceiling inlet)*	$h = C_1 + C_2 J^{0.5}$	J : Momentum number
Fisher and Pedersen *(Ceiling inlet)*	$h = C(ACH)^{0.8}$	ACH: air change per hour
Fisher *(Sidewall and ceiling inlet)*	$Nu_e = c_1 + c_2 \mathrm{Re}_e^{0.8}$ $Nu_e = c_1 + c_2 \frac{\mathrm{Re}_e^{0.8}}{Ar}$	Re_e : Enclosure Reynolds number Nu_e : Enclosure Nusselt number

4.3 Mixed Convection Model

Mixed convection models for building simulations have been developed from flat plate experiments and from model sized and office sized chambers. Both water and air have been used as experimental fluids.

Neiswanger (1987)

Neiswanger investigated mixed convection heat transfer in enclosures using a rectangular test section with inlet and outlet "doorways" and water as the test fluid. Two sets of preliminary tests were carried out before conducting the mixed convection experiments. The first is a series of natural convection experiments with heated sidewalls, and the second is, forced flow visualization to determine the flow characteristics.

Mixed convection experiments were conducted with both heated sidewalls and forced flow through the test section. Convection coefficients were obtained from the measured heat flux and temperature differentials. It was assumed that the convection coefficient was equal to the pure forced convection coefficient at low heat fluxes and high flow rates and was equal to the pure natural convection coefficient at high heat fluxes and low flow rates. Analysis of the forced convection data resulted in a forced convection correlation: $h_{fc} = 0.5(k / z_m)\mathrm{Pr}^{0.6}\,\mathrm{Re}_{zm}^{0.6}$ as shown in Table 4.3. To determine the mixed convection coefficient in terms of the natural and forced convection coefficients, a series of experiments covering three convection regimes were performed. The natural part of the convection coefficient was based on the correlation given by Fujii and Fujii (1976). The forced part of the convection coefficient was calculated from Neiswanger's own forced convection correlation. Based on a postulated form for the mixed convection coefficient:

$h = (h_{nc}{}^{a} + h_{cf}{}^{a})^{1/a}$ and the experimental data, the optimal value of "a" was found to be 3.2. The two boundaries of the mixed convection regime were determined by $h / h_{nc} > 1.05$ and $h / h_{fc} > 1.05$.

The averaged fluid temperature measured at two different elevations in the entrance of the test section was used as a reference temperature. This is not applicable for convection heat transfer in buildings since the ceiling jet or wall jet core mixes quickly with the bulk flow. In addition, the correlations are only applicable to fluids with Prandtl numbers in the range of (6.11-6.45) and can't be used directly for air (Pr = 0.7). However, Neiswanger's procedure for studying all regimes of a convection heat transfer configuration has been generally accepted.

Kamlesh Kapoor and Yogesh Jaluria (1991)

Kamlesh Kapoor and Yogesh Jaluria studied mixed convection heat transfer for a heated horizontal ceiling jet. The ceiling jet turned downward at a corner and became a wall jet with opposing thermal buoyancy. The heated air jet was discharged as shown in Figure 4.2. The diffuser could be moved to adjust the horizontal distance (L) between the ceiling diffuser and the corner. The width of the slot diffuser (D) could also be adjusted. The jet flow separated from the ceiling before the corner and reattached itself to the wall at some distance below the corner. A recirculation zone was formed because of the separation and reattachment. The flow characteristics determined the local heat transfer rate. The local Nusselt number decreased downstream of the diffuser on the ceiling and reached a valley near the corner but then increased and reached another peak on the upper part of the vertical surface and then decreased again. Average Nusselt number (Nu_D) correlations were obtained for ceilings, walls and the combined ceiling and walls in the following form.

$$(\overline{Nu}_D)_{ceiling} = 250.47(Gr / \mathrm{Re}^2)^{-0.15}(L / D)^{-1.0} \tag{4.15}$$

$$(\overline{Nu}_D)_{wall} = 82.77(Gr / \mathrm{Re}^2)^{-0.25}(L / D)^{-0.8} \tag{4.16}$$

$$(\overline{Nu}_D)_{ceiling+wall} = 61.35(Gr / \mathrm{Re}^2)^{-0.09}(L / D)^{-0.5} \tag{4.17}$$

where:

$$\mathrm{Re} = \frac{U_0 D}{\nu}$$

$$Gr = \frac{g\beta(T_0 - T_\infty)D^3}{\nu^2},$$

L = horizontal distance between ceiling diffuser and the corner

D = width of the slot for jet discharge

U_0 = velocity at the discharge of the jet

T_0 = temperature at the discharge of the jet

T_∞ = surrounding temperature

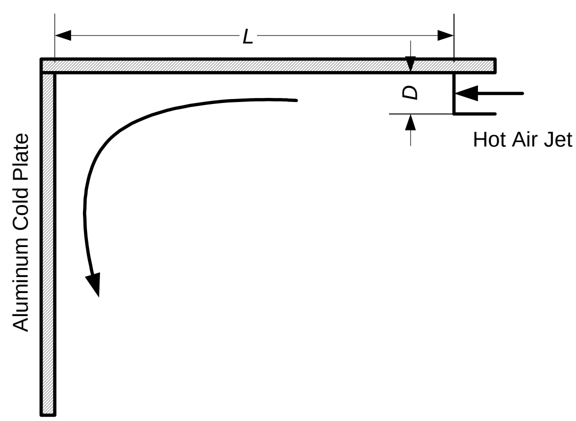

Figure 4.2 Experimental Configurations (Kamlesh Kapoor and Yogesh Jaluria)

These correlations have not been used in building simulations since the experimental configuration is significantly different from the building applications. However, the airflow and heat transfer characteristics provide a preview on how to scale the parameters for the proposed local convection model.

Awbi (2000)

Awbi (2000) extended his natural convection heat transfer research to mixed convection. Experiments for six configurations labeled with numbers in Figure 4.3 were carried out in the same test chamber.

Convection correlations were developed for each configuration in the form of $h_c = (h_{cn}{}^{3.2} + h_{cf}{}^{3.2})^{1/3.2}$, which is presented in Table 4.3. In this correlation, h_{cn} is the natural convection coefficient and h_{cf} is the forced convection coefficient.

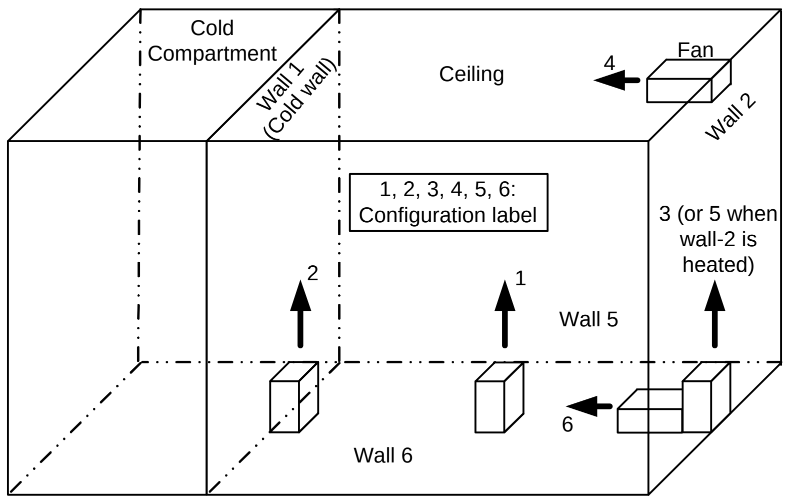

Figure 4.3 Experimental Chamber (Awbi)

Awbi pointed out that when the mixed convection coefficient was equal to the pure forced convection coefficient, the natural convection heat transfer could be neglected, and vice versa. However, he did not present the mixed convection upper and lower limits. The mixed convection configuration of a fan driven flow opposing a buoyancy driven flow was also not considered.

Awbi directly used Neiswanger's results for his mixed convection relation: $h_c / h_{cn} = (1 + \Gamma^{3.2})^{1/3.2}$ where $\Gamma = h_{cf} / h_{cn}$. The Γ values were obtained from the experimentally determined forced and natural convection coefficients. He developed a relation between Γ and jet parameters including nozzle width, jet velocity at nozzle opening, and surface-air temperature difference from experimental data. The mixed convection correlations were derived from the Γ relation and the natural convection correlation.

Beausoleil-Morrison (2000)

Beausoleil-Morrison established a method to obtain mixed convection correlations from available natural and forced convection correlations. The Alamdari and Hammond and the Fisher correlations were selected as natural and forced correlations respectively. Using Churchill and Usagi's (1972) "blending" approach, mixed convection correlations were derived in the form shown in Table 4.3. Comparing the magnitude of the convection coefficients predicted by the natural and forced convection correlations, the mixed convection regime could be identified. If the convection coefficients from both correlations are of the same order of magnitude, the mixed convection regime is identified. Beausoleil-Morrison considered mixed convection with both assisting and opposing interaction of buoyant and inertial forces.

Table 4.3 summarizes the mixed convection correlations.

Table 4.3 Mixed Convection Correlations

Developer	Correlation	Nomenclature
Neiswanger *(Model sized chamber with water)*	$h^{3.2} = h_{cn}^{3.2} + h_{cf}^{3.2}$ $h_{fc} = 0.5(k/z_m)\Pr^{0.6}\mathrm{Re}_{zm}^{0.6}$ $h_{nc} = \frac{k}{x}\left[\frac{\Pr}{4+9\Pr^{1/2}+10\Pr}\right]^{1/5}(Ra_x^*)^{1/5}$	Ra_x^* : Local Rayleigh number z_m : Overall length of heated wall k: Fluid thermal conductivity Re_{zm} : Reynolds number based on mean horizontal velocity in test section and z_m
Awbi *(Office sized chamber)*	$h^{3.2} = h_{cn}^{3.2} + h_{cf}^{3.2}$ $h_{fc} = c_1 (W)^{c_2} (U)^{c_3}$ $h_{cn} = \frac{c_1}{D^{c_2}}(\Delta T)^{c_3}$	D: Hydraulic diameter of room surface U: Velocity at nozzle opening ΔT : Surface to air temperature difference W: Width of nozzle opening
Kapoor and Jaluria *(Unconfined surfaces)*	$(\overline{Nu}_D) = C_1 (Gr/\mathrm{Re}^2)^{C_2} (L/D)^{C_3}$	L: Horizontal distance between ceiling diffuser and the corner D: Width of the slot for jet discharge
Beausoleil-Morrison *(Combined free and confined surface)*	$h_{c,mixed,assisting} = \left\|(h_{c,forced})^a + (h_{c,buoyant})^a\right\|^{\frac{1}{a}}$ $h_{c,mixed,opposing} = \left\|(h_{c,forced})^a - (h_{c,buoyant})^a\right\|^{\frac{1}{a}}$	$h_{c,forced}$: Fisher's forced convection correlations under conventional ceiling jet $h_{c,buoyant}$: Alamdari-Hammond natural convection correlations

4.4 Summary

All but one of the papers reviewed in the previous sections on developing natural convection correlation are based on experiments performed in confined spaces, such as room sized or model sized chambers. The flat plate natural convection correlation of Alamdari and Hammond is reviewed because of its demonstrated accuracy (Arnold et al. 1998). The temperature difference between the surface and the adjacent air was considered in all correlations. The length scales used in the Alamdari and Hammond correlations are the surface height for vertical surfaces and the hydraulic diameter for horizontal surfaces. Awbi used hydraulic diameter for both vertical and horizontal surfaces. Khalifa didn't consider the length scale. For forced convection correlations, ventilative flow rate and room volume are considered by both Spitler and Fisher. Spitler also considered jet flow characteristics and room inlet area. For mixed convection correlations, all researchers except Kapoor – Jaluria applied Churchill's "blending" approach combining natural and forced correlations. Neiswanger used a model-sized chamber with water as the experimental fluid. As a result, Neiswanger's correlation is difficult to implement in building simulations. Beausoleil-Morrison's mixed convection model was implemented in ESP-r. These correlations were blended from Alamdari and Hammond's free surface natural convection model and Fisher's forced convection model. Kapoor – Jaluria's correlations have not been used in any energy/load calculations. It is reviewed here because these correlations were developed without using Churchill's "blending" approach and the parameters involved are more suitable for the proposed local convection model. Local air velocity and a local length scale were considered in these correlations.

All the above correlations were developed for the whole surface convection heat transfer and are not suitable for the coupled HB and air model as discussed in Chapter 2. However, these studies provide a starting point for developing the proposed local variable based convection model.

Chapter 5: Experimental Measurements

Detailed room surface and air flow information are needed to develop the proposed local variable based convection model. The required experimental data include surface convection heat flux, surface temperatures, local air temperatures and velocities, room inlet and outlet conditions, etc. This chapter provides a detailed description of the Oklahoma State University (OSU) experimental room.

5.1 Facilities and Instrumentation

5.1.1 Experimental enclosure

An office-sized experimental room was built at OSU for studying convection heat transfer in buildings. The enclosure has inside dimensions of 12' x 16' x 10' high and is elevated 5' from the laboratory floor to provide a guard space for each surface. The walls are constructed of 2' x 4' “honeycomb” cells with removable panels mounted inside and outside of the room. Each cell is filled with a rockwool pillow to reduce conduction heat transfer across the wall. This honey comb structure provides flexibility in experimental configurations. Detailed room construction information is given by Sanders (1995) and Ferguson (1997).

A cold wall and a hot wall were constructed and instrumented as described in the following sections. The cold and hot walls as well as all passive walls are covered with low-E paint to reduce the radiation exchange among room surfaces. Figure 5.1 shows the side view of the OSU experimental system.

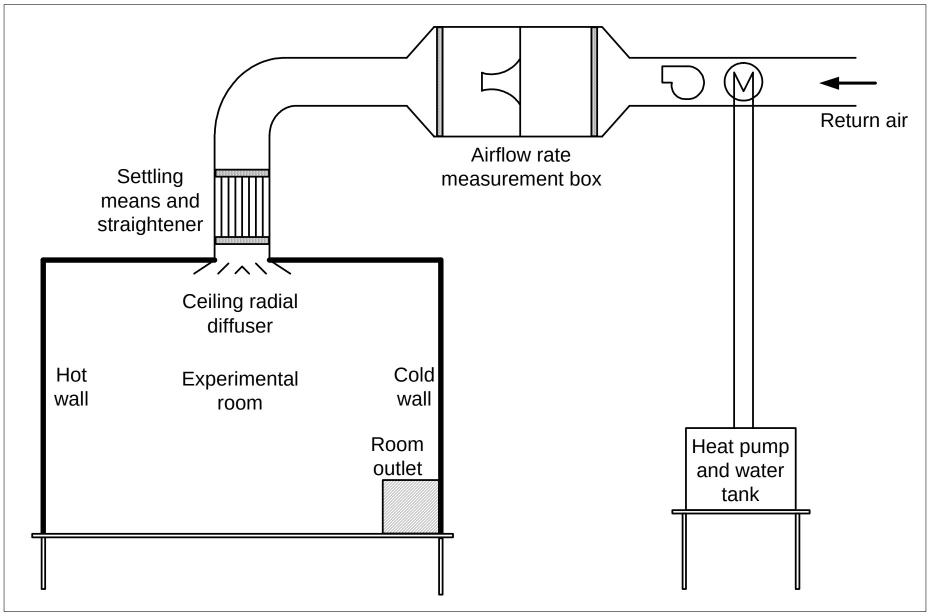

Figure 5.1 Side View of the OSU Experimental System

Hot wall

The hot wall consists of twenty 2' x 4' individually controlled panels as shown in Figure 5.2. The panel numbers correspond to the data logging channels and the surface numbers used in the radiation calculation. Each heated panel was constructed on a 5/8-inch gypsum board base by attaching Nickel-Chromium wire to the board and covering the wire with a ½" thick layer of gypsum plaster. Sanders (1995) provides additional information on the panel design. These heated panels replaced the original removable panels on the west wall.

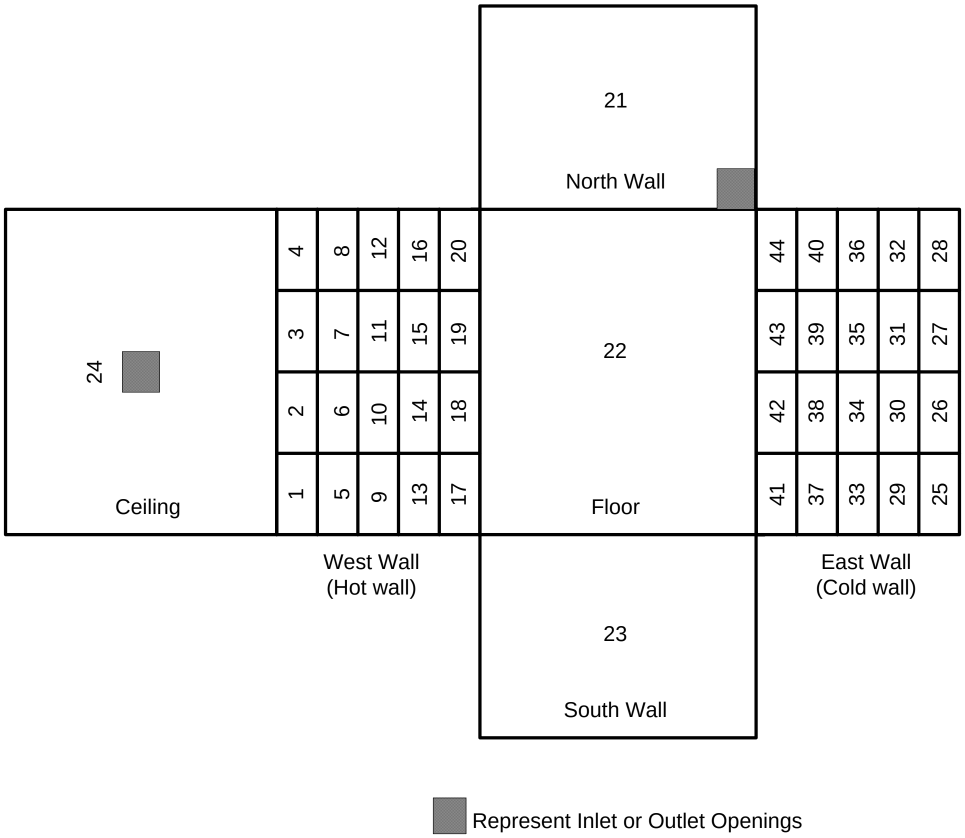

Figure 5.2 Plan View of the OSU Experimental Room

Two thermocouples are embedded in each panel and are positioned as shown in Figure 5.3. Two thermocouple readings are averaged to obtain the panel surface temperature measurement. Panel surface temperatures are computer controlled through a digital I/O board (PIO-96 board) and twenty solid-state relays. The I/O board sends 5VDC (ON) or 0VDC (OFF) to each solid-state relay and triggers on/off the controlled heated panels. The detailed control panel wiring is given in Fisher (1989). For this research, these heated panels only have on and off modes, rather than high heating, low heating, and off modes as used in Fisher's room.

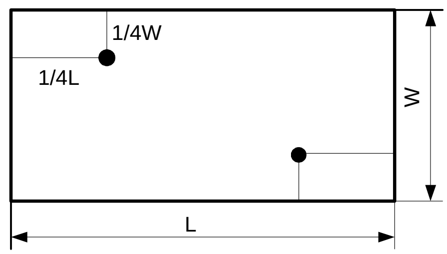

Figure 5.3 Thermocouple Layouts on Heat Panels

Simply controlling the heated panels based on instantaneous surface temperature readings leads to temperature fluctuations in the range of 2-2.5˚F with a 0.5˚F temperature differential. Fisher's (1989) pattern control strategy, which is also used in this research, reduces the temperature fluctuation range to 1˚F.

The hot wall surface convection heat flux is calculated from the electric power input to each heated panel corrected for the radiation heat exchange and panel back heat loss. Detailed heat flux calculations and error analysis will be presented in Section 5.2.

Cold wall

Twenty 2' x 4' chilled water panels form a complete cold wall as shown in Figure 5.2. The cold panels are constructed of 14-gauge aluminum sheet with five passes of ½ inch diameter copper tubing, as shown in Figure 5.4. The tubes are attached to the cold panel with PEX plate and heat transfer epoxy. Two layers of insulation are used to reduce the panel back heat transfer. Rock wool pillows mounted in the wall behind the panels provide additional insulation.

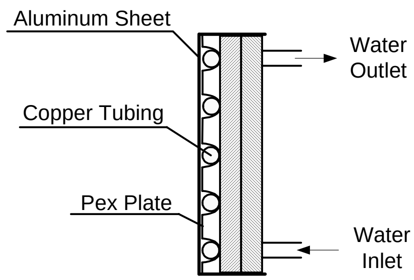

Figure 5.4 Cold Panel Structure

Cold panel surface temperatures are obtained from two thermocouples attached to the surface of the panel. The thermocouple layouts are shown in Figure 5.3. The cold panels are adjusted individually to specific surface temperatures by manually changing the water flow rates. The water temperature is maintained at a constant temperature by heat pump control of the water tank.

Accurate surface heat flux measurements on the cold wall panels are a critical part of experimentally determining surface convection coefficients. There are two options for determining the surface heat transfer rates on hydronic panels. 1). Measure the water mass flow rate and the water inlet and outlet temperatures and calculate the surface heat flux. 2). Directly measure the surface heat flux with a heat flux sensor. In general, the highest accuracy can be achieved through water flow rate and temperature measurements and the most uniform surface temperatures through direct flux measurements. Since this research requires both accurate measurement of the heat transfer rate and uniform surface temperatures and heat fluxes, the measurement methods are combined. A heat flux sensor ("Hukseflux" HFP01) is installed on each cold panel and calibrated with water flow rate and temperature measurements so that the sensor reading reflects the average heat flux over the entire panel rather than the small area covered by the heat flux transducer. The water inlet and outlet temperature difference is controlled to be as small as possible so that the uncertainty of the temperature difference is satisfactory. A calibration curve is obtained for each heat flux sensor. Once installed in the room, a uniform surface temperature is maintained by a high water flow rate and the heat flux sensor readings are corrected with the calibration curve to give the average panel flux. Calibration of the heat flux sensors is described in Section 5.3.3.

5.1.2 Air System

The air system includes a radial ceiling diffuser, a rectangular room outlet, an airflow measurement chamber, and a centrifugal fan as shown in Figure 5.1. Two sizes of Titus TMR-AA round ceiling diffusers were installed interchangeably for different test cases. The room outlet is a 2.0' x 2.0' square opening located on the bottom of the north wall on the east side. The airflow measurement chamber is constructed according to the ANSI/ASHRAE 51-1985 standard and is installed upstream of the room inlet diffuser. Three sizes of flow nozzles, 1.6-inch, 3-inch and 7-inch, are mounted in the chamber for airflow rate control and measurement. Combinations of the uncapped nozzles give various airflow rates. Four pairs of pressure taps are installed across the nozzle bank. The pressure taps are connected to manifolds using ¼" plastic tubing. The pressure drop through the nozzles is measured with a Setra (0-1 in. WC) differential pressure transducer. The airflow rate is then calculated from the pressure drop with equations provided in the ASHRAE standard. The airflow rate can also be adjusted by changing the fan pulleys.

5.1.3 Bulk Air Measurement System

A bulk air measurement system (Figure 5.5) was built to measure air temperatures and velocities throughout the entire room with a limited number of sensors. Driven by a computer program through a motor control board, a 10 foot rotating pole can move in both north-south and east-west directions. Two independent rails, mounted with DualVee tracks on aluminum base plates are fastened to the room floor. Sliding perpendicular to these rails is a 12-foot sheet of aluminum channel, also fitted with the steel tracks. A square trolley plate, mounted with the rotating pole, is then attached to this 12-foot section to allow for the second axis of linear motion. Detailed construction information is given in the capstone design project report of Lucas et al. (2002).

TSI 8470 (8475 for the new model) omni-directional velocity transducers and Type-T thermocouples are mounted on the rotating pole in pairs to measure local air velocities and temperatures. The air velocity transducer can only measure the velocity magnitude not vectors. Even though velocity vectors can improve the airflow analysis, the velocity scalars are considered satisfactory for this research, which focuses on convection heat transfer. The air data are downloaded to a computer through a wireless data logger mounted at the base of the rotating pole.

In this investigation, each cold or hot panel is considered as one surface node in the local convection model. For the purpose of getting local convection coefficients, one surface node is related to one air node, which is one set of air data including temperature and velocity. There are five rows of hot and cold panels in the experimental room and at least five pairs of thermocouples and air velocity transducers are needed on the rotating pole. To increase the air measurement accuracy, two pairs of air velocity transducers and thermocouples are laid out for each panel. The two sets of readings are averaged to correspond to the surface resolution.

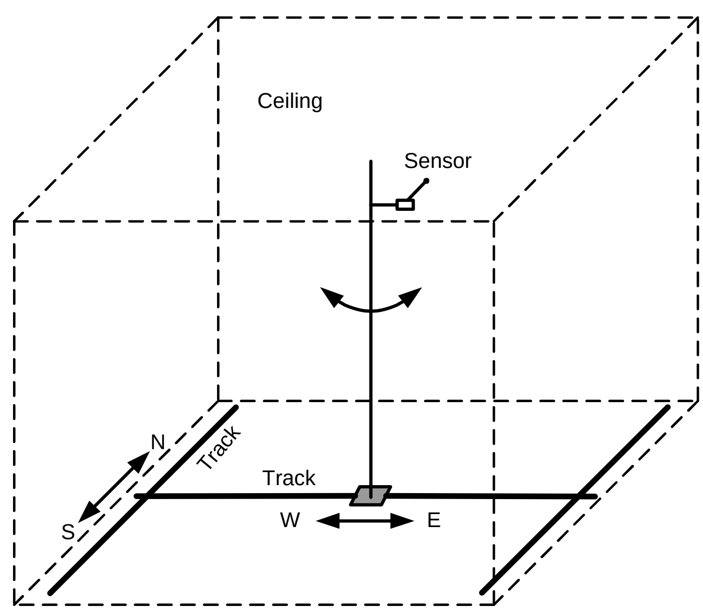

Figure 5.5 Linear Bulk Air Measurement System

5.1.4 Hydronic System

Two hydronic systems are required to run the experiments. One supplies water to the cold panels and the other supplies water to the cooling coil. The cooling coil water supply system consists of a three-ton ClimateMaster water-to-water heat pump, a 225-gallon water tank, and a heat exchanger. The cold panel hydronic system consists of a three-ton FHP water-to-water heat pump, a 225-gallon water tank and the cold panels. Both heat pumps are computer controlled using the same control hardware and software as the heated panels. A simple on/off control strategy is used throughout the experiments.

5.1.5 Data Acquisition System

The data acquisition system includes four data loggers: a Fluke Helios data logger, a Fluke Hydra data logger, a Fluke wireless Hydra data logger and a Supco (Sealed Unit Parts Co) AC Voltage (DLAV) Data Logger. The thermocouple outputs for surface temperature, room inlet and outlet temperatures, heat exchanger outlet temperatures, panel back surface temperatures, passive wall surface temperatures, water tank temperature and flow nozzle pressure differential output are multiplexed by the Fluke Helios data logger and downloaded to a computer at a user defined time interval. Table 5.1 shows the channel allocation of the Helios data logger.

Table 5.1 Channel Allocation of the Helios Data Logger

Channel No.	**Measured Parameters**
0~39	Cold wall panels
40~79	Hot wall panels
80, 86,87,89	Room inlet
81~84	Room outlet
85	Fan coil unit outlet
90	Nozzle pressure drop
91	North wall
92,93,95	Hot wall back
94	South wall
96	Ceiling
97	Floor
98	Cold air water tank
99	Cold wall water tank

The cold panel surface heat flux sensor outputs are downloaded by the Fluke Hydra data logger. The channel assigned to each heat flux sensor corresponds to the cold wall panel. The bulk air temperatures and velocities are downloaded through the Fluke wireless data logger mounted on the trolley. Channels 1-10 on the wireless data logger are allocated to air speed transducers while channels 11-20 are allocated to thermocouples. The DLAV data logger is used to monitor AC line voltage for heat panel power input calculations. Table 5.2 summarizes all the recorded parameters.

Table 5.2 Recorded Parameters

Data Loggers	Measured Parameters	
Helios Data Logger	Temperature	Room inlet air
		Room outlet air
		Panel back
		Panel surfaces
		Passive surfaces
		FCU outlet
	Air Volumetric Flow Rate	
Wireless Data Logger	Air Temperature	
	Air Speed	
Hydra Data Logger	Cold Panel Heat Flux	
DLAV Data Logger	Line Voltage	

The data acquisition system also includes two control programs; one turns on/off the hot wall panels and two heat pumps, the other runs the bulk air measurement trolley system. The heat panel on/off status is recorded at each time step in order to calculate total and average power input. Since the wireless data logger mounted on the trolley can't be controlled by the trolley motion control program, the trolley's current position and relative time variables (including start time and time interval) are recorded at each trolley stop in order to identify valid local air data measurements. Data acquisition system procedures are diagrammed in Figure 5.6, which is not a flow chart for one computer program but a flow chart for obtaining a complete set of experimental data.

Steady state operation is determined by a balance between energy input and output. The energy calculation is made in a data processing program using the latest fifty time steps of data and the panel on/off status. Panel surface temperatures are monitored and graphed in the Helios data acquisition program interface. After the surface temperature reaches a constant, a set of data is collected and the heat balance is examined. If steady state has been reached, then the bulk air data acquisition is started and heated panel control is switched to pattern control as described in section 5.1.1. If steady state has not been reached, the system continues to run and check the heat balance until steady state is reached.

The trolley positions and time intervals are specified in an input file. The time intervals must be long enough to allow the trolley pole to stabilize at each measurement point. Data from different data loggers are matched with each other using time variables. Air data are assigned to specific positions in the room according to the positions and times recorded by the trolley system.

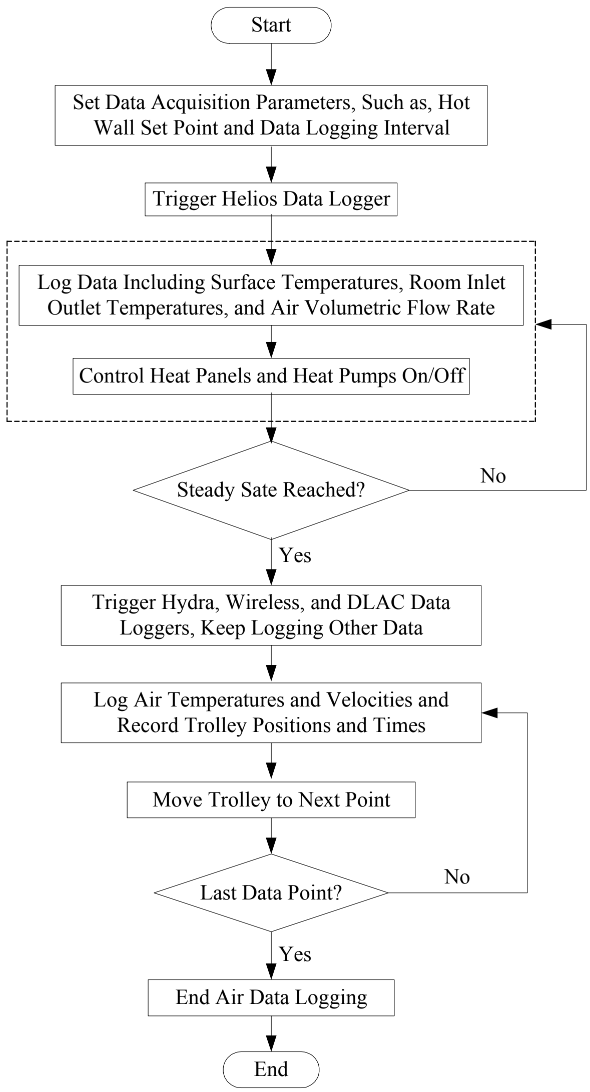

Figure 5.6 Data Acquisition Procedures

5.2 Experimental Calculation and Uncertainty Analysis

Uncertainty analysis is a critical procedure in that it quantifies the limitations of the experimental setup and determines whether the experimental procedure should be modified or not. Experimental uncertainties come from two types of errors: systematic error and random error. Random error can only be corrected by improving the precision of the measurement, but systematic error, which always affects the experimental result in the same direction, can often be corrected by calibration. This section will present the error in both directly measured values and calculated values.

The raw data obtained from experiments are processed for the proposed local variable based convection model. To meet the objectives of this research, procedures are used to calculate the following final results and intermediate results:

1. the hot panel power input
2. radiation heat transfer between room surfaces
3. heat loss from hot and cold surfaces to the guard space
4. convection heat flux
5. convection coefficient by location and reference temperature

These calculations are made with the data obtained under steady state room conditions. According to Taylor (1982) for directly measured variables, the propagation of errors can be obtained using either direct or quadratic summation of all error sources. The direct summation may underestimate the error by canceling error sources. Therefore, quadratic summation is used in this research:

$$ev = \pm\sqrt{es_1^2 + es_2^2 + \cdots + es_n^2} \qquad (5.1)$$

where:

ev = variable total error

es_n = error source

The uncertainty for the calculated results using Holman's (1989) non-linear relation is:

$$eR = \pm\sqrt{\left(\left.\frac{\partial R}{\partial v_1}\right|_{vo_1 \cdots vo_n} ev_1\right)^2 + \left(\left.\frac{\partial R}{\partial v_2}\right|_{vo_1 \cdots vo_n} ev_2\right)^2 + \cdots + \left(\left.\frac{\partial R}{\partial v_n}\right|_{vo_1 \cdots vo_n} ev_n\right)^2} \tag{5.2}$$

where:

eR = uncertainty interval in calculated result

ev_n = variable uncertainty interval

v_n = variable number n

vo_n = variable value

5.2.1 Error Estimation of Individual Measurement

Temperature

Temperature measurements of room surfaces, room inlet and outlet, and flow nozzle inlet use the FLUKE Helios data acquisition system. The error sources include the thermocouple wire, rated as $\pm 0.5°C$ according to ANSI Standard MC96.1-1982, cold conjunction compensation, estimated as $\pm 0.1°C$ (Spitler 1990) and the voltage measurement, estimated as $\pm 0.1°C$ (Spitler 1990). Using the quadratic summation for directly measured variables, the temperature error can be estimated as $\pm 0.5°C$.

This temperature error is too large for this research, which requires accurate measurement of small temperature differences between panel surface and near wall air. In order to reduce the uncertainty of the temperature measurement, each thermocouple was calibrated in-situ. Each calibration curve is both thermocouple and channel specific. The precision thermometer used in calibration is marked at $0.1°C$ intervals and can be read to an accuracy of $\pm 0.05°C$. After calibration, each thermocouple had a correction curve with an error estimated at $\pm 0.1°C$.

Air speed

The local air velocities are predicted from the following equation, Equation 7.5, which is described in detail in Chapter 7.

$$u = \frac{0.12 U_0}{(L_{ceiling} + Y)^{1.12}}$$

The diffuser outlet velocity U_0 are measured with Dwyer 640 with the selected range of $(0 - 3000\, fpm)$. The accuracy for this range is $\pm 0.3 m/s$ given by the manufacturer. The accuracy of the coefficient 0.12 is estimated to be ± 0.016 based on the velocity measurement given in Table 7.1. The error due to the jet travel length $(L_{ceiling} + Y)$ is neglected compared to other two error sources. Therefore, the uncertainty of the local air velocity is estimated as:

$$eu = \frac{\sqrt{(0.12 \cdot 0.3)^2 + (0.03 \cdot U_0)^2}}{(L_{ceiling} + Y)^{1.12}} \tag{5.3}$$

Air volumetric flow rate

The air volumetric flow rate is measured using flow nozzles. According to ASHRAE standard 51-1985, the fractional uncertainty of the volumetric flow rate is given as:

$$e'v_{air} = \sqrt{e'C^2 + e'A^2 + \left(\frac{e'f}{2}\right)^2 + \left(\frac{e'\rho}{2}\right)^2 + e'N^2} \tag{5.4}$$

where:

$e'C$ = fractional error in nozzle discharge coefficient

$e'A$ = fractional error in nozzle area

$e'f$ = fractional uncertainty of static pressure measurement

$e'\rho$ = fractional uncertainty of the air density

$e'N$ = fractional uncertainty of the fan speed measurement

The standard also gives the typical error for the nozzle discharge coefficient and the nozzle area:

$e'C \approx \pm 0.012$

$e'A \approx \pm 0.005$

From the standard, the air density error is estimated as:

$e'\rho \approx \pm 0.005$

Static pressure error and fan speed error are estimated as:

$e'N \approx \pm 0.005$

$e'f \approx \pm 0.01$

In total, the fractional uncertainty of the volumetric flow rate is ± 0.015 .

Temperature difference

Temperature difference will be used in calculations such as the surface heat back loss and the convection heat transfer coefficient. The estimated error can be calculated as:

$$e\Delta T_{a-b} = \pm\sqrt{eT_a^2 + eT_b^2} \quad (5.5)$$

The temperature measurements of T_a and T_b have an error of $\pm 0.1°C$ as estimated above, so the accumulated error for the temperature difference is estimated to be $\pm 0.14°C$.

Heat Flux

The heat flux sensors used on cold panels have fractional errors of ± 0.07 after calibration. Section 5.4 discusses the calibration procedure.

5.2.2 Calculation Algorithms and Uncertainty Analysis

Hot panel power input

The heated panel energy input is a function of line voltage and panel resistance according to Equation 5.6.

$$q_{power} = \frac{V^2}{RA_i} \quad (5.6)$$

where:

q_{power} = heat flux to each panel, W/m^2

V = line voltage, volts

R = resistance or the panel, Ω

A_i = panel area, m^2

The nominal line voltage for this experiment is 120 volts and the estimated error from the line voltage fluctuation can be as large as $\pm 4V$. An AC data logger from Supco (Sealed Unit Parts Co.) Inc. is used to monitor the line voltage, the voltage measurement error is estimated as $\pm 0.5V$. Together with the voltage fluctuation error between two data samples, the voltage is estimated to have an error of $\pm 1.0V$. The nominal resistance of the heated panel is 80Ω and is measured individually with an error of $\pm 0.5\Omega$. Therefore, the estimated error for heat panel power input is:

$$eq_{power} = \sqrt{(\frac{\partial q_{power}}{\partial R} e_R)^2 + (\frac{\partial q_{power}}{\partial V} e_V)^2} = \sqrt{(-\frac{V^2 e_R}{R^2})^2 + (\frac{2Ve_V}{R})^2} \tag{5.7}$$

Radiation heat transfer

Twenty heated panels and twenty cold panels together with the passive walls give a total of 44 surfaces in the experimental room. The radiation heat transfer from the i th surface to the j th surface can be calculated using Hottel's gray interchange area method (Spitler 1990):

$$q_{rad(i-j)} = \frac{1}{A_i} \overline{S_i S_j} \sigma (T_i^4 - T_j^4) \tag{5.8}$$

where:

$\overline{S_i S_j}$ = gray interchange area, which has the dimension of area and depends on surface emissivity ε_j only

σ = Stefan – Boltzman constant

T_i = temperature of the i th surface

T_j = temperature of the j th surface

A_i = surface area (m^2)

The uncertainty of the radiation heat transfer from the i th surface to the j th surface is:

$$eq_{rad(i-j)} = \pm\sigma\sqrt{e\overline{S_i S_j}^2 (T_i^4 - T_j^4)^2 + 16\overline{S_i S_j}^2 (eT_i^2 T_i^6 - eT_j^2 T_j^6)} \tag{5.9}$$

where $e\overline{S_i S_j} = e\varepsilon_j$

The total radiation heat transfer rate from the i th surface to all other surfaces can be calculated with:

$$q_{rad(i-s)} = \frac{1}{A_i}\sum\left[\overline{(S_i S_j}\sigma(T_i^4 - T_j^4)\right] \tag{5.10}$$

And the uncertainty is estimated as:

$$eq_{rad(i-s)} = \pm\sqrt{eq_{rad(i-1)}^2 + eq_{rad(i-2)}^2 + \cdots + eq_{rad(i-n)}^2} = \pm\sqrt{\sum_{j=1}^{n} eq_{rad(i-j)}^2} \tag{5.11}$$

Heat loss from experimental room to environment

The surface heat transfer back loss is also recorded to using the equation:

$$q_{back} = \frac{k}{\delta}A(T_i - T_o) = \frac{A(T_i - T_o)}{R} \tag{5.12}$$

where:

q_{back} = heat loss from room

k = thermal conductivity of the surface

δ = surface thickness

T_i = inside surface temperature

T_o = outside surface temperature

R = thermal resistance value

The thermal resistance was estimated as R-67 (Ferguson, 1997), 11.80 $m^2 \cdot K/W$ in SI units. For all the passive surfaces in the experimental room, the heat loss can be neglected since the passive walls are also well insulated and the temperature difference between the inside surface and outside surface is small.

The uncertainty of the back loss is calculated with the following equation:

$$eq_{back} = \pm e\Delta T_{i-o}\frac{k}{\delta}A = \pm 11.80 e\Delta T_{i-o}A = \pm 1.23W \tag{5.13}$$

Compared to the error from other sources, this error can be neglected.

Convection heat transfer flux

The convection heat flux to cold panels is calculated with the equation:

$$q_{conv} = q_{flux} - q_{rad(i-s)} \tag{5.14}$$

where:

q_{flux} = heat flux sensor measurement for the cold panel

$q_{rad(i-s)}$ = radiation from the i th surface to other surfaces

The convection heat transfer rate from the heated panels is calculated as:

$$q_{conv} = q_{power} - q_{rad(i-s)} - q_{back} \tag{5.15}$$

where:

q_{back} = heat transfer back loss from heated panel

Therefore, the uncertainty of convection heat transfer rate can be calculated as:

$$eq_{conv} = \pm\sqrt{eq^2_{flux} + eq^2_{rad(i-s)}} \tag{5.16}$$

for cold panels, and

$$eq_{conv} = \pm\sqrt{(eq_{pwr})^2 + (eq_{rad(i-s)})^2 + (eq_{back})^2} \tag{5.17}$$

for heated panels.

Convection heat transfer coefficient

The convection heat transfer coefficient is calculated as:

$$h_c = \frac{q_{conv}}{(T_{surf} - T_{ref})} \tag{5.18}$$

where:

h_c = convection heat transfer coefficient

T_{surf} = surface temperature

T_{ref} = reference air temperature

The uncertainty associated with the convection coefficient is given by:

$$eh = \sqrt{(\frac{\partial h}{\partial q} eq_{conv})^2 + (\frac{\partial h}{\partial \Delta T_{surf-ref}} e\Delta T_{surf-ref})^2} = \frac{1}{\Delta T_{surf-ref}{}^2}\sqrt{(\Delta T_{surf-ref}\, eq_{conv})^2 + (q_{conv} e\Delta T_{surf-ref})^2} \tag{5.19}$$

Air heat transfer rate

The ventilation air heat transfer rate is calculated by Equation 5.20.

$$q_{air} = \dot{v}_{air}\rho_{air}Cp_{air}(T_{out} - T_{in}) \tag{5.20}$$

where:

T_{in} = room inlet temperature

T_{out} = room outlet temperature

$\dot{v}_{air}$ = air volumetric flow rate, m^3/s

Since the uncertainty associated with the air density, ρ_{air}, and the specific heat, Cp_{air}, are small compared to the uncertainty associated with the temperature difference and the air volumetric flow rate, both errors are neglected. The uncertainty of the air heat transfer rate is estimated as:

$$e'q_{air} = \sqrt{e'v_{air}{}^2 + \left(\frac{e\Delta T}{\Delta T}\right)^2} \tag{5.21}$$

The fractional error in the volumetric flow rate is ± 0.02 as given above and the error in the temperature difference can be calculated from the error propagation formula given in equation 5.5.

For this experiment, the uncertainty of air ventilation heat transfer rate will be:

$$e'q_{air} = \sqrt{0.02^2 + \left(\frac{e\Delta T}{\Delta T}\right)^2} \tag{5.22}$$

5.2.3 Systematic Error Estimation

A heat balance of the whole system is used to check the systematic error associated with hot wall, cold wall, and air system measurements. The experimental room energy input and output errors are accumulated separately to estimate the systematic error. For this experimental room, there was one source of energy, the heated panels. There were two energy sinks, the cold panels and the cold air system. Since the errors associated with the heated panel voltage and resistance measurements are small compared to the error associated with the heat flux measurement, the systematic errors are estimated as heat sink errors, associated with the cold wall and air system.

For a typical experimental case, with cold wall heat flux errors of +/-0.07, and of air system heat transfer rate errors of +/-0.05, the systematic error is roughly +/-10%.

5.3 Calibration of Experimental Devices

5.3.1 Thermocouples

Thermocouples on both the Helios data logger and the wireless data logger were calibrated in-situ. An insulated water bath was used in the calibration to measure four temperature points as shown in Figure 5.9. A NIST standard thermometer with a minimum scale of 0.1ºC and an accuracy of +/-0.05ºC was used to calibrate the thermocouples.

Figure 5.7 and Figure 5.8 show typical calibration curves for thermocouples in the wireless and the Helios data loggers. The calibration curve for each thermocouple is shown in Appendix A.

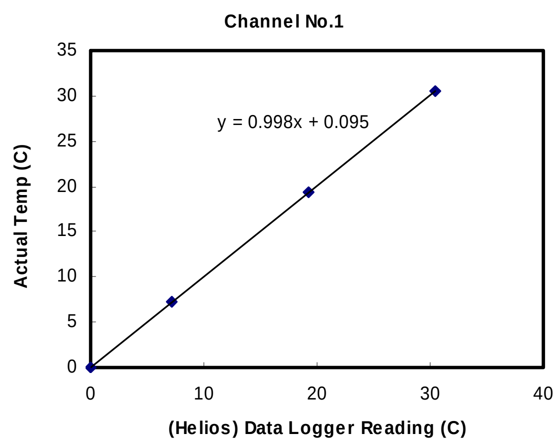

Figure 5.7 Thermocouple Calibration Curve for Channel No.1 on Helios Data Logger

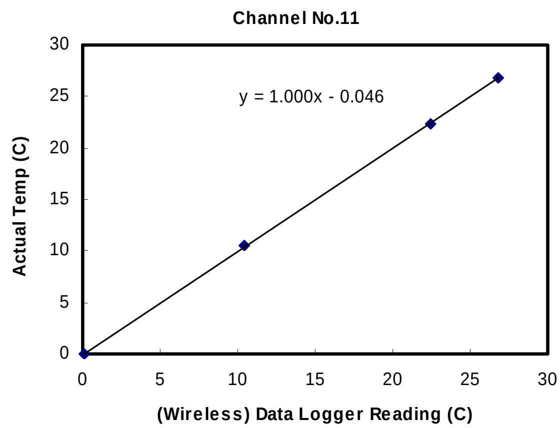

Figure 5.8 Thermocouple Calibration Curve for Channel No.11 on Wireless Data Logger

The uncertainty of the thermocouple readings is estimated as +/-0.1ºC after calibration. Together with the thermometer uncertainty (+/-0.05ºC), the total error is estimated as +/-0.1ºC.

5.3.2 TSI Air Velocity Transducers

The TSI-8470 air velocity transducers were calibrated by Davis-Inotek Calibration Laboratory. Table 5.3 shows the calibration curves correlated with the tabulated data provided by Davis-Inotek. Figure 5.9 shows one of the calibration curves.

Table 5.3 TSI Calibration Curves

Sensor serial No.	Calibration Curve
89030236	y = 0.97x + 11.20
89010056	y = 1.00x - 14.77
88070018	y = 1.01x + 3.70
89010058	y = 1.05x - 15.75
88070020	y = 0.99x + 13.55
89030238	y = 1.00x + 4.13

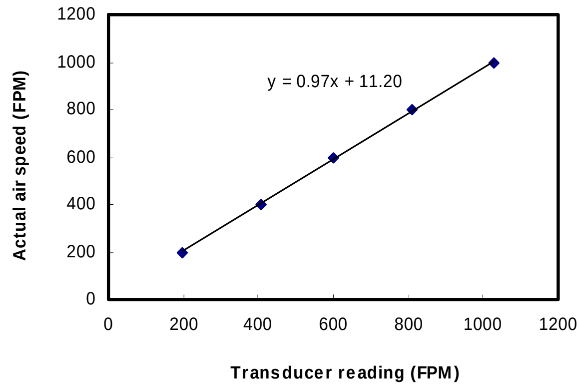

Figure 5.9 A Typical TSI Air Velocity Transducer Calibration Curve

The calibrated TSI air velocity transducers have a published uncertainty of +/-(3% + 10FPM).

5.3.3 Heat Flux Sensor Calibration

The heat flux sensor is used to measure the total cold panel surface heat flux. The heat flux sensor area together with the guard area is about 0.005m^2. This is a small fraction of the total surface area of the cold panel. The sensor output was therefore calibrated to the total panel surface heat flux.

The heat flux sensor itself has two main error sources; these are due to changes in the operating temperature and the surface conductivity. The accuracy ($\pm 20\%$) given by the manufacturer assumes that the operating temperature would change at most 40˚C from the factory calibration temperature and that conductivity would change from 0.2 to 4.0W/m-K. Under the experimental conditions in the test room, where temperature and surface conductivity changes are much smaller than the manufacturer's assumption, the heat flux sensor accuracy should be significantly higher than the published accuracy. In addition, the published accuracy was determined for soil heat flux measurement, in which the heat flux sensor is embedded in the medium. In this research application, with the heat flux sensor mounted on the surface, the deflection error due to sensor conductivity should be estimated differently. The calibration procedure described below uses the measured heat transfer rate from the water to estimate the heat flux sensor accuracy.

5.3.3.1 Calculation Design and Error Analysis

The total panel heat flux was experimentally determined by maintaining a measurable temperature difference between the water inlet and outlet. A calibrated ΔT thermocouple was used to measure the temperature difference. Using ΔT thermocouples has two advantages. First, it reduces two temperature measurement errors to one. And second, logging a voltage signal instead of temperature signal has a higher accuracy for the Fluke data loggers. Water mass flow rate is measured directly using a precision scale and a stop watch. The heat transfer rate is calculated as:

$$q_w = cm\Delta T / A \tag{5.23}$$

where:

q_w = heat transfer rate from cold water, W/m^2

c = water specific heat, J/g-˚C

m = water mass flow rate, g/s

ΔT = water inlet and outlet temperature difference, ˚C

A = cold panel surface area, m^2

The error from each component of this equation is accumulated using Holman's non-linear relation:

$$eq = \pm\sqrt{\left(\left.\frac{\partial q}{\partial m}\right| em\right)^2 + \left(\left.\frac{\partial q}{\partial \Delta T}\right| e\Delta T\right)^2 + \left(\left.\frac{\partial q}{\partial c}\right| ec\right)^2 + \left(\left.\frac{\partial q}{\partial A}\right| eA\right)^2} \tag{5.24}$$

The relative error of the heat flux is:

$$e'q = \pm\sqrt{\left(\frac{em}{m}\right)^2 + \left(\frac{e\Delta T}{\Delta T}\right)^2 + \left(\frac{ec}{c}\right)^2 + \left(\frac{eA}{A}\right)^2} \tag{5.25}$$

The systematic error described in Section 5.3.3 is determined by heat sink errors associated with the air system and cold wall. With an air system heat transfer rate error of +/-5%, the heat flux sensor measurement should be equal to or less than +/-5%. Considering the limitation of measurement devices, the heat flux sensor errors are aimed to within +/-10%. Therefore, the uncertainty associated with each component in the above equation must be reduced to less than +/-10% so that the accumulated error could be within +/-10%.

5.3.3.2 Test Setup

Figure 5.10 shows the calibration setup. Water mass flow rate is measured using a precision scale and a stopwatch. With a scale error of +/-0.1g, and a stopwatch error of +/-0.5s, the mass flow rate error can be easily controlled to within +/-0.0001 when the recording time is longer than 120 seconds. The error in measured panel surface area can be easily controlled at +/-0.001 with a medium accuracy length scale. The relative error in temperature difference is related to its magnitude. To get a specific relative error, a minimum temperature difference is required. For example, if the maximum acceptable error in the temperature difference is +/-0.05˚C, the temperature difference should be at least 1˚C. The uncertainty associated with the specific heat is assumed to be negligible compared to the measurement error.

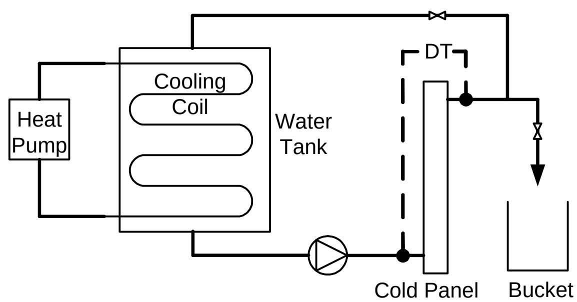

Figure 5.10 Calibration Test Setup

The temperature difference between panel inlet and outlet is measured using two ΔT thermocouples. Figure 5.13 shows the ΔT thermocouple wiring. The coefficients for these two thermocouples are calibrated using a NIST certificated thermometer with an accuracy of +/-0.05ºC. The coefficients are found to be 24764.06ºC/V and 24755.62ºC/V respectively. Two temperature readings accumulated the error to +/-0.07ºC.

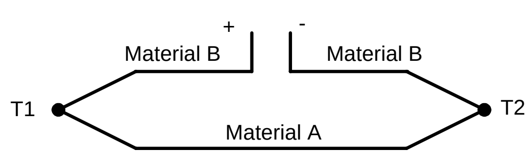

Figure 5.11 ΔT Thermocouple Wiring

The precision of a measurement is the random error around its real value. The precision of the temperature data-logging system was obtained by submerging the thermocouples into a constant temperature water bath for 10 minutes, and logging data at 20-second intervals. This procedure was repeated three times. Typical results are shown in Figure 5.12. The fluctuations of the thermocouple readings were found to be +/-0.07˚C, which is the data logger resolution. Therefore, the random error is estimated as +/-0.07˚C. In this calibration procedure, the random error was minimized by sampling for a long period of time and is neglected in the total error estimation.

The temperature measurement system error that contributed to the systematic error has two sources, one is from the thermocouple and the other is from the data logger. Using a standard thermometer to calibrate the whole measurement system can reduce the systematic error to the accuracy of the standard thermometer. Since the accuracy of the NIST certified standard thermometer is +/-0.05˚C, the calibration curve also has an error of about +/-0.05˚C. As a result, the error of the temperature measurement system was estimated at +/-0.07˚C.

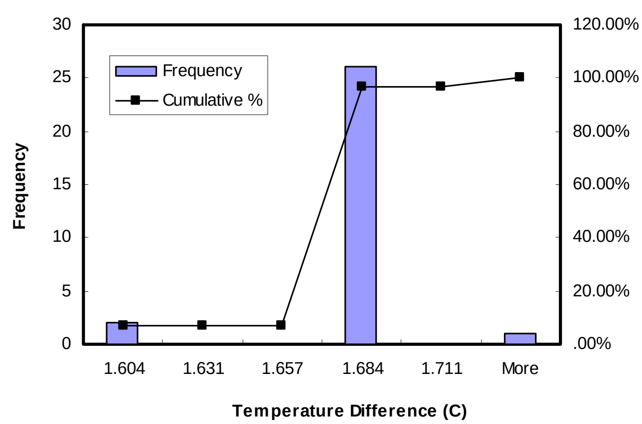

Figure 5.12 Data Logger Readings for Temperature Differential of 1.7ºc

To calibrate each panel flux transducer, the panel surface temperature, near wall air temperatures and velocities were monitored with thermocouples and air velocity transducers (TSI8470) as shown in Figure

5.13. The air speed transducers and the thermocouples were mounted on a stand for stability. The heat flux back loss are estimated and considered in the calibration. A wind tunnel as shown in Figure 5.14 was constructed to provide uniform airflow. The cold panel was flush-mounted on one side of the wind tunnel. A variable speed fan was mounted at one end of the wind tunnel and three separate settling means were positioned upstream of the test panel. A damper was installed at the fan outlet to control the volumetric flow rate. Two heaters were located upstream of the test panel to control the air temperature. The calibration tests covered all conditions expected in the experimental room.

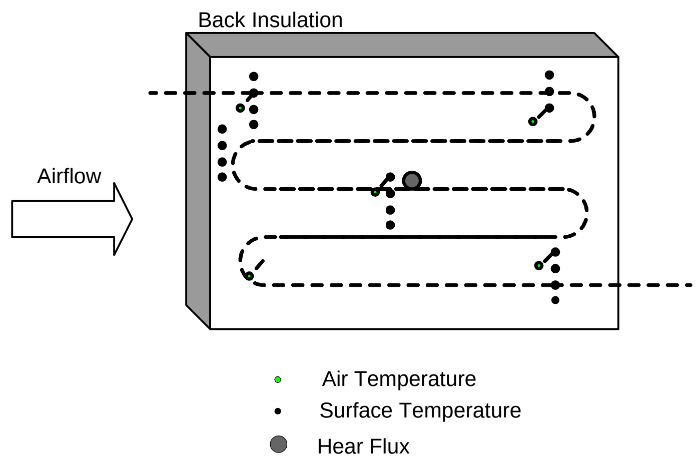

Figure 5.13 Monitored Surface and Air Parameters

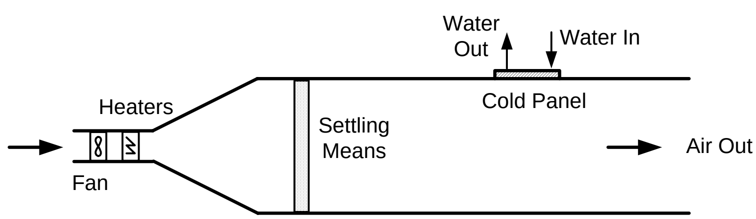

Figure 5.14 Calibration Wind Tunnel

5.3.3.3 Test Parameter Setup

Considering the measurement error and the surface temperature and heat flux uniformity requirement, the temperature difference between panel inlet and outlet was controlled at $1.4°C \le dT \le 2.0°C$ by adjusting the water flow rate.

For each panel, a set of calibration tests was performed as shown in Table 5.4. This set of tests was designed to cover natural, mixed, and forced convection conditions in the experimental room. Since one of the characteristics of the thermopile embedded in the heat flux sensor is temperature dependence, the calibration tests also cover the expected temperature range of experiments. More than 7 points were tested for most panels to improve the accuracy. A calibration curve was calculated for each panel in the form of:

$$q_{water} = A(q_{sensor})^B \tag{5.26}$$

where:

q_{sensor} = heat flux sensor reading, W/m^2

A, B = coefficients

Table 5.4 Test Parameter Setup

Test Number	Chiller Temp.	Heater	Fan Speed	MFR_Control
1	0ºC	On	Full	$1.4°C \le dT \le 2.0°C$
2	0ºC	On	¾	$1.4°C \le dT \le 2.0°C$
3	0ºC	On	½	$1.4°C \le dT \le 2.0°C$
4	0ºC	Off	Full	$1.4°C \le dT \le 2.0°C$
5	0ºC	Off	½	$1.4°C \le dT \le 2.0°C$
6	0ºC	Off	0	$1.4°C \le dT \le 2.0°C$
7	5ºC	Off	0	$1.4°C \le dT \le 2.0°C$

The system required about 1 hour to reach steady state for the first point of each panel. Adjusting the mass flow rate to reach steady state at the next point required about 20 minutes. On average, each panel required about 6 hours of testing.

5.3.3.4 Calibration Results

Table 5.5 shows typical test results using panel number 2 as an example, and Figure 5.15 shows the measured and correlated data for panel 2 and panel 6. The total error in predicted water heat flux is within +/-7% for this calibration test. The differences between the calibrated sensor readings and the average heat transfer rates are also within +/-7%. Therefore, the uncertainty on panel surface heat flux measurement is estimated as +/-10%. Table 5.6 shows the heat flux correlations for all panels.

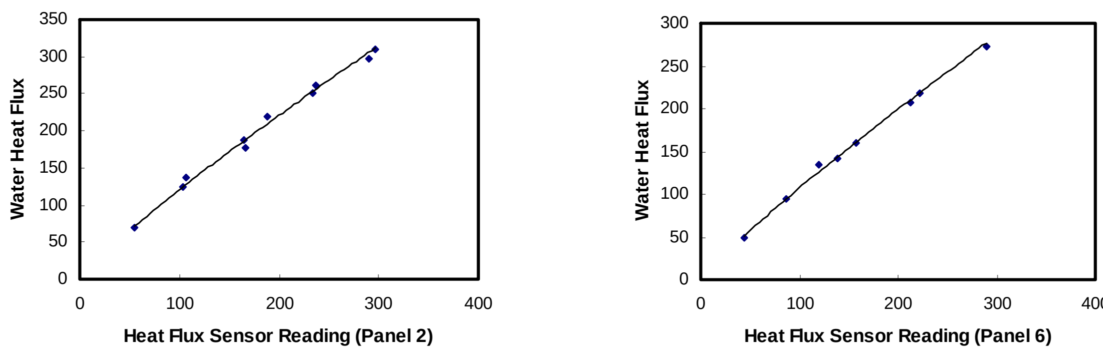

Figure 5.15 Heat Flux Sensor Calibration Results for Panel No.2 and No.6

Table 5.5 Calibration Results for Panel No.2

Test Number	Delta T	$Q_{heatFluxsensor}$	Q_{water}	$Q_{Correlated}$	Error
1	1.47	104.1	124.2	125.1	0.0070
2	2.10	165.5	177.4	187.4	0.0560
3	1.47	165	188.2	186.9	-0.0069
4	1.52	233.7	251.7	253.1	0.0056
5	1.50	289. 7	296.7	305.2	0.0288
6	1.60	296.9	310.7	311.8	0.0037
7	1.75	237.5	260.6	256.7	-0.0149
8	1.47	188.9	218.8	210.3	-0.0389
9	1.80	106.2	137.0	127.3	-0.0708
10	1.59	55	69.2	71.7	0.0358

Table 5.6 Calibration Correlations for All Panels

Panel Number	Calibration Curve	Max Error
1	$y = 1.799\ x^{0.882}$	-0.06
2	$y = 2.179\ x^{0.872}$	-0.07
3	$y = 2.644\ x^{0.804}$	0.04
4	$y = 2.259\ x^{0.840}$	-0.07
5	$y = 2.633\ x^{0.817}$	0.05
6	$y = 1.758\ x^{0.893}$	0.04
7	$y = 2.771\ x^{0.820}$	-0.05
8	$y = 2.536\ x^{0.844}$	0.06
9	$y = 2.536\ x^{0.821}$	-0.02
10	$y = 1.803\ x^{0.887}$	-0.04
11	$y = 1.613\ x^{0.916}$	0.03
12	$y = 2.3159\ x^{0.856}$	0.05
13	$y = 2.2119\ x^{0.845}$	0.01
14	$y = 2.2074\ x^{0.850}$	-0.04
15	$y = 3.0139\ x^{0.792}$	-0.07
16	$y = 2.9555\ x^{0.792}$	-0.06
17	$y = 2.2468\ x^{0.844}$	-0.02
18	$y = 2.2773\ x^{0.859}$	-0.05
19	$y = 2.1319\ x^{0.827}$	0.02
20	$y = 1.9984\ x^{0.857}$	-0.01

Chapter 6: Obtaining Nondimensional Numbers for Local Variable Based Convection Model

A valid convection model must have a properly defined reference temperature. To be generally applicable, a convection model also needs a properly defined length scale so that it can be applied in cases that are dynamically similar but with different dimensions. Currently, no agreement has been reached on how to select either the reference temperature or the length scale for room convection models. This chapter discusses the selection of length scales for the radial ceiling diffuser room configuration. Chapter 7 discusses the selection of the reference temperature.

6.1 Nondimensionalization Method

Selection of length scales is difficult for room airflow, and previous investigations have not reached an agreement on how to define it. Length scales define the nondimensional numbers that allow experimental results to be applied to dynamically similar configurations. Awbi and Hatton's natural convection model used surface hydraulic diameter defined by the surface area and the perimeter as a length scale. Khalifa's natural convection model is dimensional and doesn't include a length scale. Kapoor and Jaluria's (1991) mixed convection model used nozzle width (D) as length scale for nondimensional numbers, Gr_D, Re_D, and Nu_D. The ratio of ceiling length to nozzle width (L/D) was also considered to have an effect on surface convection heat transfer and was included in the correlations. Other length scales, such as surface height (used in Alamdari and Hammond's (1983) natural convection model), overall length of heated wall (used in Neiswanger's (1987) forced convection model), and nozzle width (used in Awbi's (2000) forced convection model), were all used without theoretical analysis.

In order to reduce the randomness associated with selecting length scales for room convection models, a general method is desired. Since length scale is used to define nondimensional numbers, seeking a proper length scale can be considered in the context of dimensional analysis for a particular flow. Therefore, the objective of rationally determining the length scales is achieved in the nondimensional number definitions.

Bejan (1995) used scale analysis to determine nondimensional numbers for natural convection flow in enclosures. Scale analysis is a technique for simplifying equations by estimating the order of magnitude of each term and then eliminating the "small" ones. Bejan's (1995) scale analysis non-dimensionalized the mass, momentum, and energy conservation equations to determine the form of the Nusselt and Rayleigh numbers and their relationship to each other for natural convection in enclosures. However, scale analysis can't be applied to forced convection heat transfer in room enclosures because of the flow complexity and the unavailability of simplifying assumptions typically used in natural convection flows. Therefore, a new method is required to properly define nondimensional numbers for forced convection models of room enclosures.

The form of the proposed forced convection correlation relies on the fact that nondimensional numbers are basically ratios of two comparable parameters. Grashof number is defined as the ratio of buoyancy and viscous forces, Reynolds number is defined as the ratio of inertia and viscous forces, and Nusselt number is defined as the ratio of convection and conduction heat transfer rate. These ratios apply to any infinitesimal control volume in the flow field. The parameters that are used to describe the flow in the control volume can be scaled with macro-parameters that are characteristics of the flow field under consideration. This method of finding length scales relies on the basic definition of the non-dimensional numbers and is used in this research. The proposed non-dimensionalization method is a semi-empirical method that relies on a-priori knowledge of the basic flow field characteristics.

6.2 Description of the Room Flow Field

Airflow characteristics of most ventilated rooms depend primarily on the diffuser location and design. For a typical ventilated room, the buoyancy effect is negligible and forced convection dominates the entire flow field. A centered radial ceiling diffuser configuration was selected for this research due both to its widespread use in buildings and the accessibility of existing experimental ceiling diffuser data sets.

In the experimental room described in Chapter 5, the flow is discharged from a radial ceiling diffuser located in the center of the ceiling. The ventilative flow rate and surface buoyancy effect are controlled to ensure forced convection flow on the enclosure walls. The near-wall airflow characteristics for this configuration are dominated by the jet attached at the ceiling and walls. The near-wall flow field can be described by six distinct regions as shown in Figure 6.1. These regions are the 'recirculation' region, located adjacent to the diffuser, the 'reattachment' region, the 'wall jet' region, the 'detachment' region, the 'reattachment' region, and the 'reattached wall jet' region.

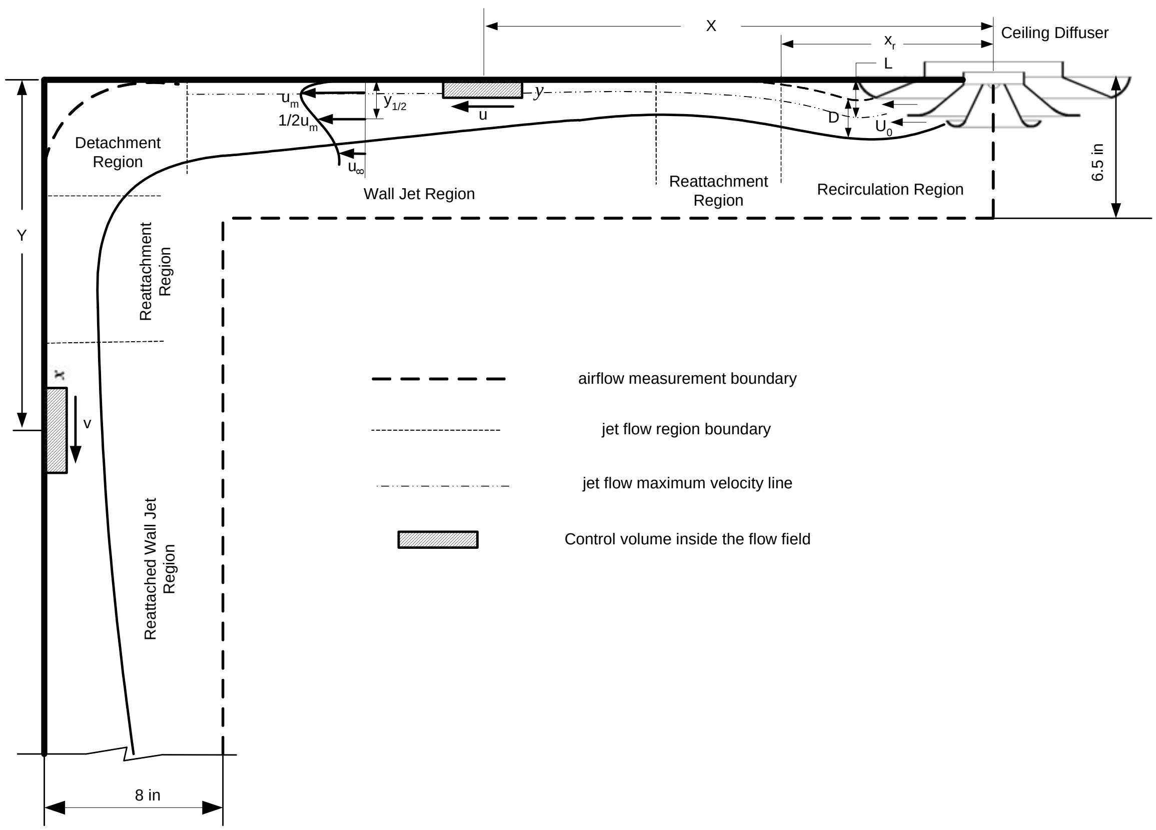

Figure 6.1 Jet Flow of the Interested Field

In order to apply the non-dimensionalization method to this flow field, the characteristic length of each region was experimentally determined. This was accomplished by measuring air speeds on a grid near the ceiling and walls. Due to the wide range of air velocities in the near wall regions of interest, two different types of air velocity transducers with different measurement ranges were used. The Dwyer Model 640-0 air velocity transmitter has four field selectable ranges, 0-200, 0-1000, 0-3000, and 0-12,000 FPM. The sensing tip is enclosed in an open window on the probe, and the measurement is actually one-dimensional. The TSI Model 8470 omni-directional sensor with a measurable range of 0-1000FPM was also used. The TSI sensors have higher accuracy but cannot be used to resolve the flow direction. The measurement grid under the ceiling is 1" x 0.5" while it is 1" x 6" near the wall. Using VTK, the measured air speed was plotted as shown in Figure 6.2a. Additional flow field details are shown in Figure 6.2b and 6.2c.

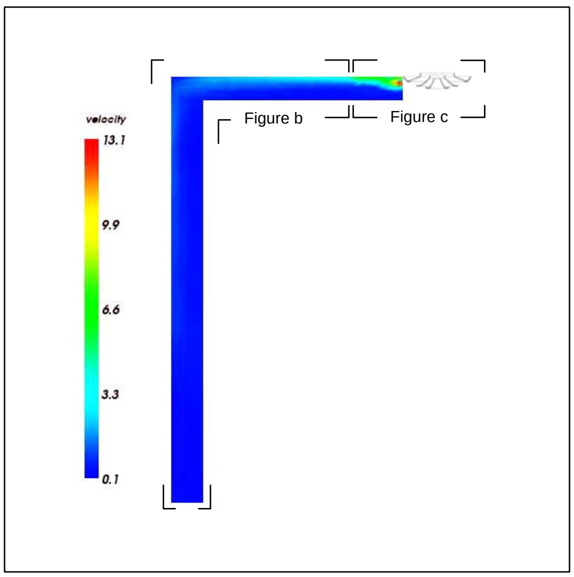

a. Whole flow field

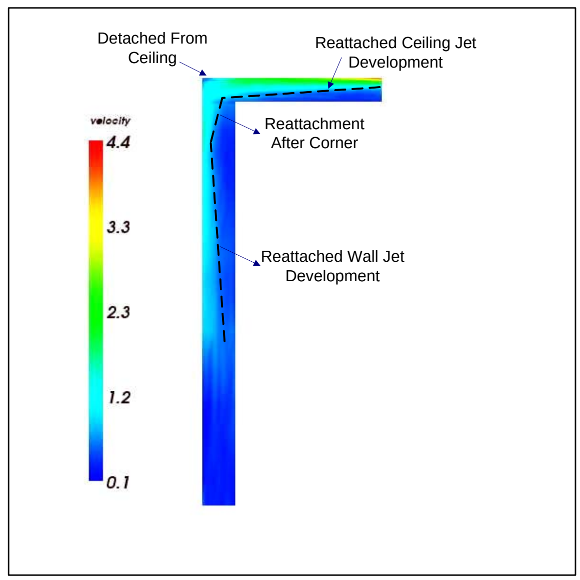

b. Reattached wall jets

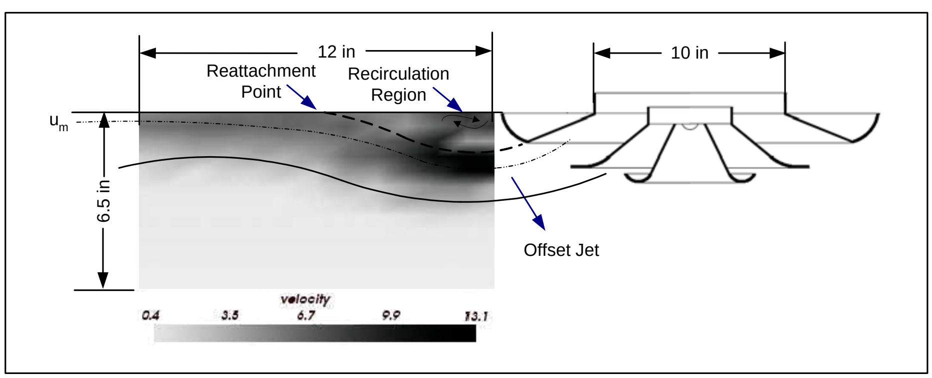

c. Offset jet reattachment

Figure 6.2 Airflow of the Measurement Field

The flow field shows that the jet flow from the diffuser behaves as an "offset jet", which leaves the diffuser as a free jet some distance from the surface, then attaches to the ceiling and develops as a wall jet. Figure 6.2c shows the reattachment and Figure 6.2b shows the ceiling jet and wall jet development. At the corner, the wall jet detaches from the ceiling and reattaches to the wall and again develops as a wall jet as shown in Figure 6.2b.

The offset ratio, L/D, is defined as the ratio of the distance from the center of the jet to the surface, L, and the jet diameter, D, at the diffuser as shown in Figure 6.1. The radial ceiling diffuser produced an offset jet with a small offset ratio as shown in Figure 6.2c.

As illustrated in Figure 6.1, the offset jet flow usually consists of three flow regions: the recirculation region, the reattachment region, and the wall jet region. The reattachment location, the center of recirculation, the jet width before and after reattachment, and the velocity and temperature distribution of the entire flow field have been previously studied. Bourque and Newman (1960) predicted the reattachment location x_r as a function of the offset ratio for the two-dimensional plane offset jet:

$$\frac{x_r}{D} = 0.332(L/D) - 0.07(L/D)^2 + 0.0169(L/D)^3 \qquad (6.1)$$

Parameswaran and Alpay (1975) proved this relation with their own data, the data of Perry (1967), and the data of Bourque and Newman. Beyond reattachment, the offset jet can be considered as a plane wall jet because velocity similarity (Parameswaran and Alpay, Song, Yoon, and Lee (2000)) and temperature similarity (Holland and Liburdy (1999)) are both reached.

Similar research results were obtained for a radial offset jet. Tanaka et al. (1978) presented a relation between reattachment location and offset ratio. A linear relation was observed for offset ratios greater than 2. This offset ratio is out of range for standard room configurations and is not shown here. A polynomial relation was also developed for offset ratios less than 2, i.e., $L/D < 2$. This relationship, which is applicable to the offset jets considered in this investigation, was given as:

$$\frac{x_r}{D} = 4.757(L/D) - 1.061(L/D)^2 + 0.112(L/D)^3 \tag{6.2}$$

Two wall jet regions, the inner layer, which is nearest the surface, and the outer layer, are separated by the maximum velocity line. The jet half width is defined as the outer layer thickness at which the magnitude of the velocity is one half of the maximum velocity. The half width velocity and the half width are usually used to define the jet's velocity and boundary layer thickness due to the complexity and instability of the inner layer. For a two-dimensional plane wall jet, Launder and Rodi (1981) presented the maximum velocity decay and gave the growth of the jet half width as:

$$\frac{dy_{1/2}}{dx} = 0.073 \pm 0.002 \tag{6.3}$$

This represents a linear relationship. For a radial wall jet, a similar relation was presented by Govindan et al. (1974) and Bakke (1957):

$$y_{1/2} \propto x^{0.915} \tag{6.4}$$

$$y_{1/2} \propto x^{0.94} \tag{6.5}$$

The exponent value on x (0.94 and 0.915) was determined to be 1.02 by Glauert (1956) and 1.0 by Dawson and Trass (1966) through theoretical analysis. The exponents from experiments and theoretical analysis are very close to 1.0. For this research, the exponent is assumed to be 1.0 for simplicity. Therefore, the half width of the radial wall jet is:

$$y_{1/2} \propto x \tag{6.6}$$

The half width of the wall jet can be scaled by 'X', the distance from the diffuser as shown in Figure 6.1, in formulating nondimensional numbers.

The maximum velocity decay of the radial wall jet was given by Baake as:

$$U_m \propto x^{-1.12} \tag{6.7}$$

6.3 Nondimensional Number Expressions

Based on the offset jet characteristics described in the proceeding section, the non-dimensionalization method can be applied to room enclosures with a centered radial ceiling diffuser. The Reynolds number and Nusselt number for this flow configuration will be defined in this section. In addition, the Grashof number for natural convection in enclosures will be developed using the non-dimensionalization method.

6.3.1 Reynolds Number

For forced convection flow in rooms, the Reynolds number and Nusselt number form the basis of the convection model. The Reynolds number characterizes momentum driven flow and determines the magnitude of forced convection heat transfer. The non-dimensionalization method is applied by defining the Reynolds number as the ratio of the inertia force to the viscous force. For the ceiling flow, defining the Reynolds number in this way as shown in Figure 6.1 gives the following relationship for the Reynolds number:

$$\mathrm{Re} = \frac{F_{inertia}}{F_{viscous}} = \frac{\rho y u \dfrac{\partial u}{\partial x}}{\mu \dfrac{\partial u}{\partial y}} \tag{6.8}$$

where:

$$F_{inertia} = ma = \rho V \frac{\partial u}{\partial t} = \rho V \frac{\partial u}{\partial x}\frac{\partial x}{\partial t} = \rho V u \frac{\partial u}{\partial x}$$

$$F_{viscous} = \mu A \frac{\partial u}{\partial y}$$

A = surface shear area of the control volume

V = volume of the control volume

Applying the result of the offset jet analysis in section 6.2 to the radial ceiling jet, the flow unit thickness is scaled as:

$$y \sim x$$

For the offset jet on the ceiling, the following scales are identified as shown in Figure 6.1:

$$x \sim X \;,\; u \sim \frac{1}{2} U_m$$

Where " X " is the local distance from the diffuser center and " $\frac{1}{2}U_m$ " is the local half width velocity. The local maximum U_m can be obtained using jet theory. Therefore, the Reynolds number for the ceiling jet flow is defined as follows:

$$\mathrm{Re} \sim \frac{1/2U_m X}{\nu} \tag{6.9}$$

Airflow on the vertical surfaces is also characterized as a reattached wall jet. According to Kapoor and Jaluria (1991) and the experimental results presented in section 2.2, the ceiling jet flow separates from the horizontal surface before reaching the corner and then reattaches itself to the vertical surface. So, the airflow near the vertical surface is another reattached wall jet after the corner. Similarly, the Reynolds number on the vertical surfaces is defined as:

$$\mathrm{Re} \sim \frac{1/2V_m Y}{\nu} \tag{6.10}$$

Here, "Y" is the distance from local point to the ceiling and wall corner as shown in Figure 6-1. The wall jet maximum velocity continuously decays from the ceiling jet. Therefore, the overall distance from the diffuser is used to evaluate the local maximum jet velocity.

6.3.2 Grashof Number

The Grashof number may be defined as the ratio of buoyancy force to viscous force. In most air-conditioned rooms, all surfaces are hot compared to the ventilation air. The buoyancy effect may result in warm plumes from the floor, a stagnant boundary layer under the ceiling, and upward buoyancy driven flow on walls.

For an infinitesimal control volume in the airflow field near the vertical surface, the fluid temperature is assumed to be the same as surface temperature, T_s, and the air density, ρ_s, is evaluated at T_s. The Grashof number is then defined as:

$$Gr = \frac{F_{buoyancy}}{F_{viscous}} = \frac{(\rho_\infty - \rho_s)gx}{\mu \frac{\partial v}{\partial x}} \tag{6.11}$$

where:

$$F_{buoyancy} = (\rho_\infty - \rho_s)Vg$$

$$F_{viscous} = \mu A \frac{\partial v}{\partial x}$$

Similarly, the variable scales and the Boussinesq approximation are applied to the Grashof number definition:

$$y \sim Y$$

$$\rho_\infty - \rho_s = \rho_s \beta (T_s - T_\infty)$$

Analysis of the energy conservation equation (Bejan, 1995) gives the scales of the buoyancy driven flow velocity:

$$v \sim \frac{\nu Y}{\Pr \delta_T{}^2}$$

Here "Y" is the relative distance from the buoyancy driven flow boundary layer starting point, which is the bottom edge of the surface for walls. The thermal boundary layer thickness, δ_T, scales x for airflow. The boundary layer thickness increases as the buoyancy driven flow develops along the vertical surfaces, and the thickness of the control volume is scaled as:

$$x \sim Y$$

The Grashof number for the walls then becomes:

$$Gr \sim \frac{\beta (T_s - T_\infty) g Y^3 \Pr}{\nu^2} \tag{6.12}$$

According to Bejan (1995), the Grashof number for the ceiling and floor, which may be characterized by stagnant air layers and plumes, is given by:

$$Gr \sim \frac{\beta g (T_s - T_\infty)(A/p)^3}{\nu^2} \tag{6.13}$$

6.3.3 Nusselt Number

By definition, the Nusselt number is:

$$Nu = \frac{h(T_s - T_\infty)A}{k\frac{\partial T}{\partial y}A} \tag{6.14}$$

For the attached wall jet, the following scales in the flow field are identified:

$\partial T \sim T_s - T_\infty$, $\partial y \sim y$, $y \sim X$

Nusselt number for forced convection on ceilings and floors is:

$$Nu \sim \frac{hX}{k} \tag{6.15}$$

The Nusselt number for natural convection is defined as:

$$Nu \sim \frac{hY}{k} \text{ for walls} \tag{6.16}$$

$$Nu \sim \frac{h(A/p)}{k} \text{ for floors and ceilings} \tag{6.17}$$

6.3.4 Summary

The non-dimensionalization method is used to find appropriate length scales for developing room convection models. The non-dimensionalization method uses the flow characteristics of the radial offset jet to find non-dimensional numbers and then the length scales are automatically obtained. The nondimensional numbers, with proper length scales are shown in Table 6.1. The detailed definition for the reference temperature will be discussed in Chapter 7.

Table 6.1 Nondimensional Numbers for the Local Variable Based Room Convection Model

Numbers		Walls	Ceilings and Floors
Reynolds Number		$\mathrm{Re}_w \sim \frac{1/2V_m Y}{\nu}$	$\mathrm{Re}_{c,f} \sim \frac{1/2U_m X}{\nu}$
Grashof Number		$Gr_w \sim \frac{\beta(T_s - T_\infty)gY^3}{\nu^2}$	$Gr_{c,f} \sim \frac{\beta g(T_s - T_\infty)(A/p)^3}{\nu^2}$
Nusselt Number	**Forced**	$Nu_w \sim \frac{hY}{k}$	$Nu_{c,f} \sim \frac{hX}{k}$
	Natural	$Nu_w \sim \frac{hY}{k}$	$Nu_{c,f} \sim \frac{h(A/p)}{k}$

Chapter 7: Developing Local Variable Based Convection Model

Chapter 6 developed the nondimensional numbers required for local variable based convection models in ventilated rooms with radial ceiling diffusers. This Chapter will use these numbers and experimental data to develop convection correlations. Experimental data from literature will be used to validate the correlations and extend their application ranges.

7.1 Validation of Experimental Data

Experimental data were considered valid only when the system reached steady state and a room energy balance had been achieved. Energy balances were checked before actually running the experiments to assess the room performance and were also checked for each set of experimental data. The experimental room has only one source of energy input, i.e. power input to the hot wall. Energy is removed from the room through the air ventilation system and the cold wall system. The heat flux calculations for all three systems are given in section 5.2.

Figure 7.1 and Figure 7.2 show the energy balance results with the hot wall, the cold wall, and the air system in operation. Ideally, the data points should fall on the diagonal heat balance curve. The error bars in Figure 7.1 represent measurement uncertainties associated with the cold wall heat flux and air system heat flux. The error bars in Figure 7.2 represent measurement uncertainties associated with the heated panel power. The figures show that the hot wall has a very small error compared to the cold wall and the air system. This is achieved with the AC line voltage data acquisition system and the measurement of the electric resistance for each heating panel. Heat balances well within the predicted range of experimental uncertainty validate both the uncertainty analysis and the calibration methodology.

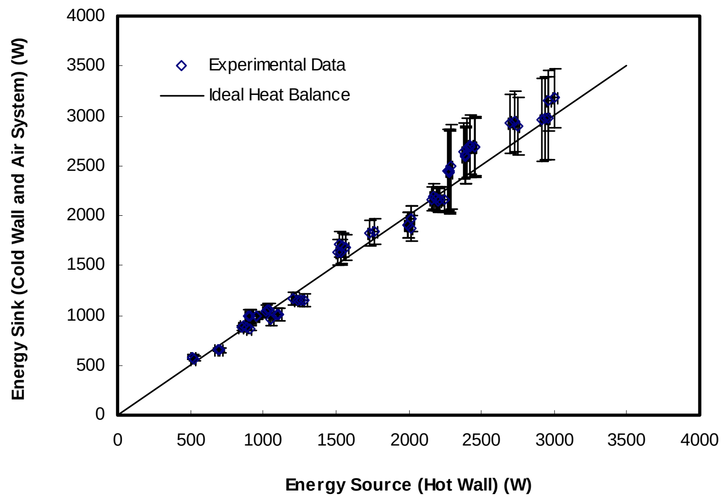

Figure 7.1 Energy Balances with Cold Wall and Air System Uncertainties

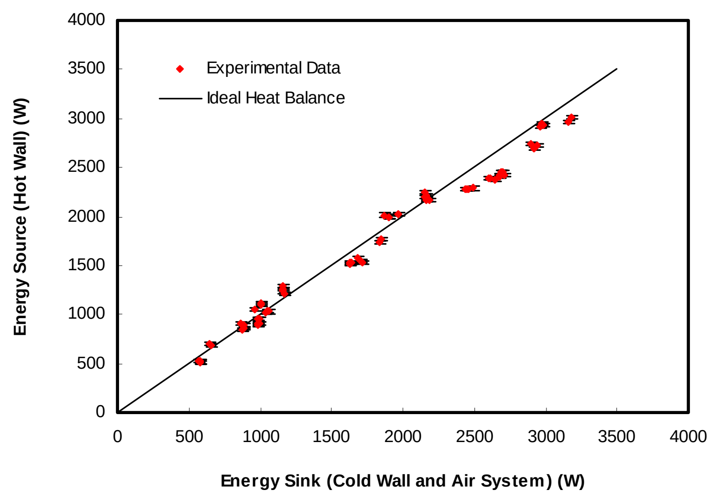

Figure 7.2 Energy Balances with Hot Wall Uncertainties

7.2 Natural Convection

The natural convection experiments were performed with both the hot wall and the cold wall on. The experimental data sets and parameters are summarized in Appendix B.2. Cold and hot panel surface data were obtained considering the buoyancy effect in both upward and downward directions.

Based on the panel data sets and the derived Grashof number and Nusselt number from Chapter 6, the natural convection correlation was developed as:

$$Nu = 0.34 \cdot Gr^{0.29} \tag{7.1}$$

The natural convection correlation was validated with experimental data from the following research: Awbi and Hatton (1999), Khalifa and Marshall (1990), Cheesewright and Ziai (1986), Bohn and Anderson (1986), and Ampofo and Karayiannis (2003). Awbi and Hatton's experiments were performed with one cold wall and different heating configurations on other surfaces. Test data were obtained on the surfaces other than the cold wall. Both room sized and model sized chambers were tested. Khalifa and Marshall investigated natural convection heat transfer on interior surfaces using a room sized test chamber. A set of experiments were performed to cover eight of the most widely used heating configurations, including a uniformly heated vertical wall and a partially heated floor and a partially heated vertical wall. Bohn and Anderson investigated natural convection in a water filled cubic enclosure. Local natural convection data were presented for the experimental configuration with one heated and three cooled walls. Cheesewright and Ziai studied natural convection in a small scale vertical rectangular cavity. The cavity had one hot wall and one cold wall facing each other. Ampofo and Karayiannis's experiments were performed with a typical 2-D natural convection configuration, i.e. one cold wall and one hot wall facing each other with all other walls adiabatic. Since the purpose of Ampofo and Karayiannis's study was to provide data to validate CFD simulations, detailed surface and air parameters were measured with high accuracy.

Figure 7.3 shows both current and previous experimental data and the natural convection correlation developed with this research data. The Bohn and Anderson data don't have the same curve as the new correlation and are not included in the plot. A possible reason is that Bohn and Anderson's experiments were conducted in a water-filled model sized chamber and the experiments are not dynamically similar to the experiments of this research. Awbi's data have the same curve but with a small systematic deviation. This is acceptable since Awbi's local data were based on the whole surface instead of smaller sub-surfaces. Awbi's data are considered to have a satisfactory match to the correlation. All other natural convection data match the correlation very well.

This research data together with the experimental data from literature give the application range of the local variable based natural convection correlation of:

$Gr = (10^3 \sim 10^{11})$

The new local correlation also applies to the whole surface with the local parameters related to the surface. Figure 7.4 shows both detailed panel data and whole surface data.

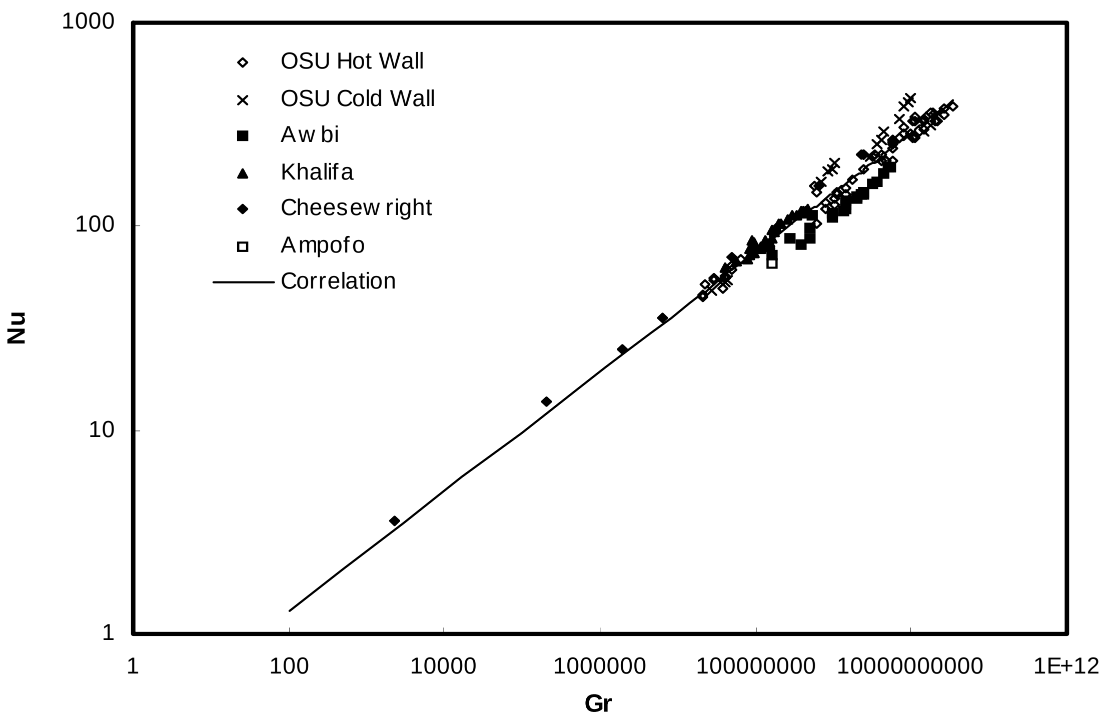

Figure 7.3 Current and Previous Experimental Data and Natural Convection Correlation

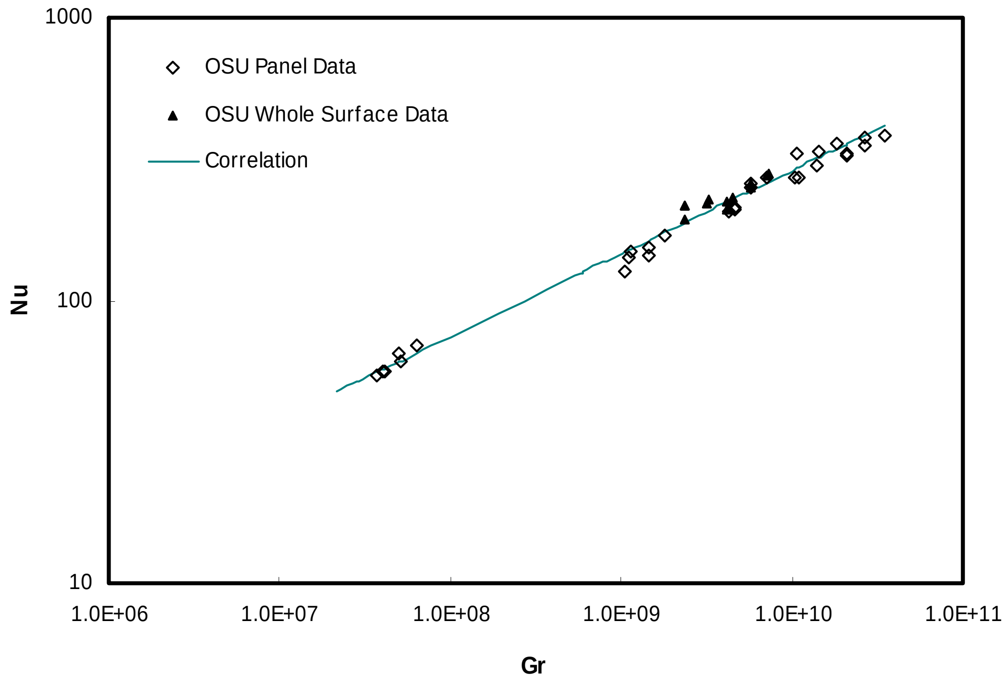

Figure 7.4 Natural Convection Data for Individual Panels and for Whole Surfaces

For natural convection, it is relatively easy to select an appropriate reference location for non-dimensionalization by simply selecting a location outside the boundary layer. Yuan (1995) found that the boundary layer thickness for natural convection in rooms ranges from 3mm to 30mm. Since both Khalifa and Awbi selected reference locations greater than 30mm from the wall, their results were consistent with Yuan's conclusion.

For the coupled HB and air model simulation, the reference temperatures are easily obtained from the air model results. The application of the local variable based natural convection correlation increased simulation accuracy for stratified rooms since it predicts the convection coefficient over sub-surfaces. The benefits of the non-mixing air model simulation are fully revealed.

7.3 Forced Convection

7.3.1 Determination of Correlation Parameters

The selection of a reference temperature is relatively obvious for simple flow configurations such as flow over a flat plate. However, there is no obvious reference temperature for room airflow. Room airflow differs from flat plate flow in two respects: there are no well-defined free stream parameters, such as temperature and velocity, and no leading edge to define the boundary layer. In addition, air temperature and velocity outside the surface boundary layer change with location.

Previously, researchers have uniformly selected the near wall air temperature as the reference temperature for room natural convection flow. This reference temperature not only determines the magnitude of the convection coefficient but also determines the surface buoyancy force. Awbi and Hatton (1999) measured local air temperatures at 100mm and 50mm from the enclosure surfaces for a room sized chamber and a small box respectively. Khalifa and Marshall (1990) measured local air temperature at 100mm away from surfaces. However, there is no agreement in defining the reference temperature for forced convection flow in rooms. Fisher (1997) selected room inlet air temperature and Spitler (1990) selected room outlet temperature. Both Fisher and Spitler's selection were based on uncertainty analysis and convenience for engineering applications.

In summary, there is no previous research to guide the selection of the reference temperature for forced convection correlations. The reference temperature for a surface grid is the adjacent air temperature at the grid center. However, the distance from the surface to the reference location is not available in the literature. In this research, local air temperatures were examined at a series of distances from the surface in order to experimentally determine the appropriate reference temperature location for forced convection correlations. Distances of 30mm, 79mm, 128mm, 177mm, and 226m from the wall were examined for all the hot wall panel surfaces. Figure 7.5 and Figure 7.6 present the local air velocities and temperatures evaluated at different locations for the first column of panels for a ventilative flow rate of 22.87 ACH. The velocity profile clearly shows the jet boundary, which is about 200mm from the surface. The temperature profile doesn't show the jet boundary, but it shows that the change in the measured surface to air temperature difference is small at all locations greater than 30mm from the surface. Even smaller differences (0.2 - 0.5°C compared to 1-2.5°C for this case) are presented among the air temperatures measured at 128mm and farther away from the surface. This temperature difference is within 0.5°C for all the experimental cases. Therefore, the local air temperature can be evaluated at 128mm or farther from the wall surface.

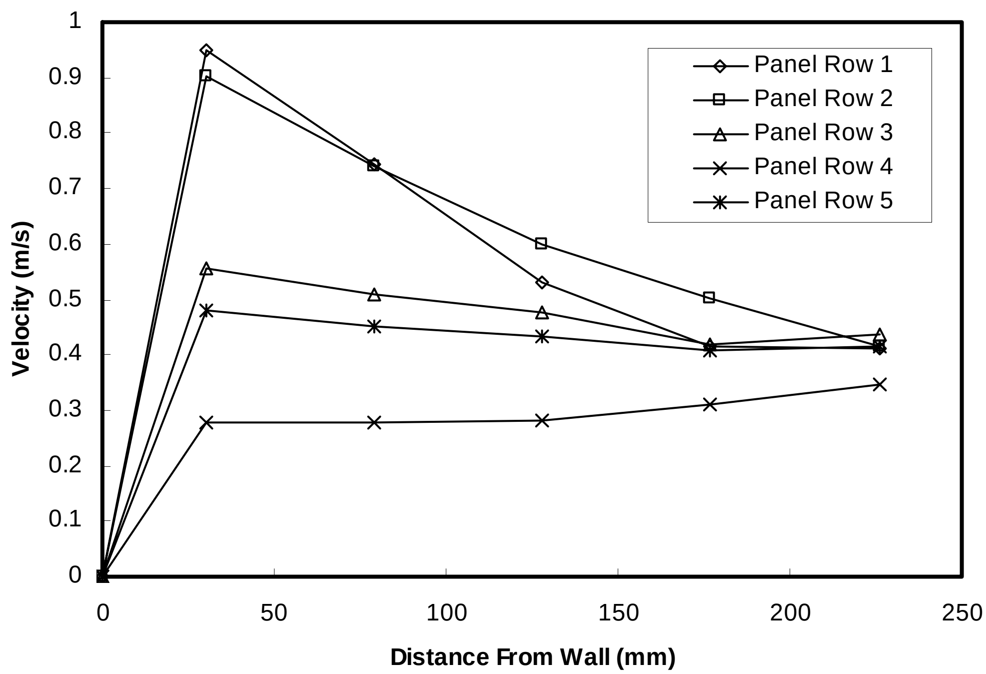

Figure 7.5 Near Wall Air Velocity Distributions

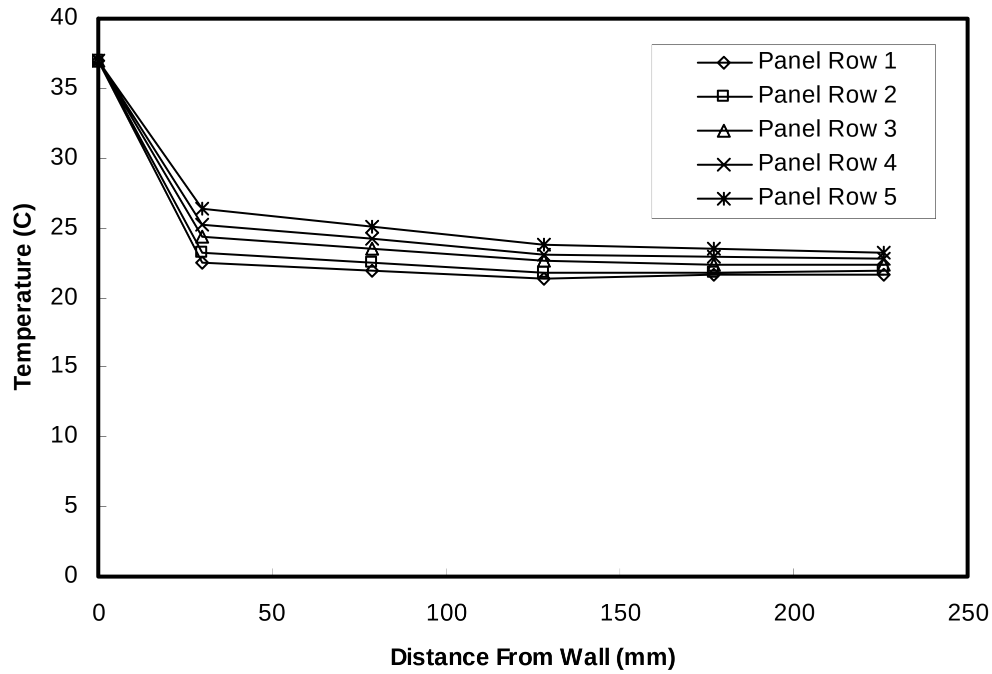

Figure 7.6 Near Wall Air Temperature Distributions

The local air velocity is defined as one half the maximum jet velocity at any point along the jet. Using the maximum jet velocity relationship given by Baake for the radial wall jet, $U_m \propto x^{-1.12}$, the local air velocity is defined as:

$$1/2U_m \propto 1/2U_0 x^{-1.12} \qquad (7.2)$$

Where: U_0 = diffuser outlet velocity

For the radial ceiling diffuser, the jet outlet velocity is determined by the room ventilative flow rate and the diffuser effective area. The diffuser effective area was not provided by the manufacturer, so it was determined experimentally. At ventilative flow rate of 13.33 ACH (0.2 m^3/s), the characteristic velocity of the diffuser was averaged to be 8.18 m/s from four points of measurement at the diffuser. The effective area of the diffuser is then calculated to be 0.0246 m^2.

With equation 7.2, one half the local jet maximum velocity can be calculated for the attached wall jet under the ceiling. Since the wall jet velocity decays continuously from the ceiling to the vertical wall, the length that is used to calculate the maximum jet velocity should be the total length from the ceiling diffuser to the vertical surface. In addition, the velocity decay due to detachment and reattachment of the offset jet must be accounted for at the diffuser and at the corner. Gu (1996) observed that the jet maximum velocity decayed about 47% from the jet opening to the reattachment point for a two-dimensional turbulent offset jet with an offset ratio of 3.98. Landreth (1990) observed 26% of jet maximum velocity decay for a radial impingement jet from jet opening to reattachment point. The velocity decays for a radial offset jet at the diffuser and at the corner are not reported in the literature. In this research, a set of experiments were performed to obtain the velocity decay coefficients from the radial ceiling diffuser opening to the reattached ceiling wall jet and the decay coefficient at the ceiling and wall corner.

The velocity decay coefficient of the reattached offset jet is the ratio between the jet maximum velocity after reattachment and the velocity at the diffuser outlet.

$$F_{Offset} = \frac{U_{m-rc}}{U_0} \tag{7.3}$$

where:

F_{Offset} = velocity decay coefficient of the offset jet

U_{m-rc} = jet maximum velocity when attached to the ceiling, m/s

U_0 = diffuser outlet velocity, m/s

The velocity decay coefficient at the ceiling and wall corner is the ratio between the jet maximum velocities at the reattachment and detachment points.

$$F_{Corner} = \frac{U_{m-rw}}{U_{m-dc}} \tag{7.4}$$

Where:

F_{Corner} = velocity decay coefficient at the ceiling and wall corner

U_{m-dc} = jet maximum velocity when detached from the ceiling, m/s

U_{m-rw} = jet maximum velocity when attached to the wall, m/s

These two ratios were obtained from jet velocity field measurements. Two regions were measured, one near the diffuser, and the other near the corner. Data sets were obtained for ventilative flow rates of 23.28 ACH, 10.98 ACH, and 3.76 ACH.

Figures 7.7 and 7.8 show the velocity profiles for a ventilative flow rate of 23.28 ACH. Figure 7.7 shows the velocity profiles near the diffuser. The figure clearly shows the offset jet, the recirculation between the offset jet and the ceiling, and the reattachment of the offset jet. Figure 7.7 shows that the jet attaches to the ceiling at a distance of 13" from the diffuser, as indicated by a maximum velocity very close to the ceiling. The maximum velocity is estimated as 4.4 m/s at this point. The diffuser outlet jet velocity is estimated from the ventilative flow rate and the diffuser effective area. Figure 7.8 shows the wall jet before detachment and after reattachment at the corner. The velocity profiles show that the wall jet detaches at 9" from the corner with a maximum velocity of 1.83 m/s and reattaches 7" from the corner with a maximum velocity of 1.33 m/s. The velocity decay coefficient is calculated using these values and includes both the corner effect and the velocity decay over this distance.

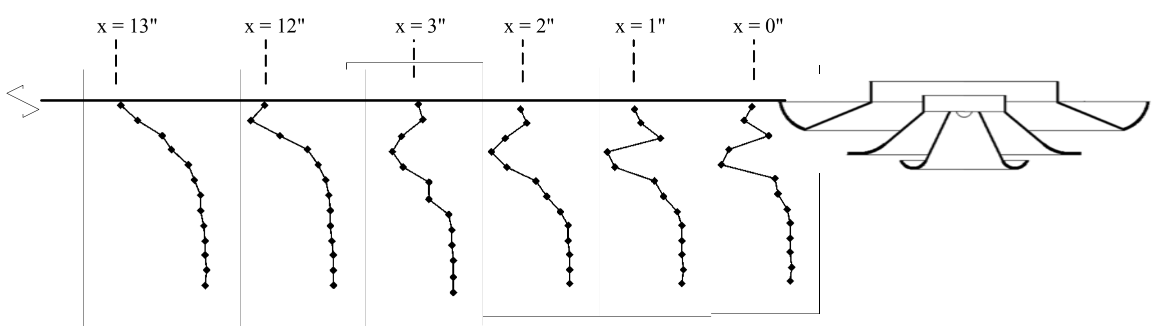

Figure 7.7 Near Ceiling Jet Velocity Profiles at Offset Jet and Reattachment Region

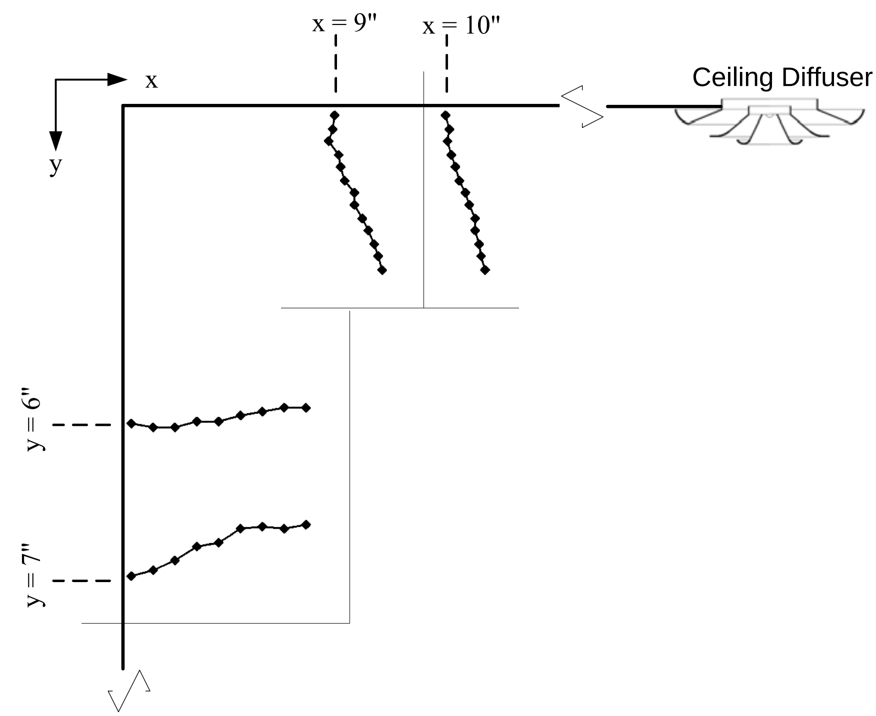

Figure 7.8 Near Wall Jet Velocity Profiles at Detachment and Reattachment Region

Table 7.1 presents all the velocities and velocity decay coefficients for the tested cases.

Table 7.1 Jet Velocity Decay Coefficients

Exp. No.	ACH	U_0 (m/s)	U_{m-rc} (m/s)	U_{m-dc} (m/s)	U_{m-rw} (m/s)	F_{Offset}	F_{Corner}
1	23.28	14.29	4.4	1.83	1.33	0.31	0.73
2	10.98	6.74	1.98	0.76	0.64	0.29	0.84
3	3.76	2.31	0.76	0.22	0.18	0.33	0.82

Over the range of ventilative flow rates (3.76 to 23.28 ACH), the velocity decay coefficients at the offset jet reattachment are almost the same and can be uniformly assumed to be 0.3. Likewise, the decay coefficients at the corner are assumed to be 0.8 for all cases. These two coefficients are considered in predicting local air velocities as demonstrated in equation 7.5.

$$u = 1/2U_0 \cdot 0.3 \cdot 0.8(L_{ceiling} + Y)^{-1.12} = \frac{0.12U_0}{(L_{ceiling} + Y)^{1.12}} \tag{7.5}$$

Where:

$L_{ceiling}$ = jet travel distance on the ceiling from diffuser center to the wall

Y = the local distance from the ceiling and wall corner

The velocity prediction equation, equation 7.5, was validated through experimentally measured maximum jet velocities. As shown in Figure 7.9, the measured velocities before the jet begins to degrade match the velocities predicted by jet theory over a range of ventilative flow rates from 10.6 to 22.9 ACH.

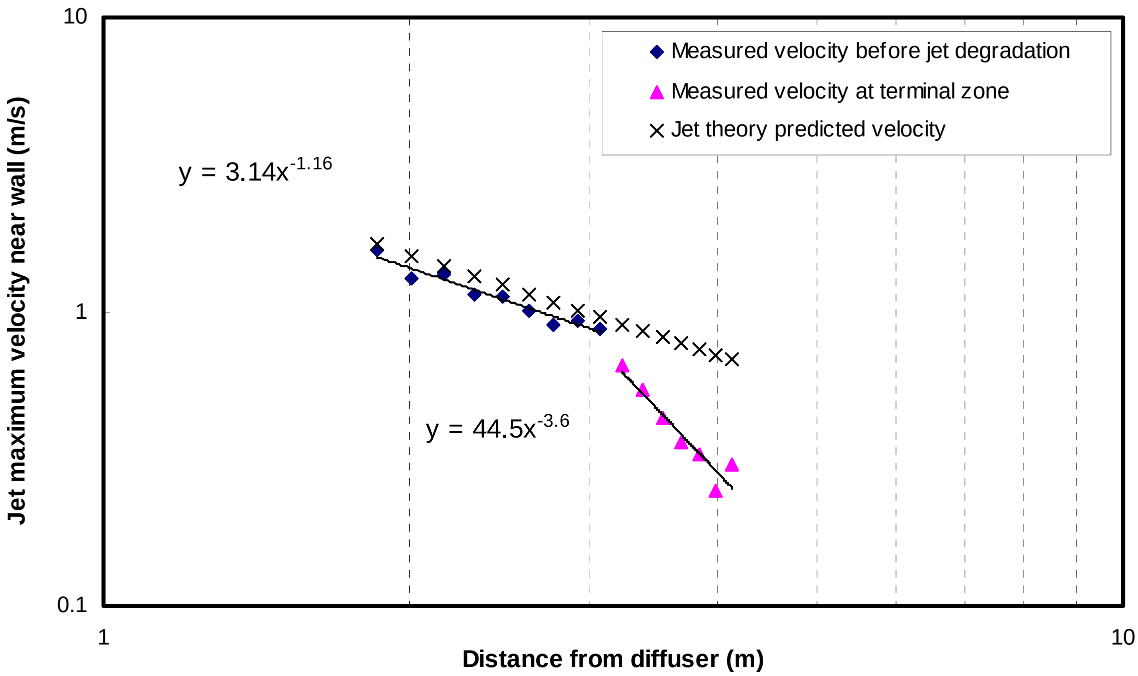

Figure 7.9-a Wall Jet Maximum Velocity Decay along the Vertical Surface Under 22.9 ACH

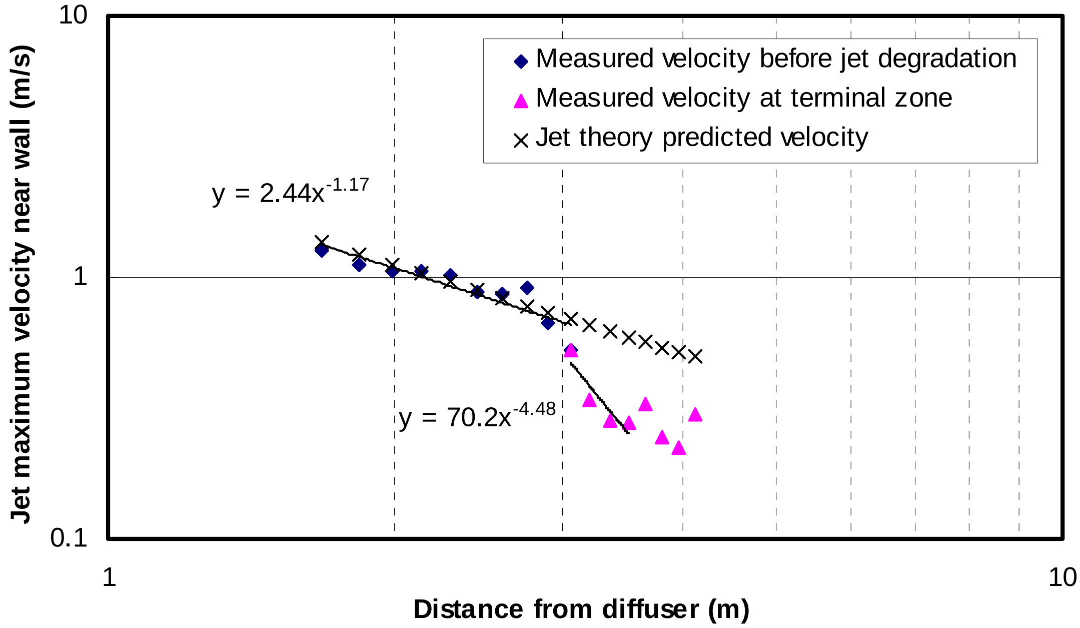

Figure 7.9-b Wall Jet Maximum Velocity Decay along the Vertical Surface Under 16.42 ACH

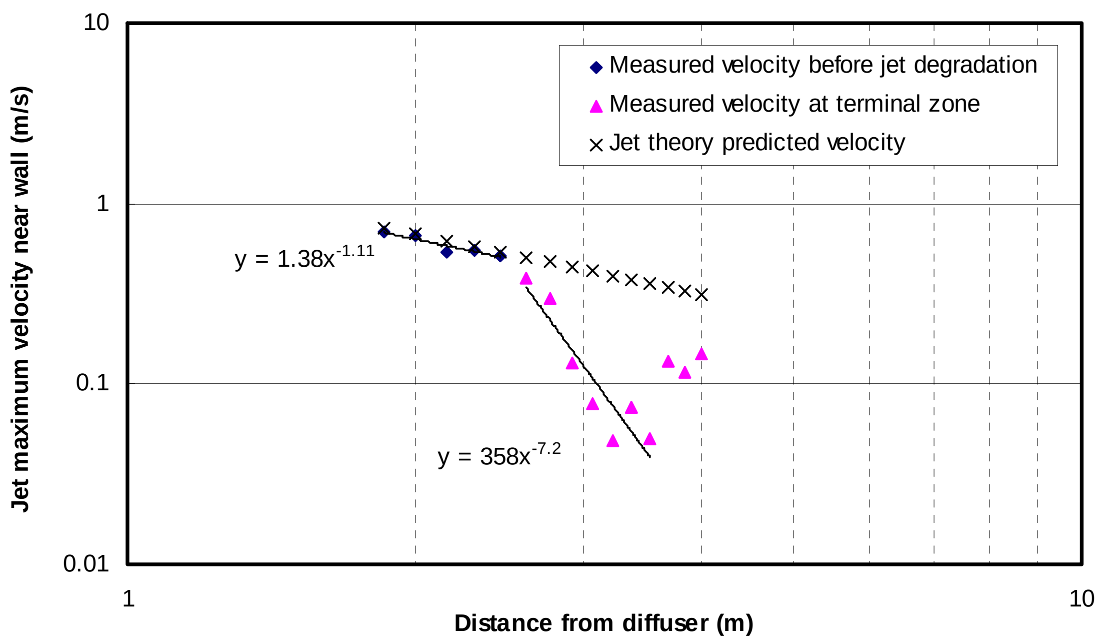

Figure 7.9-c Wall Jet Maximum Velocity Decay along the Vertical Surface Under 10.62 ACH

Figure 7.9 also shows that the jet velocity prediction equation, equation 7.5, has an application range. The jet maximum velocity decay discussed above assumes that the attached wall jet is within the fully established turbulent flow region. The ASHRAE Handbook of Fundamentals (2001) divides the jet region into four zones. For the radial ceiling diffuser configuration, the first three zones have the same correlation in terms of jet maximum velocity decay. At Zone IV, also known as the terminal zone, the velocity decays much more rapidly than for the first three zones. Therefore, the correlation that applies to the first three zones doesn't apply to Zone IV. The experimental measurements shown in Figure 7.9 demonstrate the validity of the jet velocity decay theory and clearly show the transition to Zone IV.

The limit of Zone III has not been quantitatively presented for the attached radial ceiling jet at this point. Zou (2000) found the transition point between Zone III and Zone IV using experimental measurement. The first velocity that deviates from the Zone III velocity decay trend is considered as the beginning point of the terminal zone. Linear relationships between the end velocity of Zone III and the outlet velocity were presented for both free jets and three – dimensional wall jets when $U_0 < 10 m/s$. The end velocity of Zone III becomes constant, i.e. about $1.2 m/s$, when $U_0 \geq 10 m/s$. This conclusion was validated with data from both Nottage (1951) and Malmstrom (1992). However, Zou's results can't be applied to this research due to differences in jet configurations and room dimensions.

The decay in the jet maximum velocity and the transition from Zone III to the terminal zone are examined in this research in order to define the end of Zone III. The Zone III end velocities can be obtained from figures like Figure 7.9. The Zone III end velocities for the four test cases are listed in Table 7.2.

Table 7.2 Zone III end Velocity under Different Ventilative Flow Rate

Ventilative flow rate (ACH)	U_0 (m/s)	U_e (m/s)
22.9	14.06	0.80
16.42	10.08	0.67
11.32	6.95	0.56
10.62	6.52	0.53

Based on the data presented in Table 7.2, a preliminary correlation between the ventilative flow rate and the Zone III end velocity is found:

$$U_e = 0.17 \cdot VFR^{0.5} \qquad (7.6)$$

Where:

U_e = Zone III end velocity, m/s

VFR = Ventilative flow rate, ACH

Figure 7.10 presents the correlation of the ventilative flow rate and the Zone III end velocity.

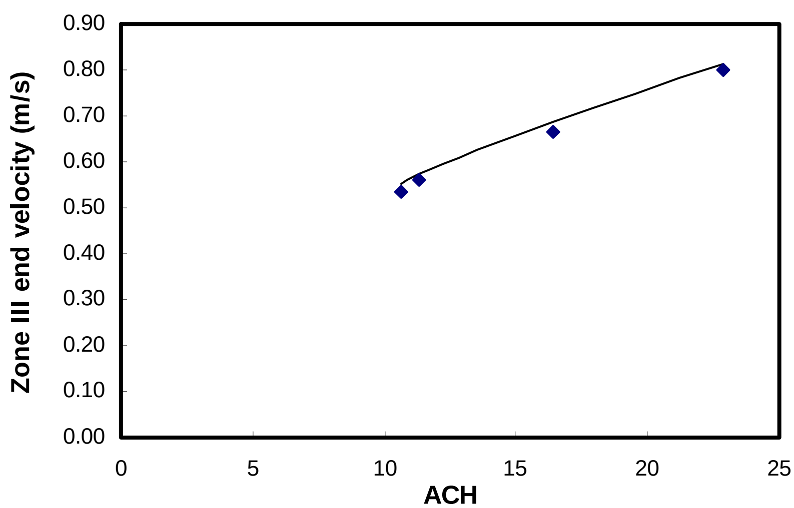

Figure 7.10 Correlations between Ventilative Flow Rate and Zone III End Velocity

For ventilative flow rates smaller than 10 ACH, the attached wall jet Zone III and the transitions from Zone III to terminal zone on walls can't be observed clearly. The limited data strongly suggests a correlation of Zone III end velocity and ventilative flow rate, equation 7.6, to define the limit of Zone III. Since the only parameter involved in equation 7.6 is ventilative flow rate, the application is very limited. A more detailed parametric study is recommended to define the limit of Zone III for future research.

The flow characteristics of the terminal zone are not well understood at this point. Figure 7.9 shows different profiles in the terminal zone as a function of ventilative flow rate. As shown, the correlation between maximum jet velocity and distance from the diffuser in the terminal zone increasingly breaks down as the ventilative flow rate decreases. For example, at 10.6 ACH (Figure 7.9-c) other forces, such as buoyantly driven plumes or recirculating flows, clearly dominate the near wall air velocity beyond approximately 3.75 m distance from the diffuser. As demonstrated in the following sections, buoyant forces can influence the flow field for ventilative flow rates as high as 16 ACH. For forced convection, the velocity in the terminal zone is assumed to follow a relation that is similar to the one given in Figure 7.9-a.

$$u = U_0 \cdot (L_{ceiling} + Y)^{-3.6} \tag{7.7}$$

7.3.2 Forced Convection Flow Regime and Correlation

The forced convection flow regime is not quantitatively defined in the literature. The proposed scaling of the Reynolds number, Grashof number, and Nusselt number makes it possible to identify both the natural and the forced convection flow regimes from the OSU experimental data. For laminar flat plate flow, three convection regimes can be identified by plotting $\frac{Gr}{\mathrm{Re}^2}$ on one axis and $\frac{Nu}{\mathrm{Re}^{0.5}}$ on the other as shown in Figure 7.11. If $\frac{Nu}{\mathrm{Re}^{0.5}}$ doesn't change with $\frac{Gr}{\mathrm{Re}^2}$, the flow is in the forced convection regime. If $\frac{Nu}{\mathrm{Re}^{0.5}}$ and $\frac{Gr}{\mathrm{Re}^2}$ have a pure power law relation, the flow is in the natural convection regime. The mixed convection regime, for buoyancy effects either assisting or opposing the momentum flow, is identified by a deviation from the natural convection and forced convection lines as shown in Figure 7.11.

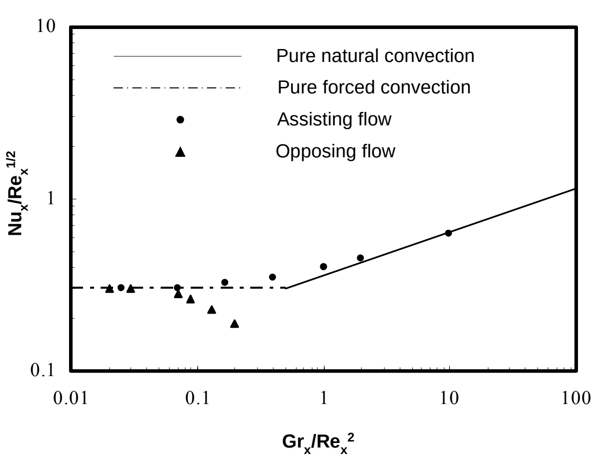

Figure 7.11 Convection Flow Regime for Vertical Flat Plate Airflow (Kakac and Yener, 1995)

The OSU experimental data for ventilative flow rates from 20 ACH to 32 ACH were used to develop a local variable based forced convection correlation for turbulent flow in enclosures. This range is selected to guarantee most of the data are in the forced convection flow regime. Over this range, a single parameter was required to fit the hot wall data as follows:

$$Nu = 0.01 \cdot \mathrm{Re} \qquad (7.8)$$

The Reynolds number range for this correlation is $10000 \le \mathrm{Re} < 88500$. The correlation curve is presented in Figure 7.12-a, Figure 7.12-b with Nusselt number uncertainty intervals, and Figure 7.12-c with Reynolds number uncertainty intervals. The whole surface data matches the correlation as shown in these figures demonstrating that the correlation is applicable to different sizes of surfaces.

Surprisingly, the cold panel data for the same experiments could not be fit to a forced convection correlation as shown in Figure 7.12-d. and Figure 7.12-e. This suggests that the forced convection correlation developed from hot panel data is limited to a cold downward flowing jet attached to a hot wall. As shown in section 7.4, the cold panel data, which corresponds to a warm downward flowing jet attached to a cold wall, requires a mixed convection correlation.

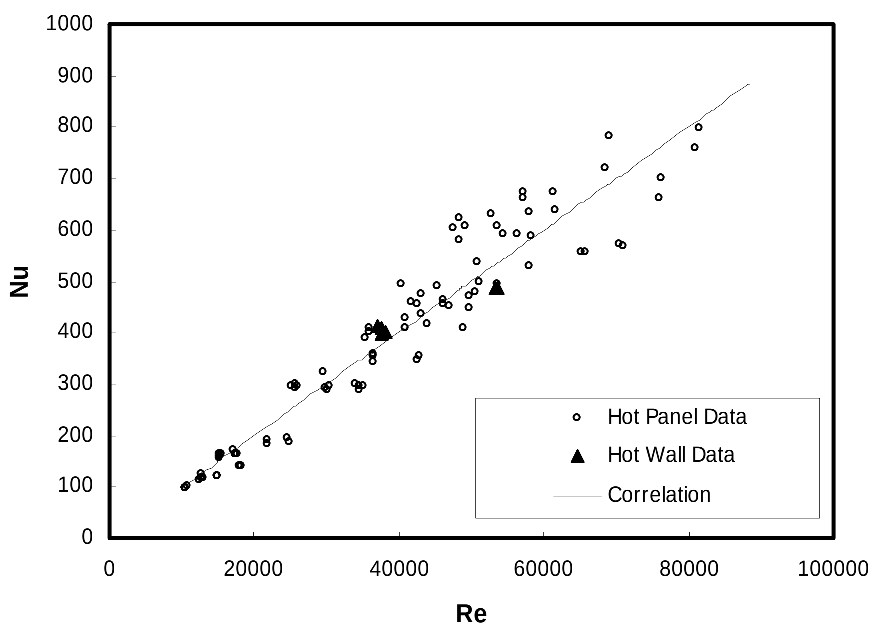

Figure 7.12-a Hot Wall Forced Convection Correlation

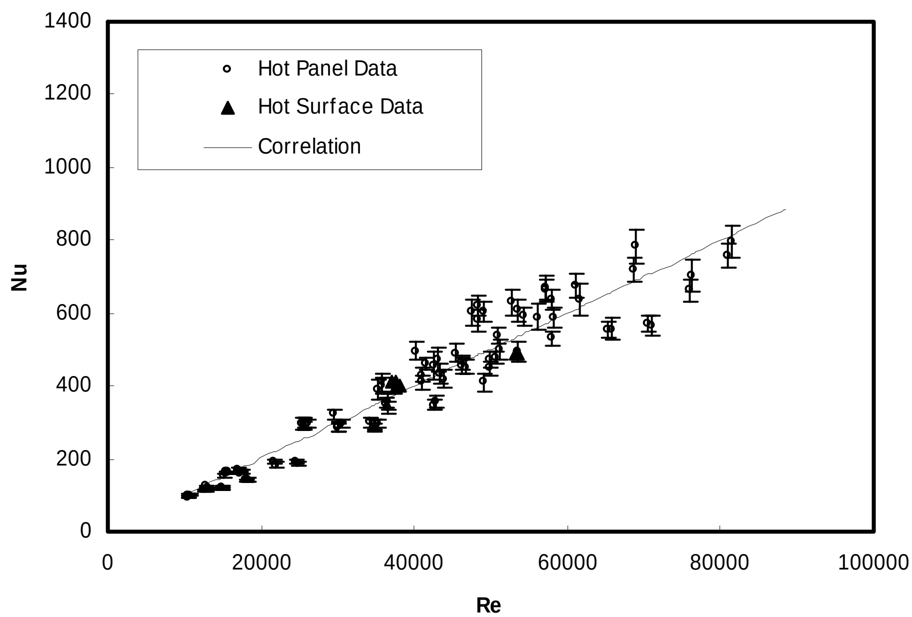

Figure 7.12-b Hot Wall Forced Convection Correlation with Nu Uncertainty Intervals

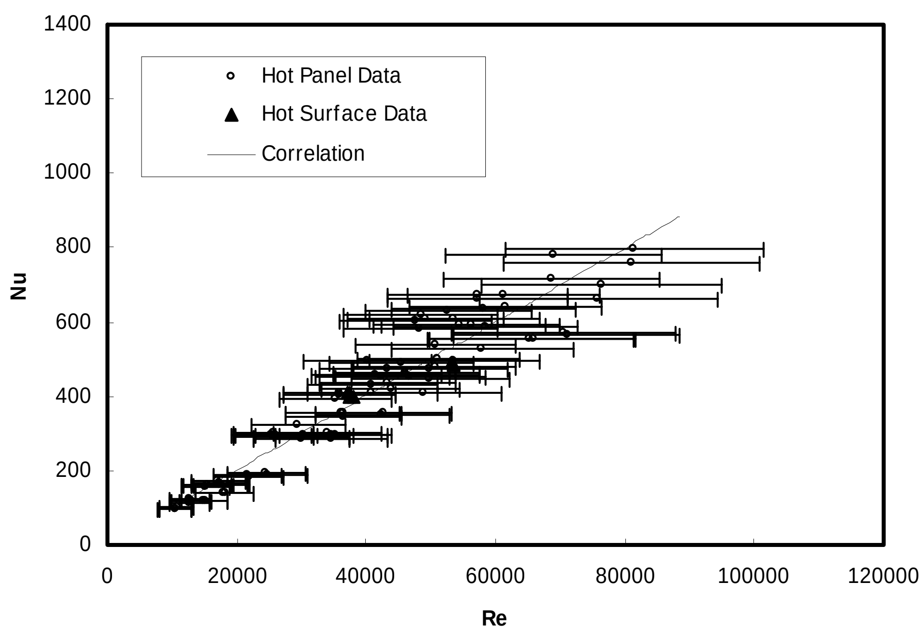

Figure 7.12-c Hot Wall Forced Convection Correlation with Re Uncertainty Intervals

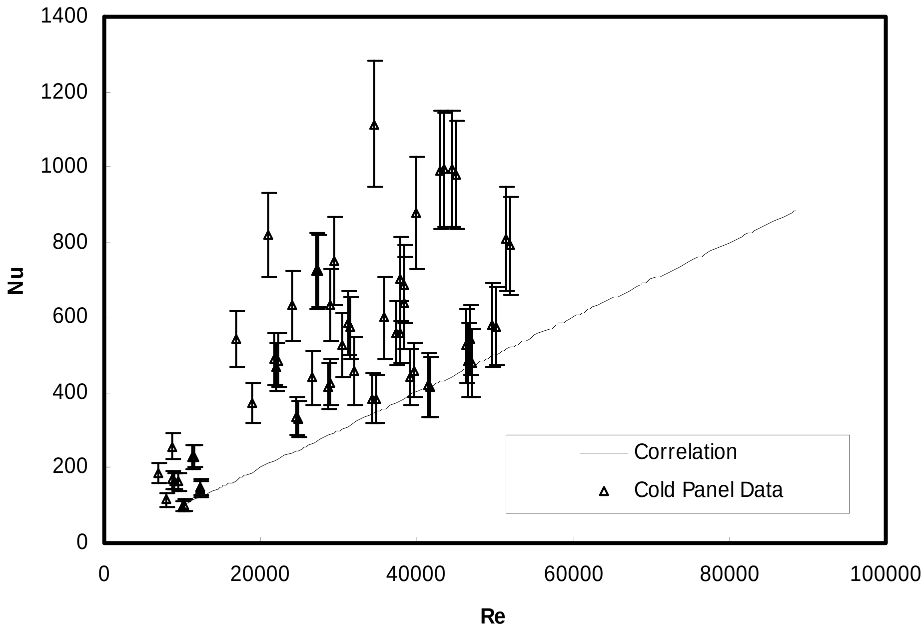

Figure 7.12-d Cold Panel Data with Nu Uncertainty Intervals

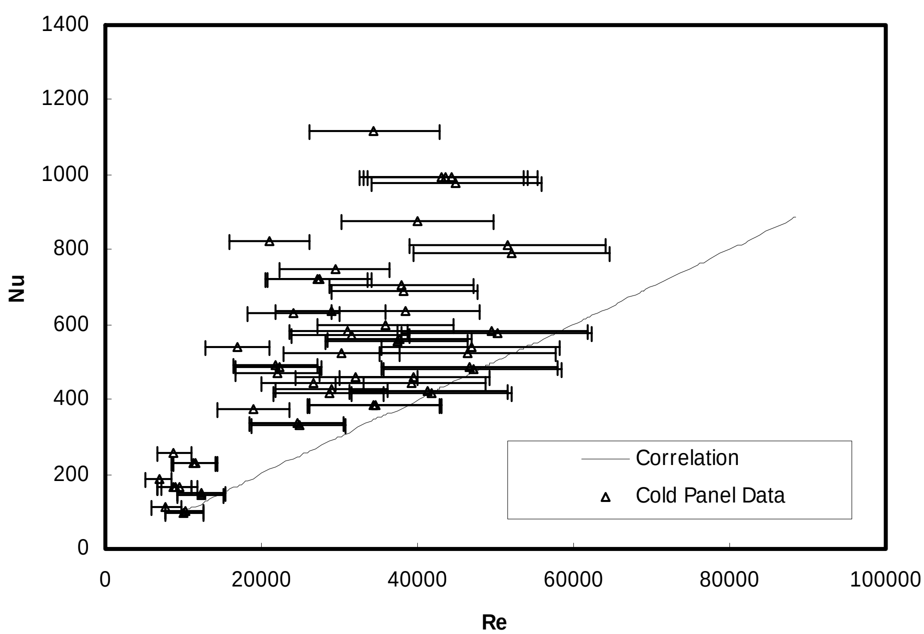

Figure 7.12-e Cold Panel Data with Re Uncertainty Intervals

In order to identify convection flow regimes, the comparison parameter of the buoyancy and momentum forces $\frac{Gr}{\mathrm{Re}^2}$, which is also called the buoyancy parameter, is usually used. If forced convection flow dominates ($\frac{Gr}{\mathrm{Re}^2} << 1$), the Nusselt number would follow the forced convection correlation, and if the natural convection flow dominates ($\frac{Gr}{\mathrm{Re}^2} >> 1$), the Nusselt number would follow the natural convection correlation. Figure 7.13-a gives the relationship between Nusselt number and the buoyancy parameter and shows that the convection flow regimes could not be clearly identified using the Nusselt number and the buoyancy parameter.

The method of Kakac and Yener uses the buoyancy parameter on the x-axis and the forced convection coefficient, $\frac{Nu}{\mathrm{Re}^{0.5}}$, on the y-axis to identify the flow regimes. The hot wall forced convection coefficient of this research is $\frac{Nu}{\mathrm{Re}}$ since the local variable based forced convection correlation has a linear relationship. Accordingly, the two parameters that are used to identify convection flow regimes are $\frac{Gr}{\mathrm{Re}^2}$ and $\frac{Nu}{\mathrm{Re}}$. Processing the experimental panel data in terms of $\frac{Gr}{\mathrm{Re}^2}$ and $\frac{Nu}{\mathrm{Re}}$, the convection flow regimes can be clearly identified as shown in Figure 7.13-b.

Figure 7.13-b presents the panel data for different ventilative flow rates. It shows that when the ventilative flow rate is 3.6 ACH, the wall convection falls entirely in the natural convection flow regime. When the ventilative flow rate is increased to 10.6 ACH, most of the panel data fall in the natural convection flow regime. A few points fall in the mixed convection with opposing flow regime and the rest fall in the forced convection flow regime. Figure 7.13-b clearly demonstrates the three convection flow regimes in terms of the Grashof number and the Reynolds number. Applying the experimental limitations ($2\times10^7 \le Gr \le 6\times10^{10}$, $950 \le \mathrm{Re} \le 88500$), the flow regimes are defined as following:

$0.08 \le \frac{Gr}{\mathrm{Re}^2} \le 1$, pure forced convection flow regime

$1 < \frac{Gr}{\mathrm{Re}^2} < 10$, mixed convection with assisting or opposing flow regime

$10 \le \frac{Gr}{\mathrm{Re}^2} \le 40000$, pure natural convection flow regime (7.9)

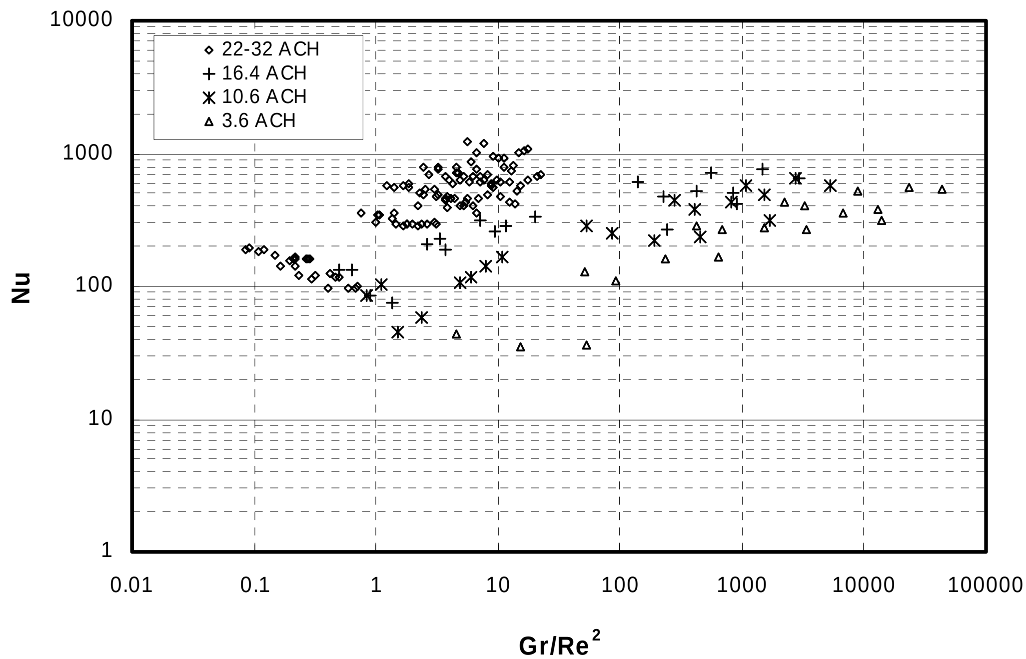

Figure 7.13-a Flow Regime Prediction Using Nusselt Number

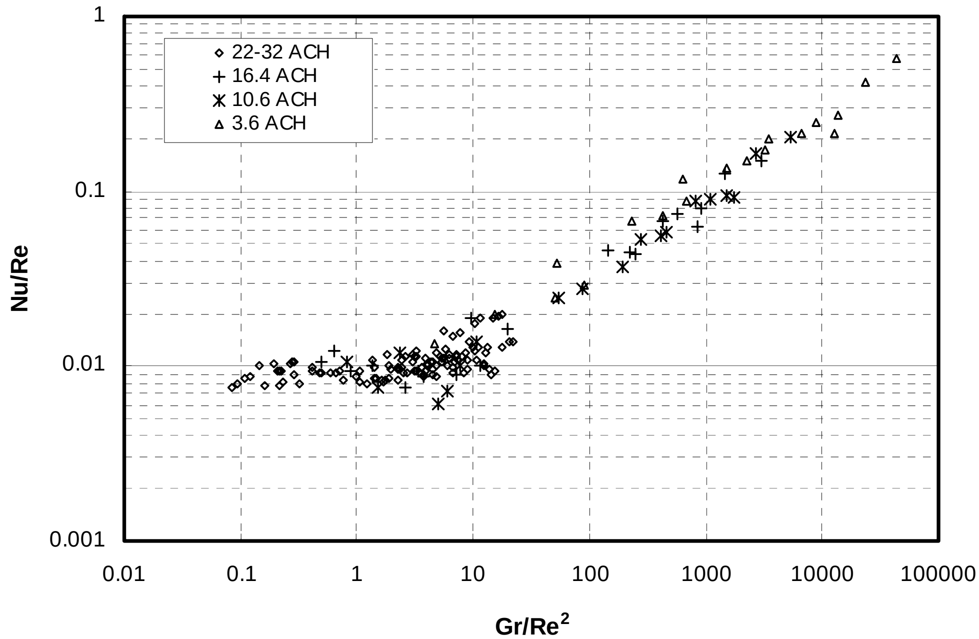

Figure 7.13-b Flow Regime Prediction Using $\frac{Nu}{\mathrm{Re}}$

For a ventilative flow rate of 10.6 ACH, the convection heat transfer on all surfaces is treated as forced convection in building simulation packages like EnergyPlus and the ASHRAE Toolkit. According to the OSU experimental data however, most of the panel data at this ventilative flow rate fall in the natural convection flow regime. The 10.6 ACH data that are identified by the criteria as falling within the natural convection flow regime match well with the natural convection correlation shown in Figure 7.14. Those in the forced convection flow regime match well with the forced convection correlation shown in Figure 7.15. This demonstrates the ability of the criteria to differentiate between convection flow regimes.

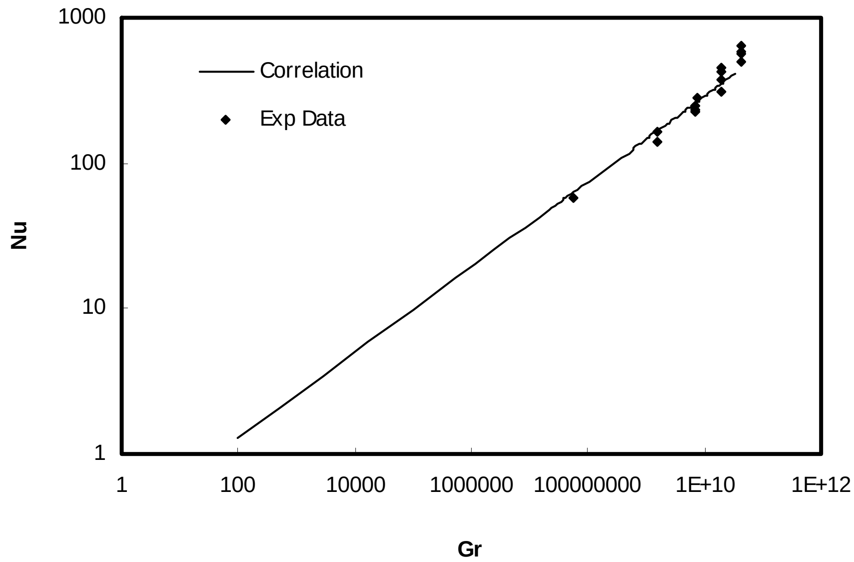

Figure 7.14 Natural Convection Data under Ventilative Flow Rate of 10.6 ACH

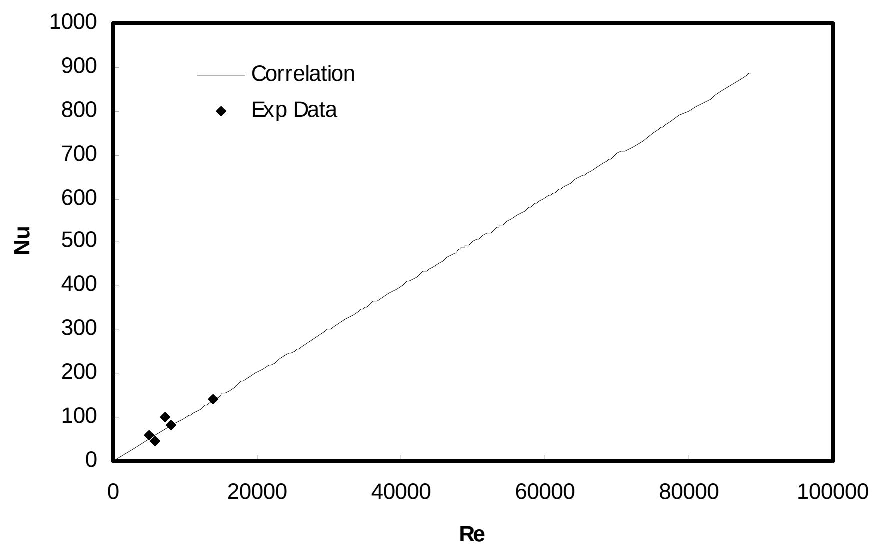

Figure 7.15 Forced Convection Data under Ventilative Flow Rate of 10.6 ACH

The experimental data presented in Figure 7.13-a and Figure 7.13-b are for a hot wall with a cold downward flowing wall jet. Theoretically, the surface convection should be in pure forced, pure natural or mixed convection opposing flow regime, with the mixed convection opposing flow regime showing data below the forced convection curve. However, the data distribution, as presented in Figure 7.16, indicates that the bottom row of panels are in mixed convection with assisting flow regime rather than the mixed convection opposing flow regime. This would indicate that the higher momentum of the downward flowing jet from the opposing cold wall dominates the flow field in the lower region of the hot wall. The upward flowing wall jet on the hot wall results in the mixed convection with assisting flow regime as observed by Fisher (1995).

Figure 7.16 indicates that the mixed convection flow regime can be predicted with reasonable accuracy by the forced convection correlation. The errors in predicting surface convection coefficients by using the forced convection correlation for the mixed convection flow regime is acceptable ($-0.25/+0.22$) compared to the errors for the pure forced convection flow regime ($-0.20/+0.06$). Figure 7.17 shows the errors of the convection coefficient predicted by the forced convection correlation for both the forced and the mixed convection flow regimes. The error distributions show that within the range of the experiments, using a forced convection correlation for both the forced and mixed convection flow regimes doesn't increase the error associated with the convection coefficient. Therefore, at this point, the forced convection correlation can be applied to both forced and mixed convection flow regimes. The room convection correlations and their application ranges become:

$$Nu = 0.01 \cdot \mathrm{Re}\text{, (}0.08 \le \frac{Gr}{\mathrm{Re}^2} < 10\text{, forced and mixed convection flow regime)}$$

$$Nu = 0.34 \cdot Gr^{0.29}\text{, (}10 < \frac{Gr}{\mathrm{Re}^2} \le 40000\text{, natural convection)} \tag{7.10}$$

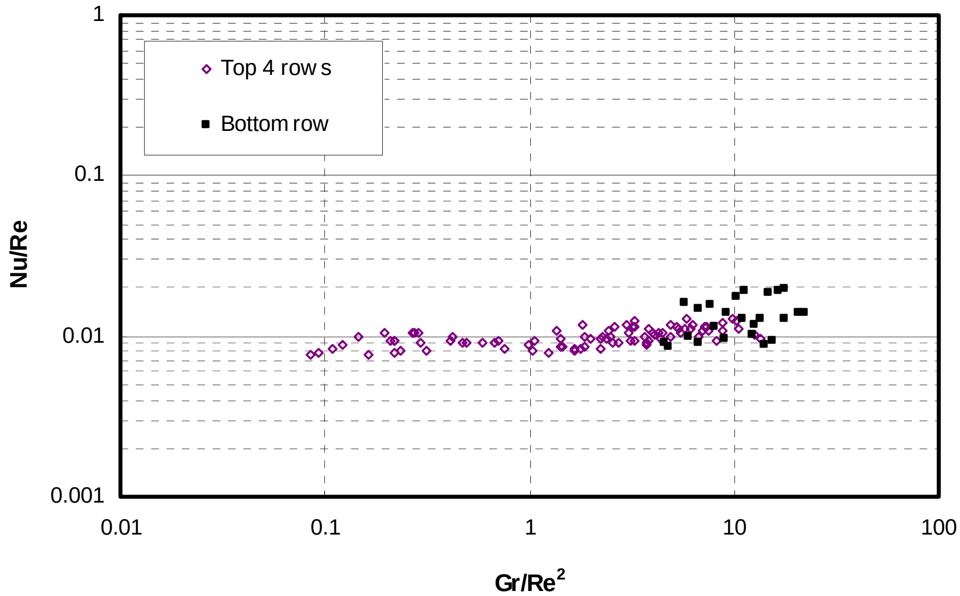

Figure 7.16 Convection Flow Regime on Panels at Different Location

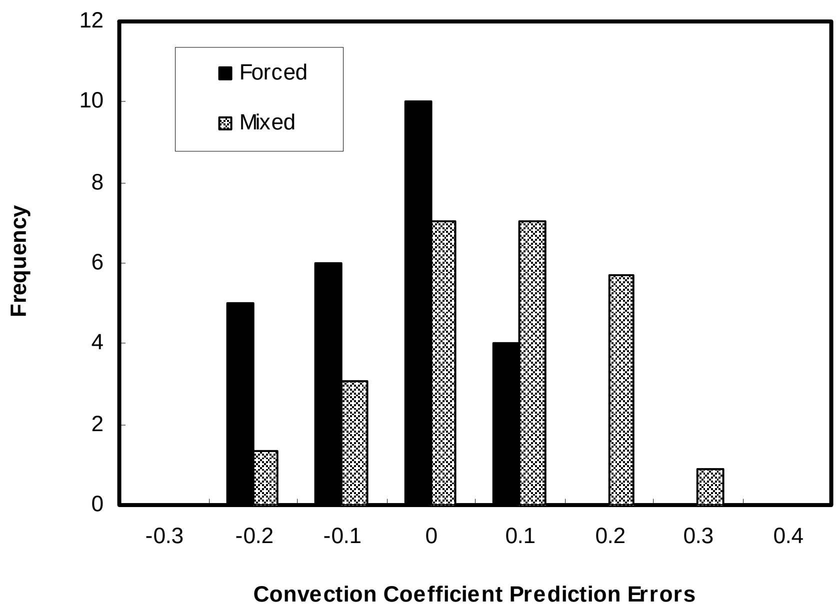

Figure 7.17 Convection Coefficient Error Distribution Using Forced Convection Correlation for both Forced and Mixed Flow Regime

7.3.3 Correlation Validation

The experimental data from the UIUC room have all the required information to validate the local variable based forced convection correlation: surface temperature, near wall air temperature, convection heat flux, and inlet diffuser conditions. Six sets of data with different ventilative flow rate were selected for validation. Appendix B gives the parameters of the data sets. The UIUC data were also obtained under the radial ceiling diffuser room configuration, so the near wall air velocities can be predicted from Equation 7.5.

The convection flow regimes are first identified using the criteria obtained in Section 7.3.2. Figure 7.18-a shows the UIUC experimental data together with the OSU data in the flow regime chart. The UIUC data distributed in all three flow regimes and the distribution is more scattered than the OSU data. The uncertainties of the UIUC data were analyzed and the errors are presented in Figure 7.18-b. The error bars show that all the forced convection data match the correlation, while there are data points in the mixed convection flow regime that don't match the forced convection correlation as the OSU data would. So the forced convection correlation is only applicable to forced convection flow regime for the UIUC data. Figure 7.18-c gives the forced convection data in the flow regime chart. Figure 7.19 shows the UIUC forced convection data with Nusselt number uncertainties, OSU data, and the forced convection correlation. The UIUC data match the correlation but are more scattered. The data that are in mixed convection flow regime are also results of recirculation flow because the mixed convection assisting flow data were obtained while the opposing flow data were expected under the experimental configuration. So the mixed convection correlation couldn't be obtained from the UIUC data either.

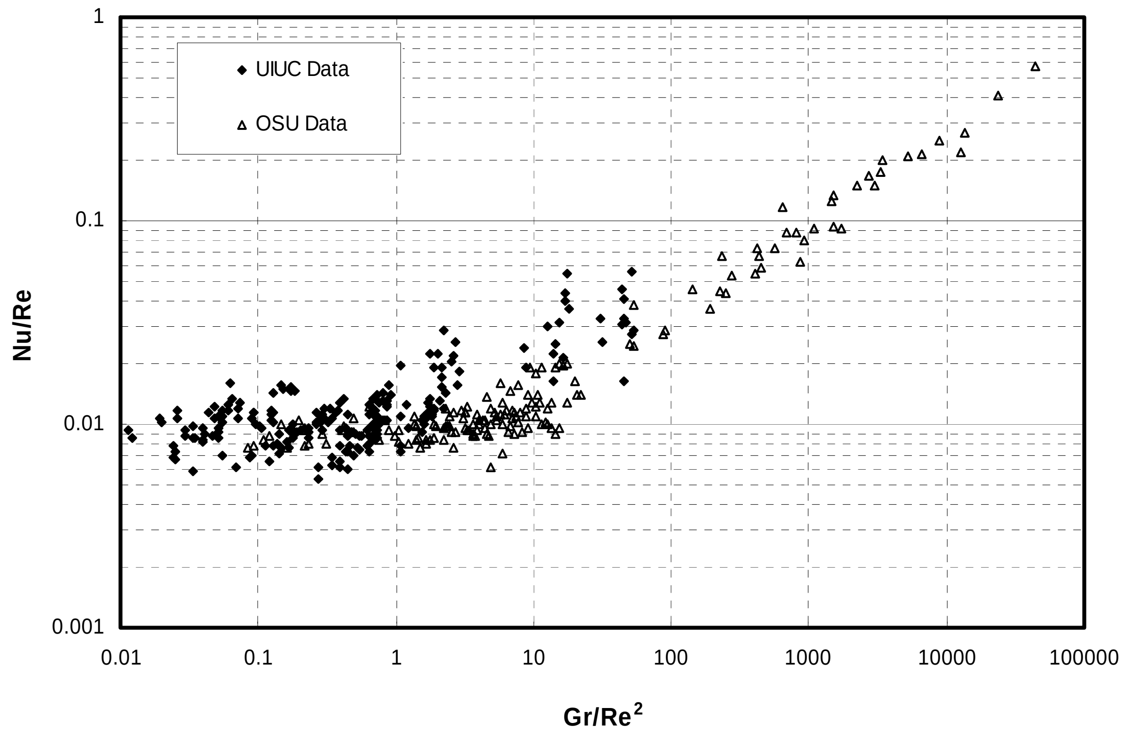

Figure 7.18-a Convection Flow Regimes of UIUC and OSU Data

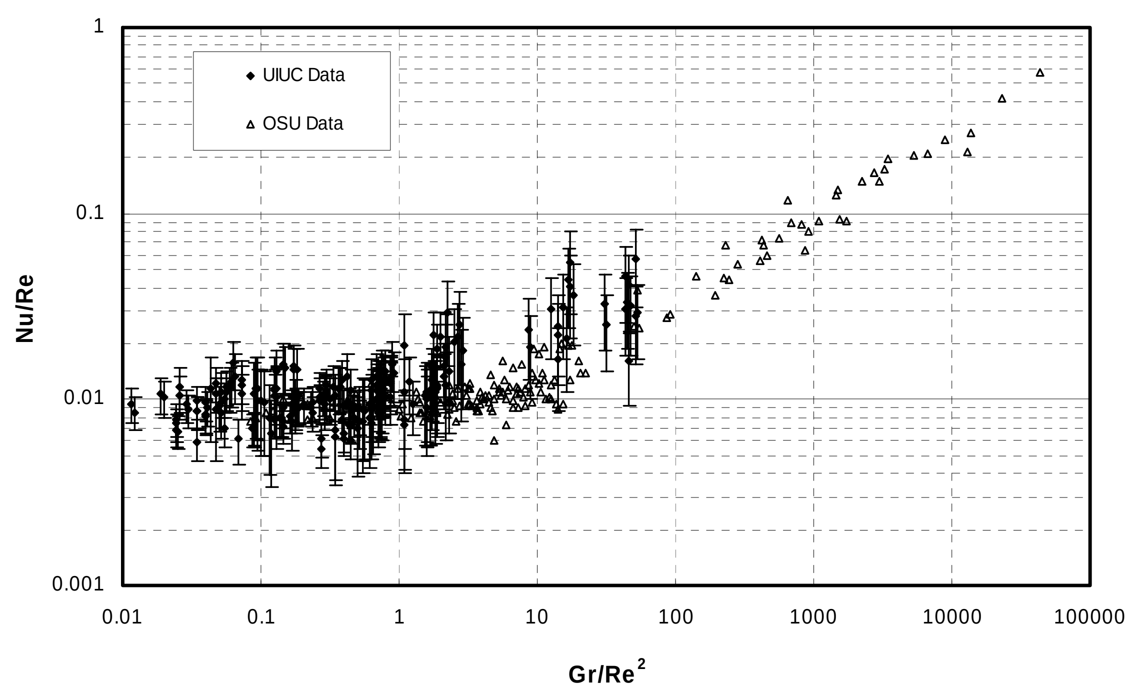

Figure 7.18-b UIUC Data Uncertainties and Convection Flow Regimes

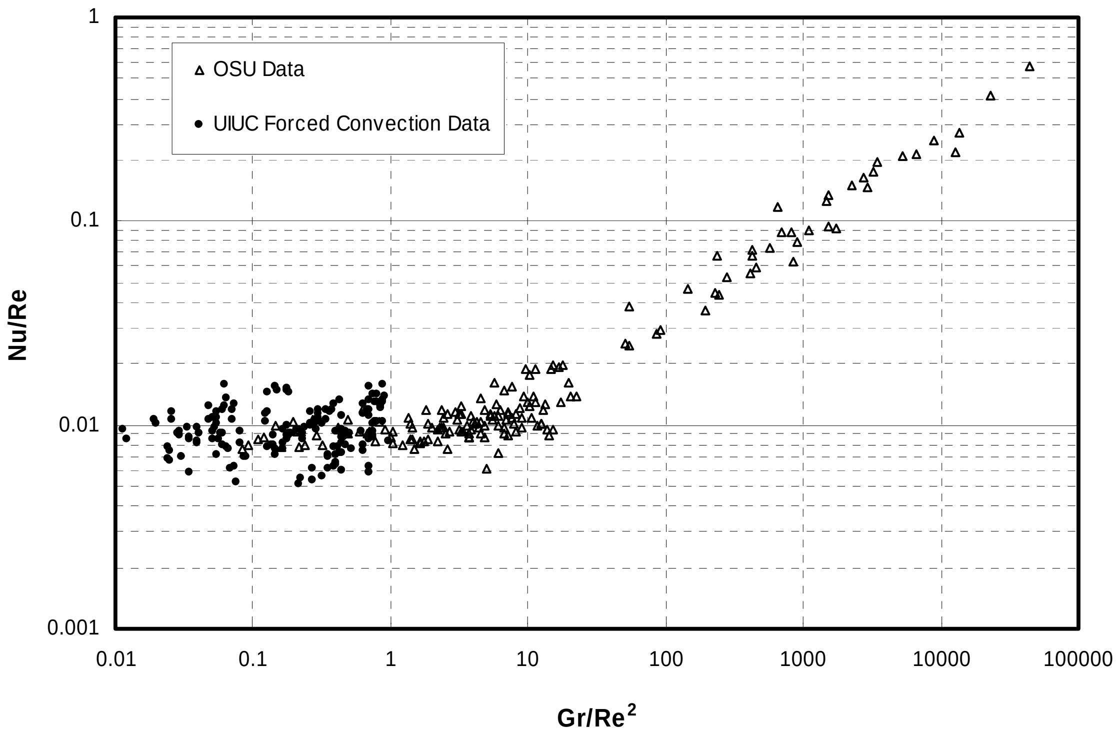

Figure 7.18-c UIUC Forced Convection Flow Regime Data

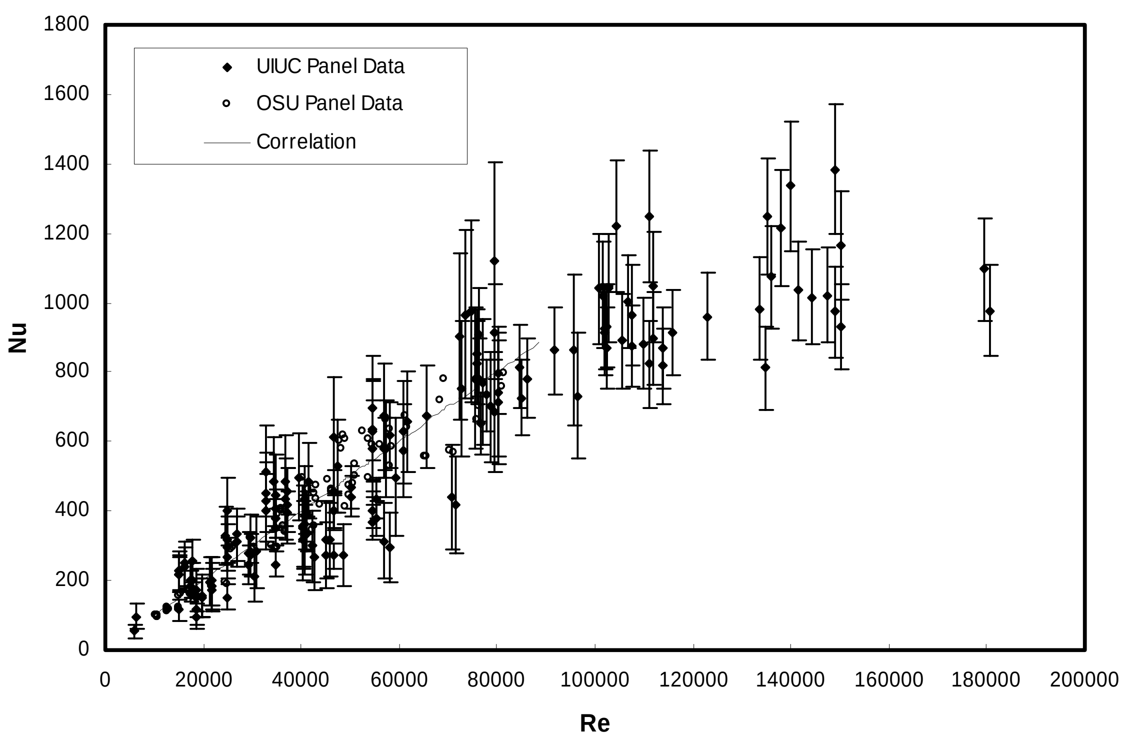

Figure 7.19 UIUC and OSU Data with the Forced Convection Correlation

7.3.4 Correlation Extension

The local variable based forced convection correlation developed from wall panel data is expected to be applicable to ceilings as long as the airflow is characterized as attached wall jet. The local air velocities on the ceiling could be predicted from Equation 7.5 without the corner decay coefficient. The local velocity prediction equation for ceilings becomes:

$$u = 1/2U_0 \cdot 0.3 \cdot (L_{ceiling} + Y)^{-1.12} = \frac{0.15U_0}{(L_{ceiling}+Y)^{1.12}} \tag{7.11}$$

The UIUC experimental data sets include detailed ceiling panel data that could be used for this analysis. There were nine panels of the same size on the ceiling of the UIUC room. To minimize the uncertainty from corner effects and the jet offset, data from the center panel and four corner panels were not included in the analysis. By applying the ceiling velocity prediction equation with the length scale obtained from Chapter 6, local nondimensional numbers were obtained for the other four panels.

Figure 7.20 shows the ceiling data and the convection flow regimes. All of the ceiling data are in the forced convection flow regime and the forced convection flow regime is extended to $0.003 \le \frac{Gr}{\mathrm{Re}^2} < 10$. Figure 7.21 gives the ceiling data and the forced convection correlation. Since most of the ceiling data is beyond the OSU wall data range, the following correlation is proposed based on all of the available data:

$$Nu = 0.09 \cdot \mathrm{Re}^{0.8} \tag{7.12}$$

As shown in the figure, at high ventilative flow rates, both the wall and ceiling data deviate from the proposed correlation. This is likely due to the fact that the local Reynolds number is based only on the characteristics of the jet and does not include a contribution from recirculating flow in the room. As the ventilative flow rate increases, recirculating flow structures are expected to have a significant effect on the convective heat transfer rate. This effect is not captured in the correlation. Although in this respect the correlation is preliminary, it is significant that a single correlation based only on the characteristics of the offset jet captures the major features of room convection for both ceilings and walls over a wide range of ventilative flow rates ($6 \times 10^3 \le \mathrm{Re} \le 4 \times 10^5$).

Additional research is required to establish and quantify the contribution of recirculating flow. In addition, the following factors also introduce uncertainty in the application of the UIUC data:

1. Jet detachment occurs on every UIUC ceiling panel (except the center panel) since every panel has at least one edge adjacent to a wall. Further investigation is required to correct for this effect.
2. The virtual origin of the attached wall jet on the ceiling is assumed to be at the diffuser center. This could lead to significant errors over the range of ventilative flow rates (3ACH to 100ACH) included in the data.
3. The ceiling panel size is relatively large and the attached wall jet does not develop linearly. So evaluation of the local velocity at the panel center could lead to significant errors.

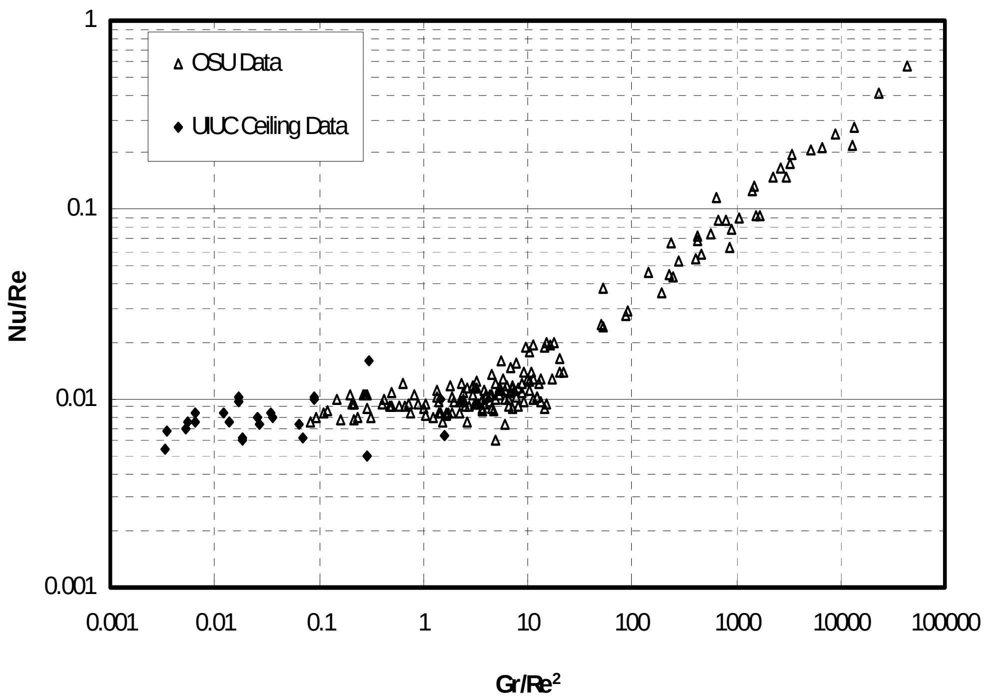

Figure 7.20 Convection Flow Regimes of UIUC Ceiling Data and OSU Wall Data

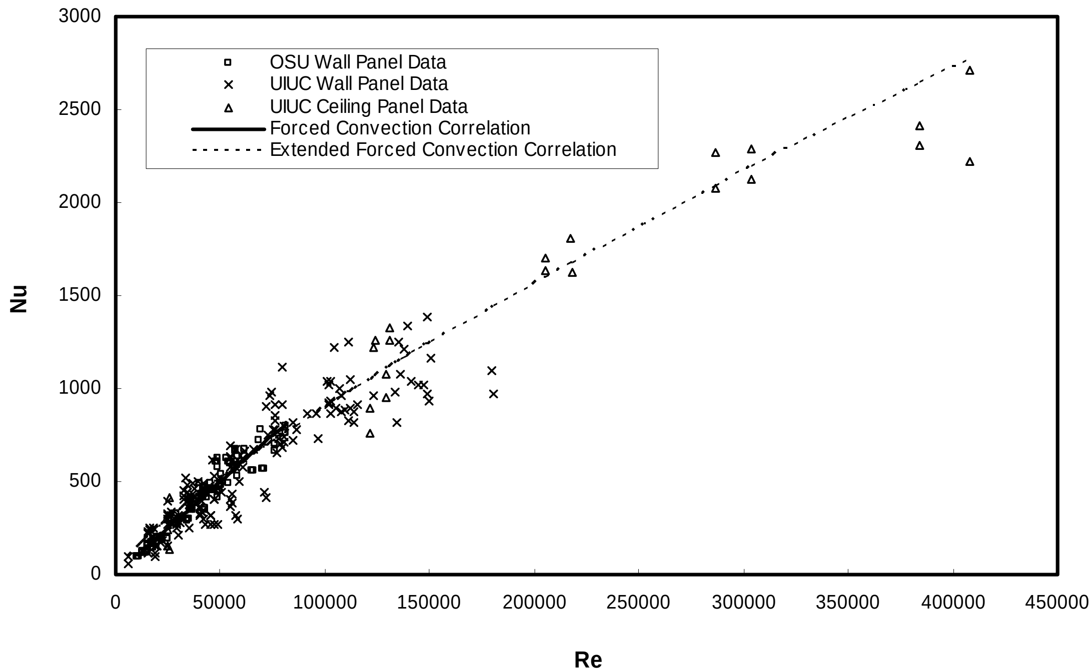

Figure 7.21 All Available Panel Data with Forced Convection Correlation and Its Extension

7.4 Mixed Convection Correlation

The cold panel data shown in section 7.3.2 does not fit the forced convection correlation developed from the hot panel data. Most of the measured nondimensional convection coefficients – Nusselt numbers are greater than those predicted by the forced convection correlation. This data distribution suggests that the buoyancy driven flow assisted the momentum driven flow on the cold panel, which is also reflected in the flow regime chart as shown in Figure 7.22. Therefore, a mixed convection correlation for the buoyancy assisted flow regime was developed based on cold panel data as given in Equation 7.13. The mixed convection correlation for the assisted flow regime is blended from the natural and generalized forced convection correlation, as shown in Equation 7.14.

$$Nu = 0.09 \cdot \mathrm{Re}^{0.8} + 0.34 \cdot Gr^{0.29} \qquad (7.13)$$

$$Nu = Nu_{forced} + Nu_{natural} \qquad (7.14)$$

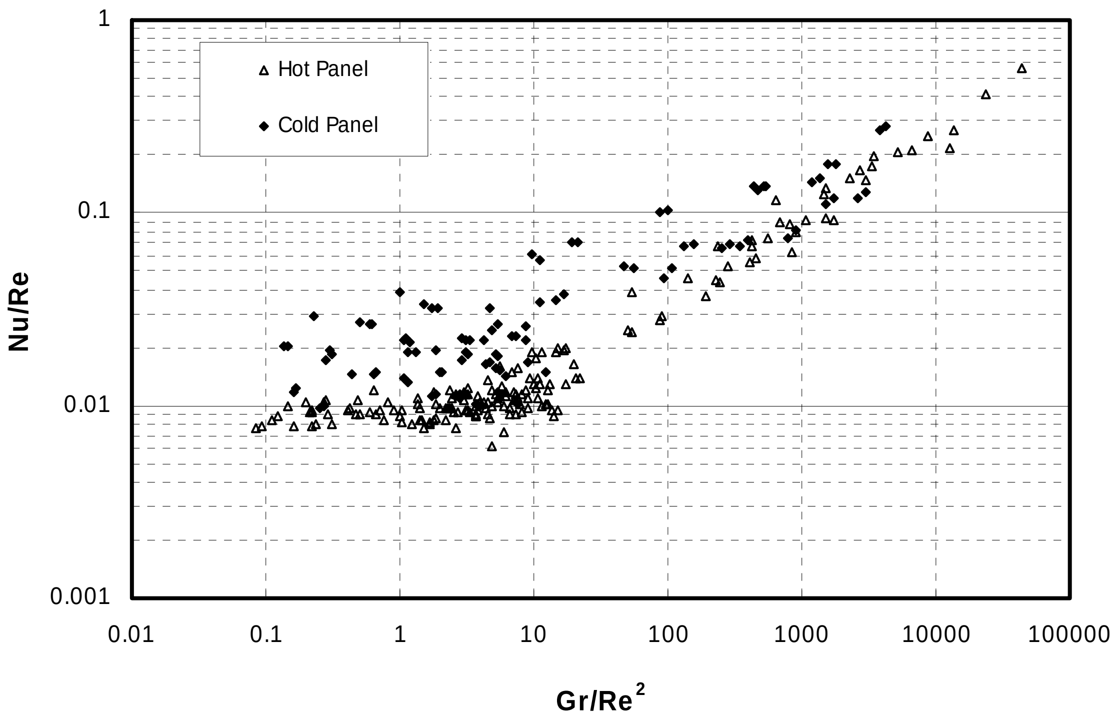

Figure 7.22 Analyzing Convection Flow Regimes for Cold Panel Data

Figure 7.23-a and Figure 7.23-b show the cold wall data and uncertainties in the flow regime chart with the mixed convection correlation, forced convection correlation, and natural convection data. The mixed convection correlation upper and lower limits are the natural and the forced convection correlations. Figure 7.24 shows that the mixed convection correlation merges to the natural convection correlation when buoyancy force dominates and with additional data it appears that it could be extended and merged to the forced convection correlation when the buoyancy effect could be neglected.

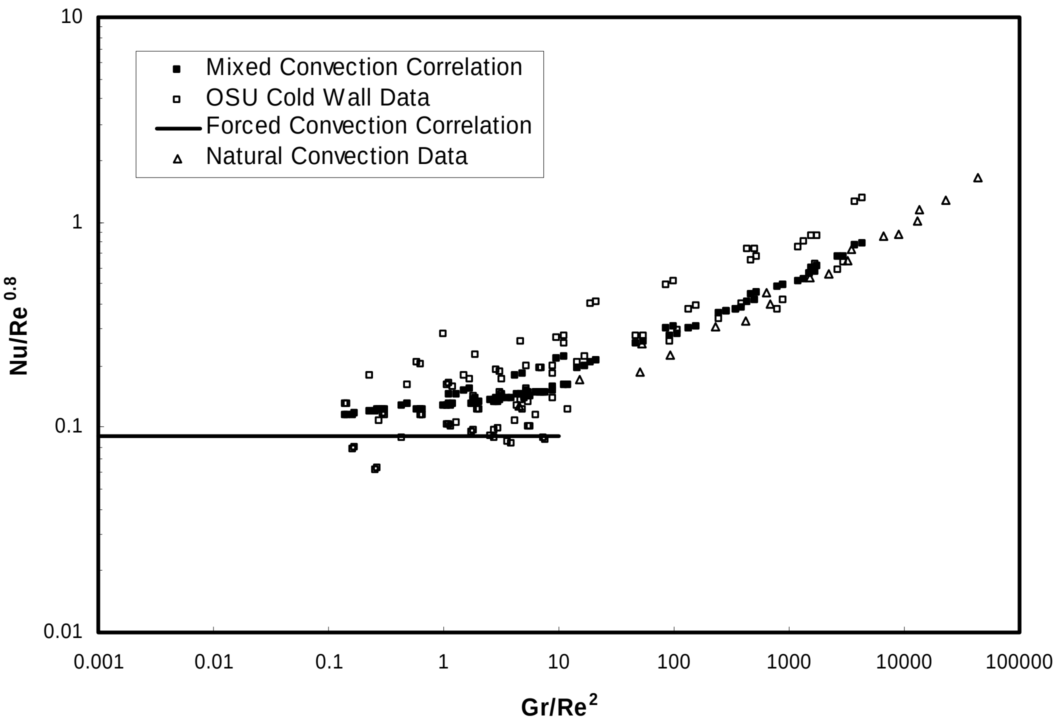

Figure 7.23-a Mixed Convection Correlation for Buoyancy Assisting Flows

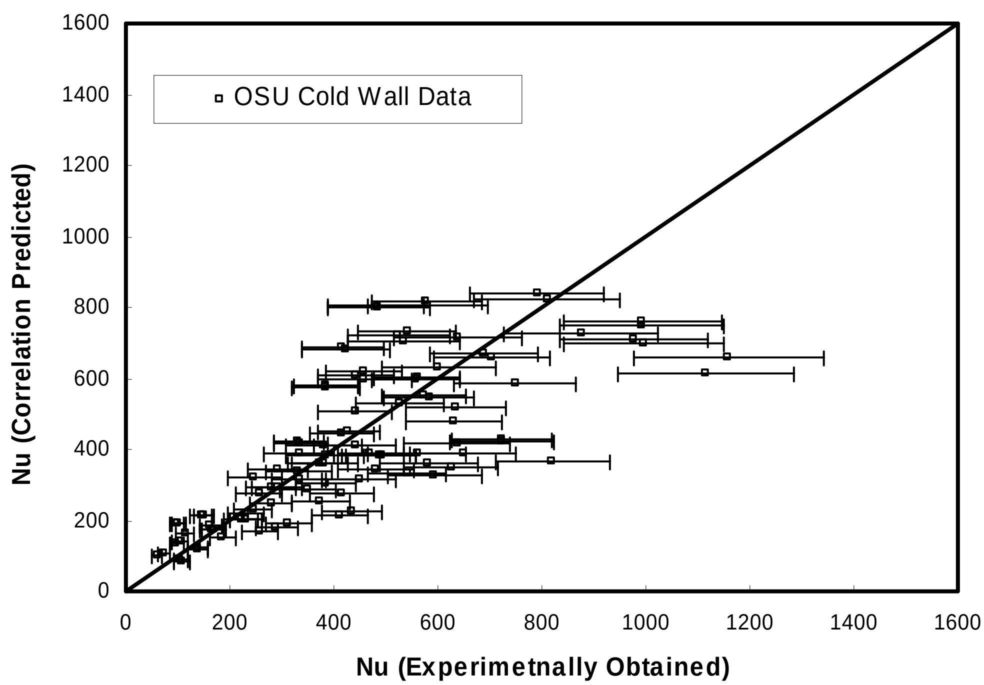

Figure 7.23-b Cold Wall Data Uncertainties

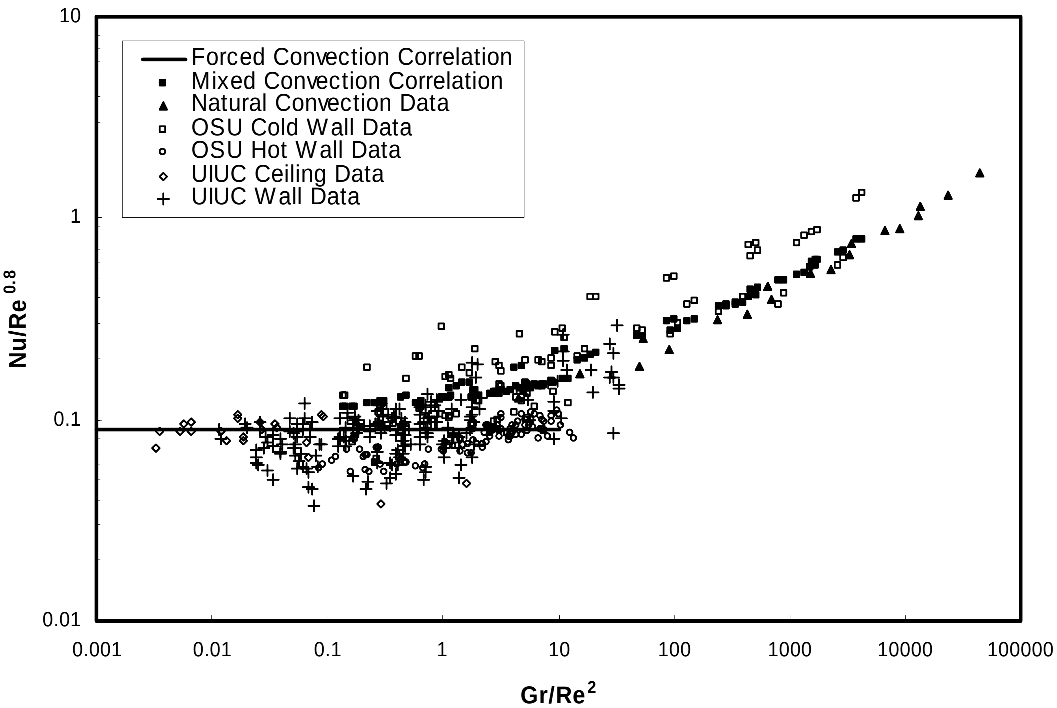

Figure 7.24 All Data and Correlations

7.5 Summary

A detailed scale analysis resulted in the following significant findings:

- Developed local air velocity prediction correlations for the attached wall jet under the radial ceiling diffuser room configuration. The correlations and application conditions are summarized in Table 7.3.
- Obtained local air parameters for local convection models as given in Table 7.3.
- Developed natural convection correlation, which is applicable to natural convection flow regime.

$Nu = 0.34 \cdot Gr^{0.29}$, ($10 \le \dfrac{Gr}{\mathrm{Re}^2} \le 40000$, natural convection flow regime)

- Developed forced convection correlation, which is applicable to both forced and mixed convection flow regimes for hot walls with a cold, downward flowing wall jet:

$Nu = 0.01 \cdot \mathrm{Re}$, ($0.08 \le \dfrac{Gr}{\mathrm{Re}^2} < 10$, forced and mixed convection flow regimes)

- A general forced convection correlation based on UIUC and OSU data is proposed: $Nu = 0.09 \cdot \mathrm{Re}^{0.8}$ ($0.003 \le \frac{Gr}{\mathrm{Re}^2} < 10$, forced and mixed convection flow regimes for hot walls with a cold, downward flowing wall jet:).
- A mixed convection correlation for assisted flow regime is developed based on OSU cold wall data. This correlation is applicable to cold walls with a warm downward flowing wall jet.

  $Nu = 0.09 \cdot \mathrm{Re}^{0.8} + 0.34 \cdot Gr^{0.29}$, ($0.1 \le \frac{Gr}{\mathrm{Re}^2} < 100$, forced and mixed convection flow regimes)

Table 7.3 Scales for Local Variable Based Convection Model for Attached Wall Jet

Parameters	Scales	Application Conditions
Velocity	$\frac{0.12U_0}{(L_{ceiling}+Y)^{1.12}}$	wall, forced, Before jet decay, i.e., $U_e \ge 0.17 \cdot VFR^{0.5}$
	$\frac{U_0}{(L_{ceiling}+Y)^{3.6}}$	wall, forced, after jet decay, i.e. , $U_e < 0.17 \cdot VFR^{0.5}$
Length	A/p	ceiling, natural
	X	ceiling forced
	Y	wall forced
Temperature	T at 128mm from surface	walls, ceilings and floors, forced
	T at 100mm from surface	walls, ceilings and floors, natural

Table 7.4 summarizes the developed and extended local convection correlations and application ranges.

Table 7.4 Local Variable Based Convection Correlations for Attached Wall Jet

Correlations	Flow Regimes	Application Ranges	Uncertainties	Applied Surfaces
$Nu = 0.34 \cdot Gr^{0.29}$	$10 \le \frac{Gr}{\mathrm{Re}^2} \le 40000$	$10^3 \le Gr \le 10^{11}$	$e'_{Gr} = \pm 16\%$	Walls
$Nu = 0.01 \cdot \mathrm{Re}$	$0.08 \le \frac{Gr}{\mathrm{Re}^2} < 10$	$10^4 \le \mathrm{Re} \le 9 \times 10^5$	$e'_{\mathrm{Re}} = \pm 25\%$	Hot walls
$Nu = 0.09 \cdot \mathrm{Re}^{0.8}$	$0.003 \le \frac{Gr}{\mathrm{Re}^2} < 10$	$6 \times 10^3 \le \mathrm{Re} \le 4 \times 10^5$	$e'_{\mathrm{Re}} = \pm 25\%$	Hot walls Ceilings
$Nu = 0.09 \cdot \mathrm{Re}^{0.8} + 0.34 \cdot Gr^{0.29}$	$0.1 \le \frac{Gr}{\mathrm{Re}^2} < 100$	$2 \times 10^3 \le \mathrm{Re} \le 5 \times 10^4$ $2 \times 10^7 \le Gr \le 3 \times 10^{10}$	$e'_{\mathrm{Re}} = \pm 25\%$ $e'_{Gr} = \pm 16\%$	Cold walls

The analysis of the UIUC data leads to possible future work:

- The local variable based mixed convection correlation needs to be developed under carefully designed experimental conditions that have no recirculation effect.
- The offset jet on the ceiling needs to be characterized in terms of the offset jet length and the virtual origin.
- The ceiling data needs to be obtained on a smaller grid in order to validate the application of the local variable based convection correlation on ceilings.

Chapter 8: Applications

Chapter 7 defined room convection flow regimes and developed local variable based convection correlations for each flow regime. This chapter focuses on applying the new local convection model to building simulation programs and analyzing the differences of simulation results using the local convection model and other available convection models. The ASHRAE air toolkit was selected for model implementation due to the availability of non-mixing air models in the toolkit. Available convection models include the Fisher model, the ASHRAE model, and the Tarp model.

8.1 Implementation of convection model in building simulation programs

The local convection model was implemented as an individual subroutine in the toolkit's "InteriorConvectionMod" module. The specific convection model used in the simulation is specified by the inside heat balance, the air heat balance, and the system load calculation subroutines of the heat balance calculation module. The new parameters required by the local convection model, such as jet discharge location and outlet effective area, were included in the input file (in.idf) and input definition file (ToolkitTest.idd) and read by a subroutine in the "InteriorConvectionMod" module. Local surface coordinates were added to the input object "Surface" to calculate the local length scale.

8.2 Verification of local convection model

The first set of simulations was to verify the calculation accuracy and the application range of the local convection model by comparing the calculated building system load to the experimentally measured load. The experimental room was simulated under six different experimental setups. Each setup was first simulated with the experimentally measured convection coefficients. The measured convection coefficients are available for individual hot wall panels, so each heated panel is specified as a surface and assigned a convection coefficient in the simulation input file. The convection coefficient values are assigned in the

“Surface Settings” objects. To use these convection coefficients in the simulation, the convection coefficient type is selected as “prescribed hc” in the “select air model’ object. In the simulation program, the convection model specified in the inside heat balance, air heat balance, and system load calculation subroutines is “ReturnPrescribedHcIn”.

Since the experimental room surfaces have different temperature settings while the outdoor condition is the same for all surfaces, the surfaces were constructed with different thermal resistances. The hot wall was constructed of thin metal, with almost no thermal resistance. Adiabatic walls were constructed with high thermal resistances and are assigned with very low inside surface convection coefficients so that there is negligible heat transfer through the adiabatic walls. The predicted hot wall inside surface temperature and the reference temperatures should match the experimentally measured near wall air temperatures.

The only air model that will correctly simulate the radial ceiling diffuser room configuration is the momentum zonal model. However, the momentum zonal air model can’t simulate the airflow discharged from the radial ceiling diffuser horizontally. Therefore half of the experimental room is simulated with a side wall inlet opening. The coordinate system is defined so as to meet the requirement that the inlet velocity should be positive.

Six experimental cases are simulated, “0708041”, “0716041”, “0717041”, “0919041”, “1008041”, and “1020041”. Appendix B gives the experimental parameters for all the experimental cases. All the input files with experimentally measured convection coefficients were tuned to match the experimental conditions. The boundary conditions from the experimental data include: ventilative flow rate, inlet temperature, surface convection coefficients, and diffuser effective area. The tuned parameters include: room set point temperature, outside temperature, and wall insulation structure. The parameters that are examined to match the experimental conditions are: hot wall inside surface temperatures, near wall air temperatures, and convective heat fluxes. For this investigation, which is primarily concerned with the sensitivity of the building system load calculation to different convection models, the only significant parameter predicted by the air models is the reference temperature. Figure 8.1-a shows both the experimentally measured and simulated near wall air temperatures for a typical experimental case.

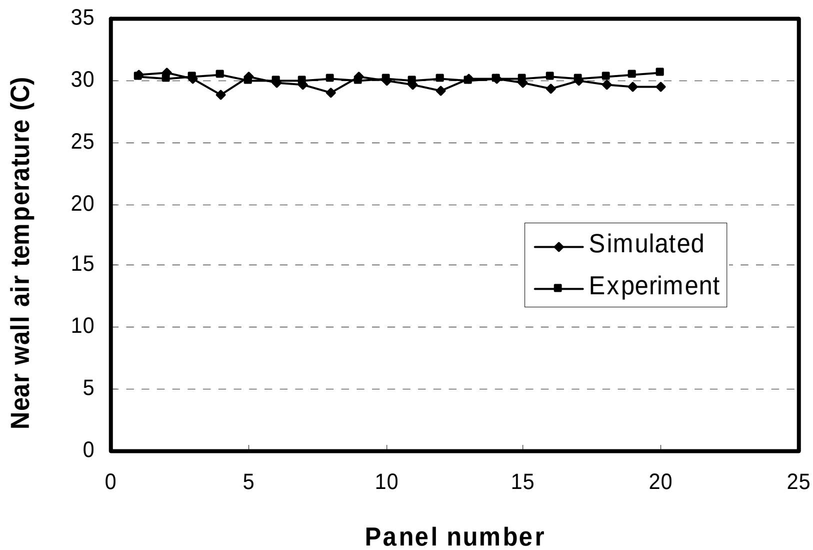

Figure 8.1-a Measured and Simulated Reference Temperatures near the Hot Panels (Case 0717041)

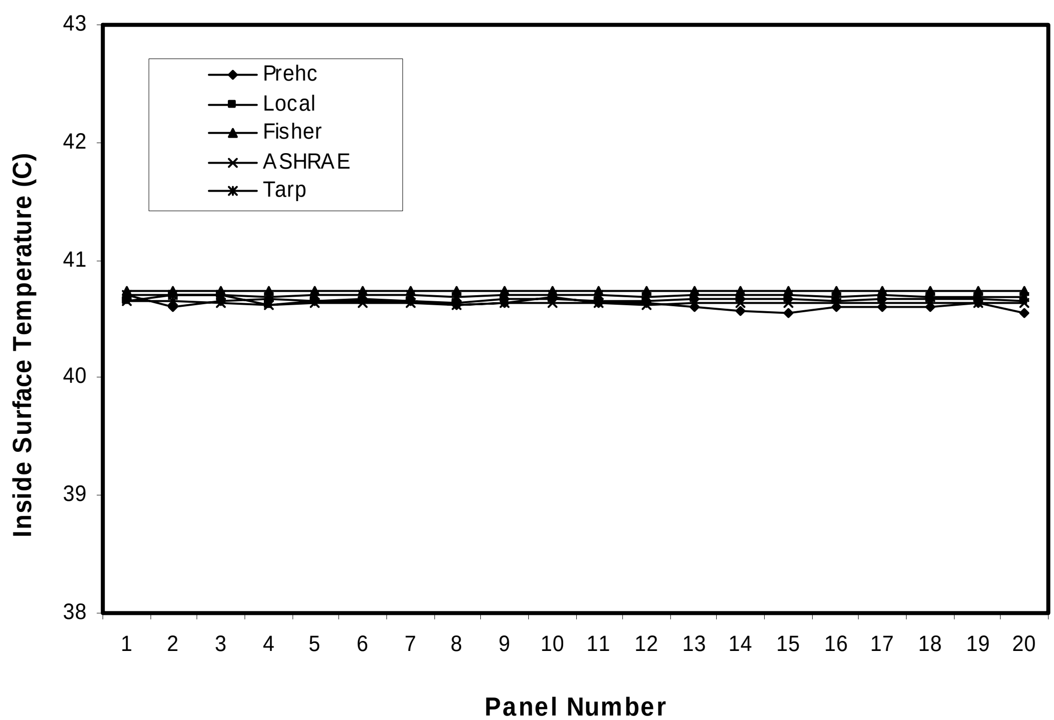

Figure 8.1-b Inside Surface Temperature (Case 0717041)

After tuning a "prescribed hc" simulation input file for each of the six experimental cases, simulations using the convection models (e.g. the local convection model, the Fisher model, the ASHRAE model, and the Tarp model) were performed for each case. The global variable based convection models (i.e. the Fisher model, ASHRAE model, and Tarp model) assume a uniform convection coefficient on the surface and are applied to individual panels. In order to make the simulation results comparable, the predicted panel surface temperatures should be the same for all convection models. Figure 8.1-b shows very good match among the inside surface temperatures from the simulation results with the "prescribed hc" and four convection models.

Figure 8.2 shows the simulation results using different convection models. The ventilative flow rates of the six experimental cases range from 0 to 32.46 ACH, and the room loads range from 350 to 2200 W. The local convection model is the only one that matches the experimental data for the entire range. The average error of the local convection model is 8.7%, which is much smaller than the average error of the ASHRAE model (29.0%), the Fisher model (51.1%), and the Tarp model (45.9%). Table 8.1 summarizes the cooling load prediction errors of each model for each experimental case.

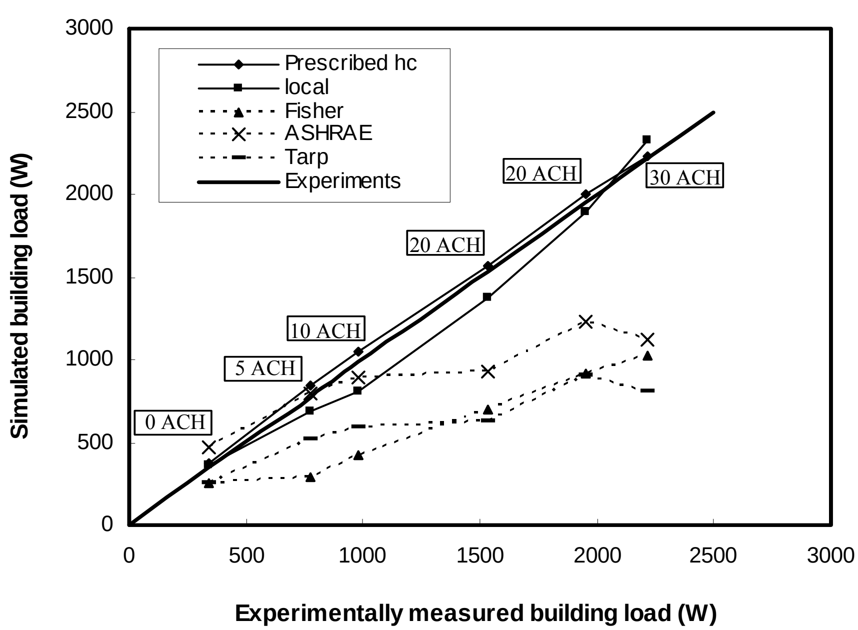

Figure 8.2 Experimentally Measured and Simulated Building Load (OSU room)

Table 8.1 Cooling Load Prediction Errors of Each Model

Exp. Case	Local	Fisher	ASHRAE	Tarp
1020041	0.043	0.257	0.356	0.257
717041	0.113	0.634	0.028	0.337
708041	0.182	0.571	0.098	0.399
916041	0.104	0.544	0.392	0.589
919041	0.029	0.528	0.370	0.537
1008041	0.049	0.535	0.493	0.638
Averaged	0.087	0.511	0.290	0.459

Three significant differences make the local convection model more accurate in load calculations:

- The local convection model has a more detailed flow regime definition. The ASHRAE model and Tarp model don't differentiate between flow regimes; they both assume that one correlation works for all. The Fisher model defines the flow regime according to the ventilative flow rate. If the ventilative flow rate is 3ACH or greater, the forced convection correlation is applied, and if the ventilative flow rate is smaller than 3ACH, the natural convection correlation (Tarp model) is applied. The local convection model compares the momentum and buoyancy forces near the surface and defines the convection flow regime by the balance of these two forces. The parameter that is used to define flow regime is $\frac{Gr}{\mathrm{Re}^2}$. Equation 7.9 gives the flow regime definition.

- The local convection model is nondimensional and could be applied to other room dimensions. This is validated through a set of simulations based on the UIUC experimental data. The UIUC experimental room is simulated following the same procedure as the OSU experimental room simulation. Six experimental cases are simulated "112933", "624921", "1015892", "1016891", "428895", and "505891". The experimental settings are given in Appendix B. The simulated surface temperatures, near wall air temperatures, and surface convection heat fluxes are tuned to match the experimental data. Figure 8.3 presents the simulation results. It shows that the local convection model works well for the UIUC room. The Fisher model also works well for the UIUC room while the ASHRAE and Tarp models are not good, especially when the ventilative flow rate is high.

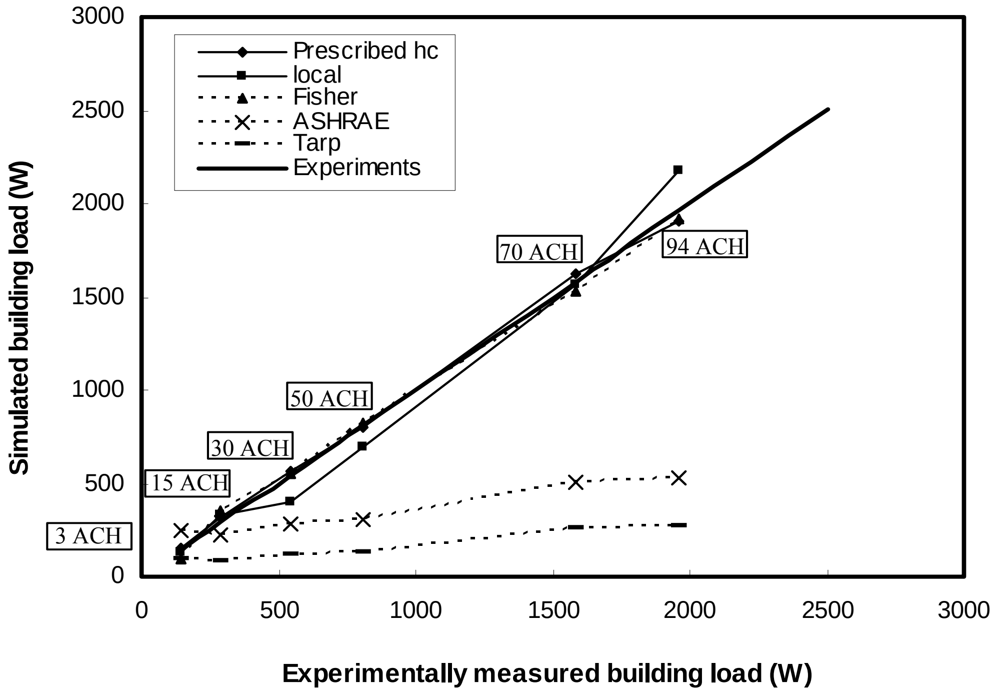

Figure 8.3 Experimentally Measured and Simulated Building Load (UIUC room)

- The local convection model is applicable to both uniform and non-uniform room surface temperature configurations. The local convection model was developed from panel data, i.e., panel surface temperatures, convection heat flux, and local air temperatures and velocities. All of the parameters, except the air velocities, are independent. It can therefore be applied to all room configurations that have the same airflow characteristics. The Fisher model correlated the convection heat transfer coefficient to a single parameter, ACH. It has limited applicable room configurations. The ASHRAE and Tarp models are applicable to whole surfaces and require uniform temperatures on the entire surface.

The local convection model works for the whole convection flow regime with satisfactory errors. However, it doesn't have a specific correlation for the mixed convection flow regime, which leads to higher errors when mixed convection occurs on a large portion of the surface. Figure 8.2 shows that the systematic error is the highest, 18%, at 10ACH where mixed convection is more likely to occur. For the UIUC experimental data, mixed convection occurs more in the 3ACH to 15 ACH range.

The Fisher model works well for the UIUC experimental data but significantly under predicts the OSU data. Two factors contribute to the error. One is that the ceiling diffuser in the OSU room is slightly off centered. When the ACH is corrected to account for diffuser placement, the Fisher model predictions improve slightly as shown in Figure 8.4. The other factor, which has a more significant effect, is that the UIUC room has a heated ceiling while the OSU room has a passive ceiling. The Fisher model - a global variable based convection model with an inlet air reference temperature cannot differentiate between different surface temperature configurations. As a result it significantly under predicts wall heat transfer in the OSU room.

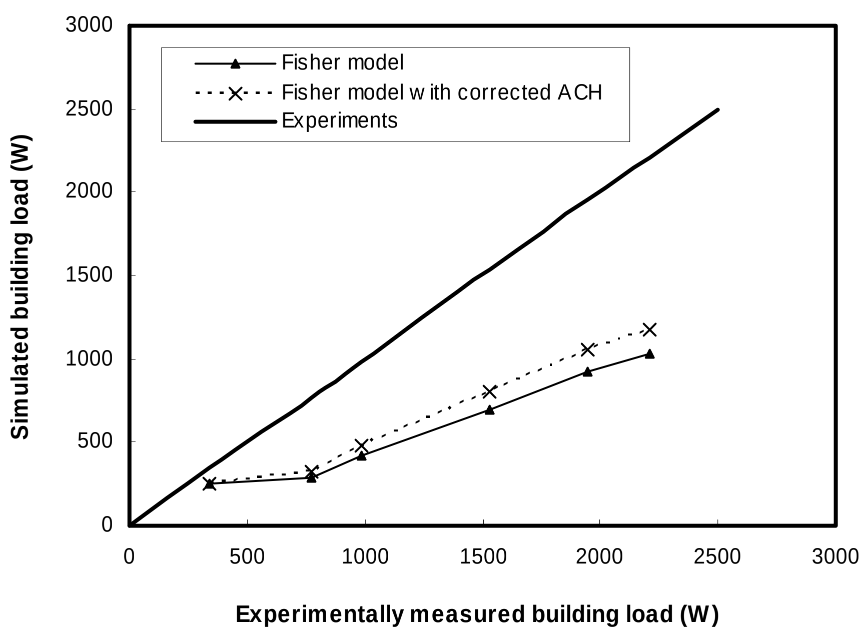

Figure 8.4 Simulated Building Cooling Load Using Fisher Model with Corrected ACH (OSU room)

The ASHRAE model has three constants for upward facing surfaces, vertical surfaces, and downward facing surfaces. The tarp model is for pure natural convection flow with correlations for upward facing surfaces, vertical surfaces, and downward facing surfaces. Both ASHRAE and Tarp models are unable to accurately predict the room cooling load when the momentum driven flow regime is dominant.

In conclusion, the Fisher model is configuration dependent, and the Tarp and ASHRAE models are regime dependent. The new local convection model works well for both uniform and non-uniform surface temperatures and for both natural and forced convection flow regimes.

8.3 Application

The application of interest for this investigation is the accuracy in building energy calculations under different ventilative flow rates. A room the same size as the experimental room with a constant volume system was simulated with different flow rates. All the room surfaces except the floor were constructed as outside walls exposed to the outside temperature, wind, and solar radiation. The convection coefficients on the ceiling and floor are specified as same values for different convection model simulations. Lighting, equipment, and people were modeled with a typical office schedule. During working hours, the lighting load was 9.0 W/m^2, the equipment load was 10 W/m^2, and the number of people was 7. During non-working hours, the lighting load was 0.5 W/m^2, the equipment load was 2 W/m^2, and the number of people was 0. Since there is no set point temperature for constant volume system, the extraction rate is reported as a simulation result. The zone exhaust temperature floated with the outside weather condition as shown in Figure 8.5.

The comparison agrees with the experimental results of section 8.2. The extraction rate predicted by Fisher model matches that obtained with the local convection model when the ventilative flow rate is greater than 10 ACH as shown in Figure 8.6-a, Figure 8.6-b, Figure 8.6-c, and Figure 8.6-d. The ASHRAE model works well when the ventilative flow rate is smaller than 10 ACH as shown in Figure 8.6-f, Figure 8.6-g, and Figure 8.6-h. When the ventilative flow rate is about 10 ACH, the peak extraction rate predicted by the

ASHRAE model and the Fisher model are almost the same as shown in Figure 8.6-e. The Tarp model always under-predicts the peak extraction rate. Both the ASHRAE and Tarp results match the local convection model results under any ventilative flow rate during non-working hours, while the Fisher model over estimates the extraction rate during this time period. When the ventilative flow rate is decreased to 3 ACH, the simulation program switches from the Fisher model to the Tarp model. Under pure natural convection conditions, the simulation results using the four different convection models agree relatively well with each other.

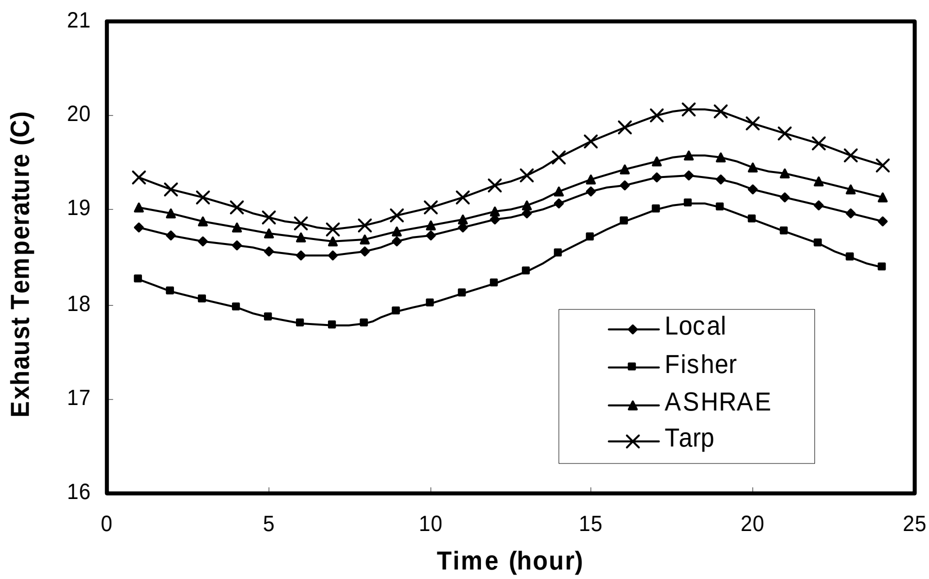

Figure 8.5 Exhaust Temperatures at Ventilative Flow Rate of 20ACH

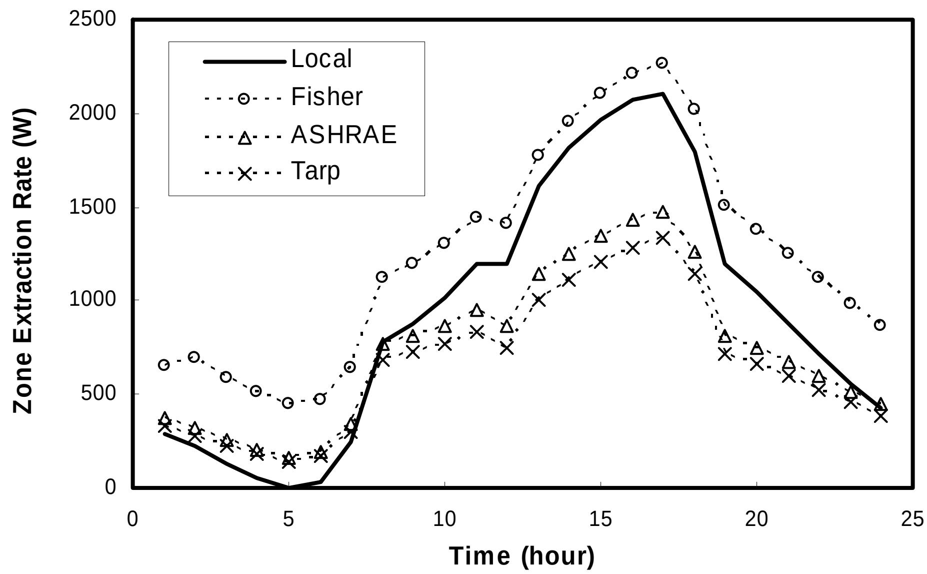

Figure 8.6-a Predicted Zone Extraction Rate under 100 ACH Using Different Convection Models

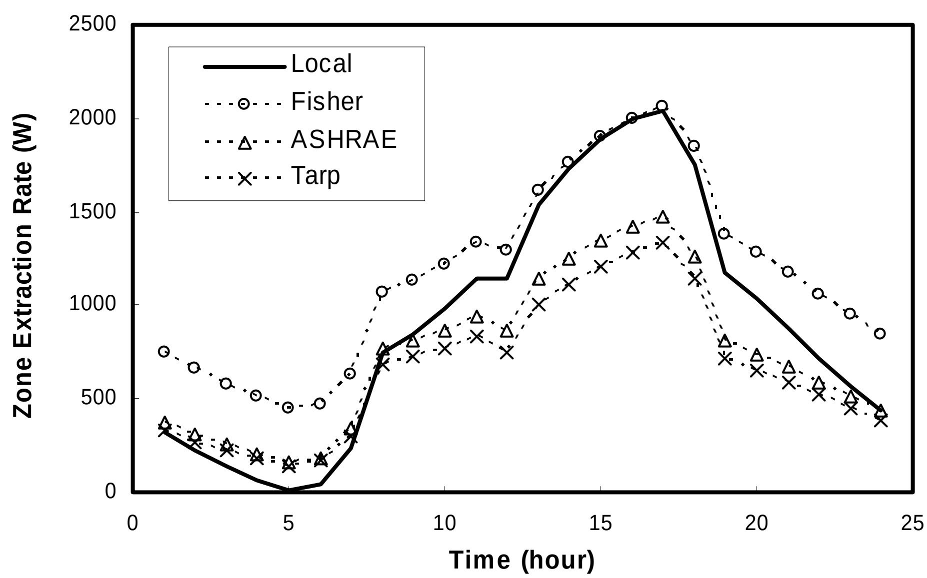

Figure 8.6-b Predicted Zone Extraction Rate under 50 ACH Using Different Convection Models

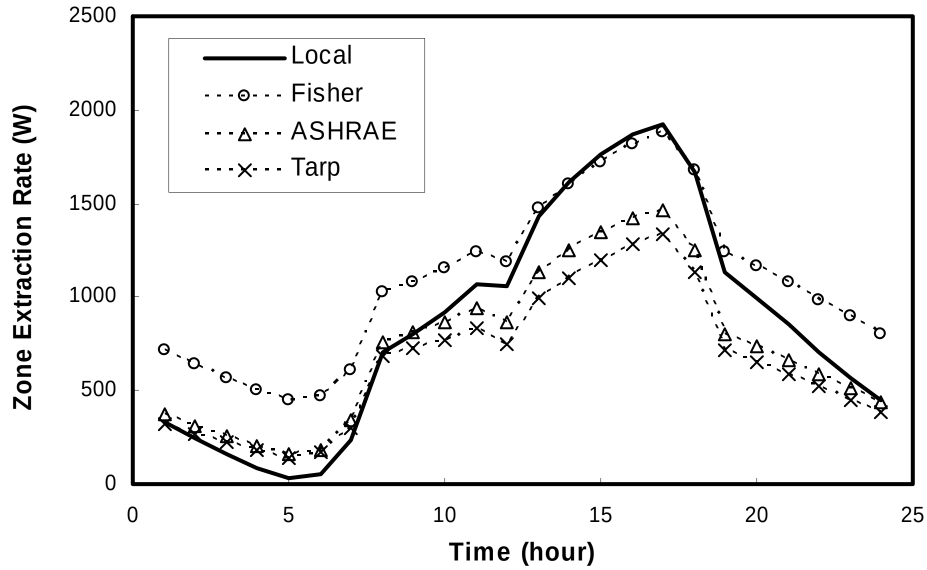

Figure 8.6-c Predicted Zone Extraction Rate under 30 ACH Using Different Convection Models

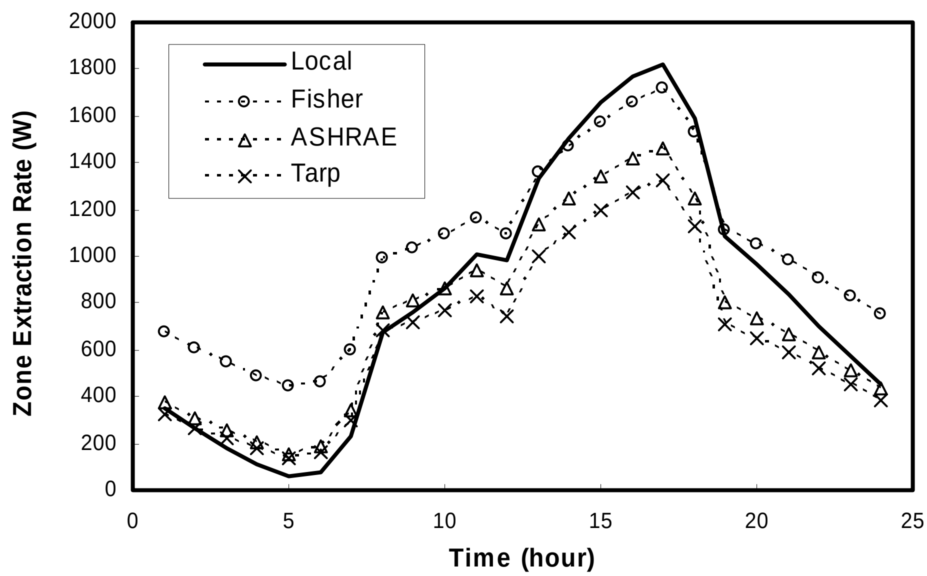

Figure 8.6-d Predicted Zone Extraction Rate under 20 ACH Using Different Convection Models

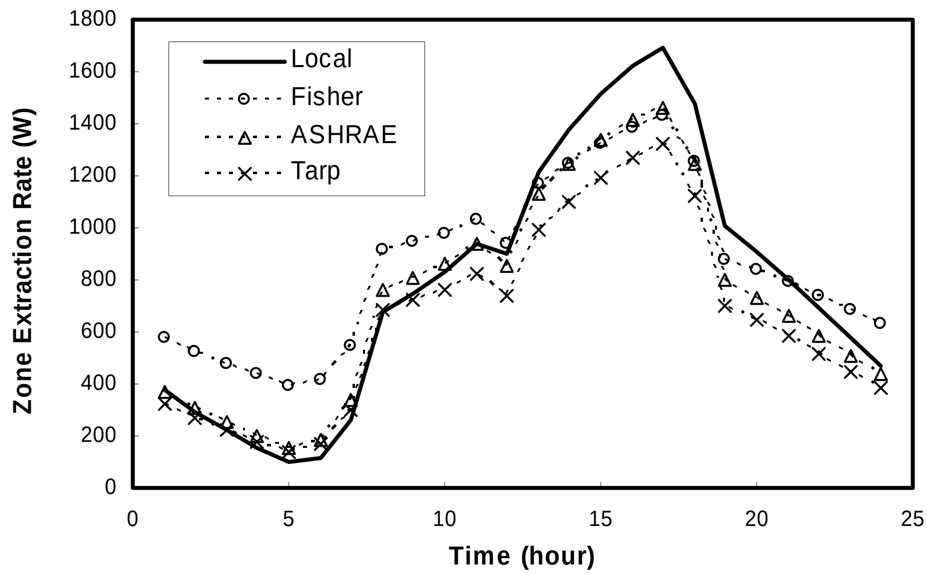

Figure 8.6-e Predicted Zone Extraction Rate under 10 ACH Using Different Convection Models

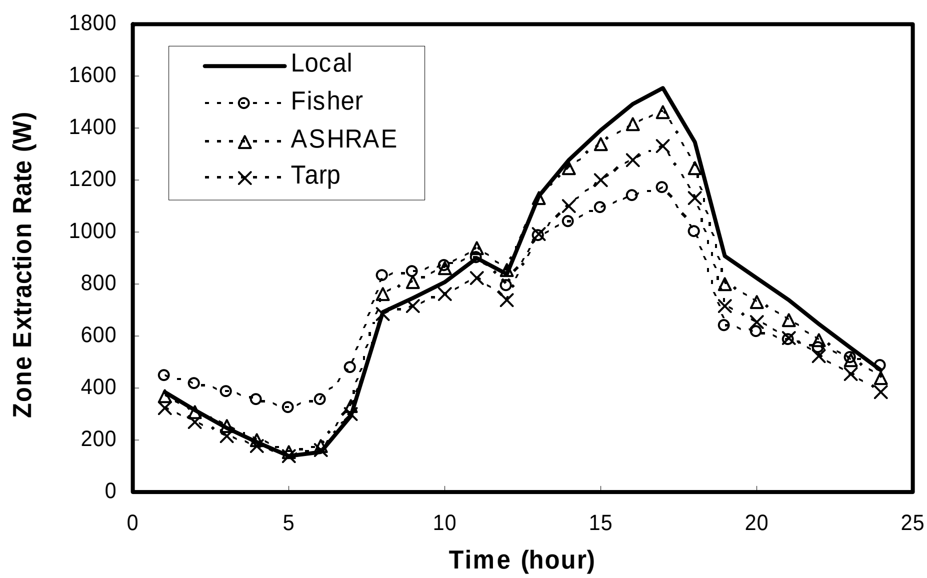

Figure 8.6-f Predicted Zone Extraction Rate under 5 ACH Using Different Convection Models

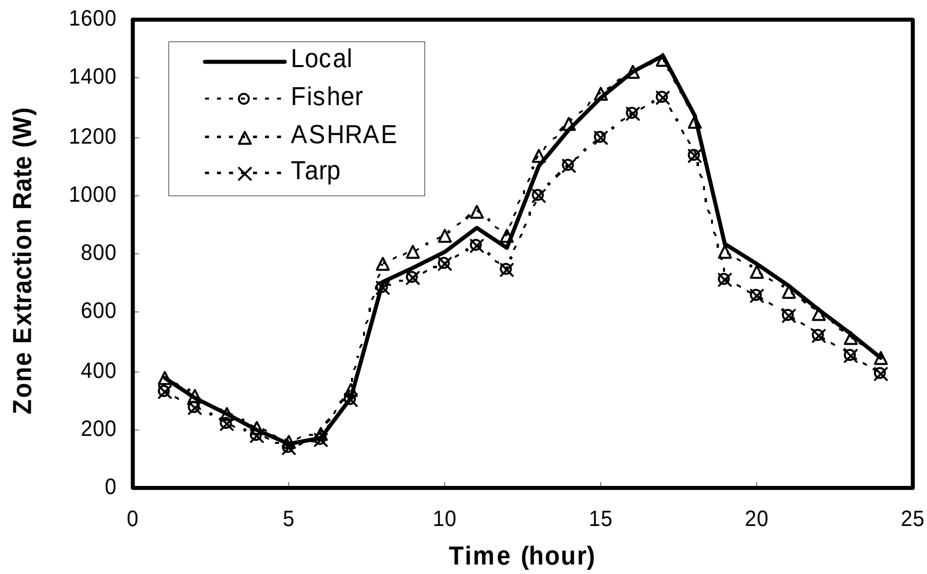

Figure 8.6-g Predicted Zone Extraction Rate under 3 ACH Using Different Convection Models

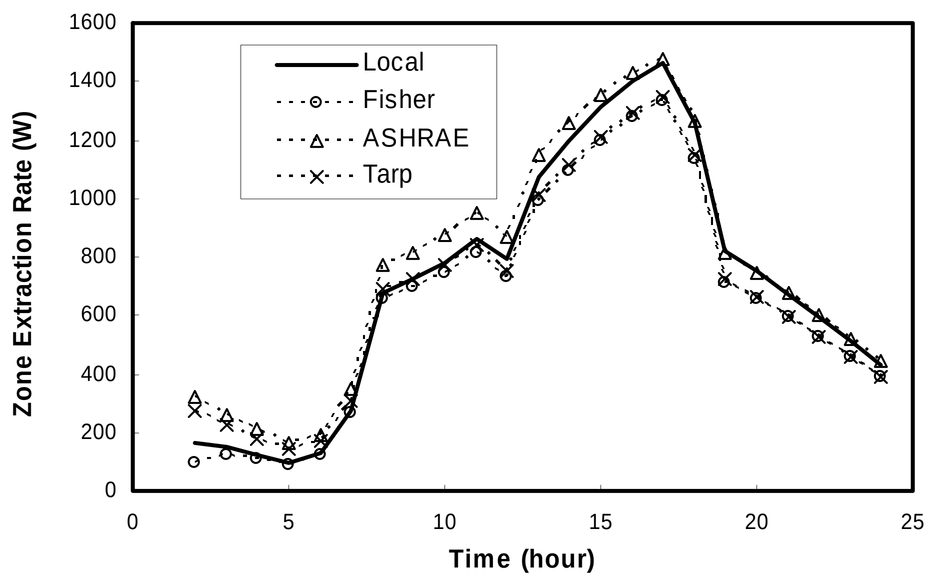

Figure 8.6-h Predicted Zone Extraction Rate without Ventilation Using Different Convection Models

Figure 8.7 shows the simulation results using the local convection model under different ventilative flow rates. The building extraction rate is similar before 8am, when the outside temperature is not high and the load due to the office lighting, equipment, and people has not been added. After 8am, the higher the ventilative flow rate, the higher the building extraction rate. This is due to lower room average air temperature and outlet temperature for higher ventilative flow rates.

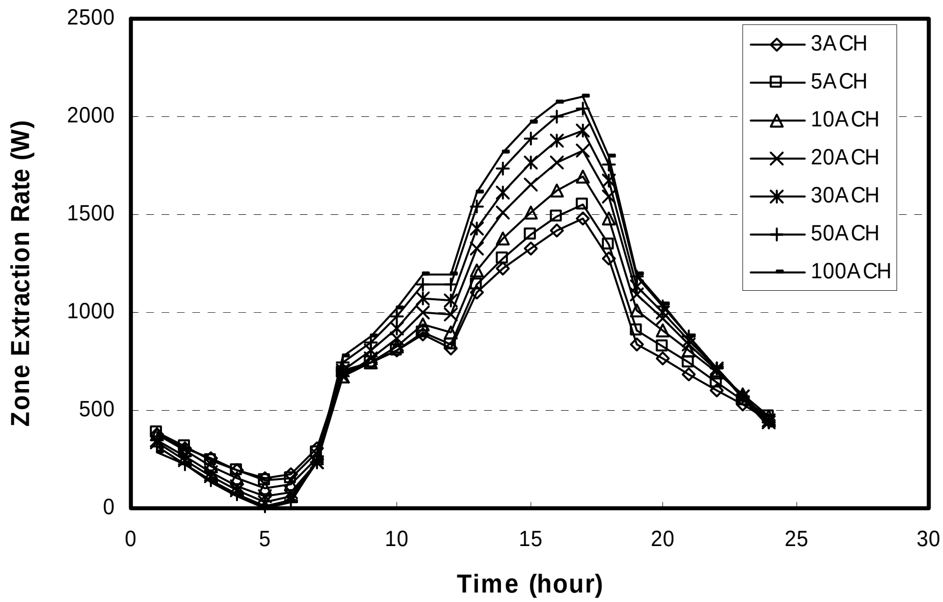

Figure 8.7 Predicted Zone Extraction Rate Using Local Convection Model for All CV Systems

A VAV system can't be simulated with the Fisher model and the local convection model because these two convection models are based on the ventilative flow rate, which changes during the iteration resulting in non-convergence of the ASHRAE Air Toolkit.

Chapter 9: Conclusions and Future Work Recommendations

The significant contributions of this work may be summarized as follows:

1. A local Reynolds number based explicitly on the characteristics of the offset wall jet has been defined. Both the local velocity and the length scale are based on a previously reported offset wall jet correlation. The local Reynolds number can be calculated in the simulation environment for any location in the room with only room geometry and diffuser inlet conditions required as input. Detailed room air models are not required to support the calculation of the local Reynolds number.
2. A forced convection model based on the local Reynolds number was developed. The correlation was based on measured ceiling and wall data from the UIUC room over a range of 3 to 100 ACH and wall data from the OSU room over a range of 10 to 30 ACH. A single correlation was developed for both walls and ceilings with uniform and variable surface temperatures over the entire range of flow rates.
3. A metric to determine the type of local flow regime (natural or forced convection) was developed. The metric is suitable for implementation in a simulation program and will allow for the application of both forced and natural convection correlations in a single room.
4. A natural convection model based on local Grashof and Nusselt numbers was developed.

A local variable based convection model was defined for coupling building heat balance models and multi-node air models. Currently available convection models can't meet the needs of airflow simulations for low energy room air management systems. The low energy systems tend to reduce energy consumption by conditioning the occupied zone only. This strategy leads to thermal stratification, non-uniform surface temperatures and mixed, natural and forced flow regimes in rooms. In order to calculate the convective heat transfer of these rooms in a simulation environment, a local variable based convection model, which represents convection coefficients with local air temperatures and velocities, has been defined in this research.

A valid convection model has a properly defined reference temperature and a generally applicable length scale so that it can be used in cases that are dynamically similar but have different dimensions. The existing literature does not include a methodology that can be generally applied to define the reference temperature and length scale for room convection models with attached wall jets. This research introduces a non-dimensionalization method, which can be applied to determine appropriate length scales and reference temperatures for rooms with various types of near-wall diffusers including floor and ceiling slot diffusers.

The airflow characteristics of the radial ceiling diffuser in an office size room have been experimentally investigated. The jet discharging from ceiling radial diffuser can be identified as offset jet. A recirculation region, reattachment region, and jet development region have been observed and a good match with offset jet theory has been found. After reattachment, the offset jet develops as an attached wall jet and wall jet theory can be applied. By applying wall jet theory, the boundary layer thickness required to define the local Reynolds and Grashof numbers is scaled with the distance from the local surface element to the point where the jet is discharged from the diffuser. With the length scale and local air temperatures and velocities obtained from the non-dimensionalization method, a local Reynolds number and Nusselt number for forced convection driven by a radial ceiling diffuser were defined. For local natural convection, a Grashof number and Nusselt number based on Bejan's scale analysis were also defined.

A local convection model based on the local Reynolds, Grashof and Nusselt numbers was developed for the room with a radial ceiling diffuser. The model includes a single forced convection correlation applicable to both ceilings and walls which applies to both the forced and mixed convection flow regimes, and a natural convection correlation which applies to walls and floors. Additional research is required to develop a suitable mixed convection correlation. However, it was observed that the forced convection correlation can be used for a wide range of room airflow and temperature configurations within a reasonable margin of error.

The local convection correlations were implemented in the ASHRAE Air Toolkit. The experimental room conditions were modeled using measured local convection coefficients the new local convection model, the Fisher model, the Tarp model, and the ASHRAE model. Good agreement was obtained between results predicted by the local convection model and the experimental data. All models work well in the natural convection flow regime and at low ventilative flow rates. The ASHRAE model under estimated the building load for ventilative flow rates greater than 5 ACH, and the Tarp model always under estimated the building load in the forced convection regime. The Fisher model worked well for ventilative flow rates greater than 20 ACH, but under predicted the building load for ventilative flow rates less than 10 ACH. In summary, the The local variable based correlation improved the predicted cooling load by at least 20% over the entire range of ventilative flow rates.

Recommendations for future work include the following:

1. The mixed convection correlation consistent with the local variable based convection model should be developed. The experimental data in the mixed convection flow regime of this research is the result of recirculation flow and it matches the forced convection correlation reasonably well. For room configurations that have small recirculation flow effect and the momentum force and the buoyancy force are comparable, a mixed convection correlation is needed.

2. An improved model of the offset associated with various diffuser types should be developed. The local air velocity prediction equation has two decay coefficients; one of them reflects the velocity decay at the offset jet attachment point. For diffusers that have much different offsets, the decay coefficient needs to be re-evaluated.

3. Data sets for common diffuser configurations including floor and ceiling slot diffusers should be collected. The local convection model of this research is limited to offset jets and attached wall jets. Local convection models for other diffuser and jet configurations should be developed.

4. A state of the art airflow measurement technique, such as PIV measurement system, is preferred for future research so that the near wall airflow can be characterized in more details. This research used omni-directional air velocity transducers to measure local air velocities point by point and very limited number of data point was obtained.

5. Limitations in existing room air models were uncovered during the course of the investigation. The zonal air model can't properly simulate the airflow discharged from radial ceiling diffuser, so half of the experimental room was simulated with a side wall inlet diffuser. The predicted near wall reference temperature was examined to match the measured air temperature. Room air models should be extended and enhanced to accurately model common room air flow configurations. In addition, the ASHRAE Air Toolkit should be extended to include VAV systems.

6. Both air models and local convection models should be implemented in commercial building simulation software to facilitate modeling of low energy systems. Well stirred room air simulation, which is used in most commercial software, is no longer valid to accurately simulate low energy systems.

References:

Alamdari, F., and G.P. Hammond. 1983. Improved data correlations for buoyancy driven convection in rooms. *Building services engineering research and technology* 4(3): 106-112.

Alamdari, F., G.P. Hammond, and L. Melo. 1984. Appropriate calculation methods for convective heat transfer from building surfaces. *U.K. National conference on heat transfer* 2: 1201-1211.

Ampofo, F., and T.G. Karayiannis. 2003. Experimental benchmark data for turbulent natural convection in an air filled square cavity. *International Journal of Heat and Mass Transfer* 46(19): 3551-3572.

Arnold, P.D., G.P. Hammond, A.D. Irving, and C.J. Martin. 1998. The Influence of Sun Patches on Buoyancy-Driven Air Movement and Heat Transfer within a Passive Solar Test Cell. *Proceedings of ASME Heat Transfer Division* 361(1): 47-57.

ASHRAE. 1985. *ANSI/ASHRAE 51-1985 standard*. Atlanta: American Society of Heating, Refrigerating, and Air-Conditioning Engineers, Inc.

ASHRAE. 2001. *2001 ASHRAE Handbook--Fundamentals*. Atlanta: American Society of Heating, Refrigerating, and Air-Conditioning Engineers, Inc.

Awbi, H.B, and A. Hatton. 1999. Natural convection from heated room surfaces. *Energy and Buildings* 30: 233-244.

Awbi, H.B. 1998. Calculation of convective heat transfer coefficients of room surfaces for natural convection. *Energy and Buildings* 28: 219-227.

Awbi, H.B., and A. Hatton. 2000. Mixed convection from heated room surfaces. *Energy and Buildings* 32: 153-166.

Awbi, H.B., and G. Gan. 1994. Numerical simulation of the indoor environment. *Building and Environment* 29(4): 449-459.

Aydin, O., and W. Yang. 2000. Mixed Convection In Cavities With A Locally Heated Lower Wall And Moving Sidewalls. *Numerical Heat Transfer Part A: Applications* 37(7): 695-710.

Bakke, P. 1957. An Experimental Investigation of a Wall Jet. *Journal of Fluid Mechanics* 2: 467-472.

Beausoleil-Morrison, I. 2000. The Adaptive Coupling of Heat and Air Flow Modeling Within Dynamic Whole-Building Simulation. Ph.D. Thesis. University of Strathclyde.

Beausoleil-Morrison, I. and P. Strachan. 1999. On the Significance of Modeling Internal Surface Convection in Dynamic Whole-Building Simulation Programs. *ASHRAE Transactions* 105(2): 929-940.

Bejan, A. 1995. *Convection Heat Transfer*. John wiley & sons.

Bourque, C., and B.G. Newman. 1960. *The Aeronautical quarterly*. 11: 201.

Calay, R.K., A.E. HoldØ, and G.P. Hammond. 1998. Natural Convective Heat Transfer Rates In Rectangular Enclosures. *Energy and Buildings* 27: 137-146.

Campbell, G. S. 1977. *An Introduction to Environmental Biophysics*. New York: Springer-Verlag.

Cebeci, T., and A.M.O. Smith. 1974. *Analysis of Turbulent Boundary Layers*. New York: Academic Press.

Cheesewright, R., and S. Ziai. 1986. Distributions of Temperature and Local Heat-Transfer Rate in Turbulent Natural Convection in a Large Rectangular Cavity. *Proceedings of the 8th International Heat Transfer Conference* 4: 1465-1470.

Chen, H.C., and V.C. Patel. 1988. Near-wall Turbulence Models for Complex Flows Including Separation. *AIAA Journal* 26(6): 641-648.

Chen, Q. 1997. Computational fluid dynamics for HVAC: successes and failures. *ASHRAE Transactions* 103(1): 178-187.

Chen, Q., A. Moser, and A. Huber. 1990. Prediction of Buoyant, Turbulent Flow by a Low-Reynolds-Number K-E Model. *ASHRAE Transactions* 96(1): 564-573.

Chen, Q., and B. Griffith. 2002. Incorporating nodal room air models into building energy calculation procedures. ASHRAE RP1222 Final Report. Atlanta: American Society of Heating, Refrigerating, and Air-Conditioning Engineers, Inc.

Chen, Q., and Z. Jiang. 1992. Significant questions in predicting room air motion. *ASHRAE Transactions* 98(1): 929-939.

Chen, Q., C.A. Meyer, and J. van der Kooi. 1989. Convective Heat Transfer in Rooms with Mixed Convection. *Proceedings of International Seminar on Air Flow Patterns in Ventilated Spaces*: 69-82.

Chen, T.S., E.M. Sparrow, and A. Mucoqlu. 1977. Mixed Convection In Boundary Layer Flow On A Horizontal Plate. *Journal of Heat Transfer* 99(C)(1): 66-71.

Churchill, S.W., and R. Usagi. 1972. A General Expression for the Correlation of Rates of Transfer and Other Phenomena. *AIChE Journal* 18(6): 1121-1128.

Clarke J.A. 1991. *Internal Convective Heat Transfer Coefficients: A Sensitivity Study*. Report to ETSU. University of Strathclyde, Glasgow U.

Costa, J.J., L.A. Oliveira, and D. Blay. 1999. Test of Several Versions for the K-E Type Turbulence Modeling of Internal Mixed Convection Flows. *International Journal of Heat and Mass Transfer* 42: 4390-4409.

Dascalaki, E., M. Santamouris, C.A. Balaras, and D.N. Asimakopoulos. 1994. Natural Convection Heat Transfer Coefficients From Vertical And Horizontal Surfaces For Building Applications. *Energy and Buildings* 20: 243-249.

Dawson, D.A., and O. Trass. 1966. Mass Transfer in a Turbulent Radial Wall Jet. *The Canadian Journal of Chemical Engineering* 44: 121-129.

Ewert, M. and M. Zeller. 1991. Turbulent parameters at supply opening (measurements). Report R.I. 1.43. International Energy Agency Annex 20.

Ferguson, J. 1997. A Full Scale Room for the Experimental Study of Interior Building Convective Heat Transfer. M.S. Thesis. Oklahoma State University.

Fisher, D.E. 1989. Design of an experimental facility for the investigation of convective heat transfer in enclosures. M.S. thesis. Department of Mechanical and Industrial Engineering, University of Illinois at Urbana-Champaign.

Fisher, D.E. 1995. An Experimental Investigation of Mixed Convection Heat Transfer in a Rectangular Enclosure. Ph.D. thesis. Department of Mechanical and Industrial Engineering. University of Illinois at Urbana-Champaign.

Fisher, D.E., and C.O. Pedersen. 1997. Convective heat transfer in building energy and thermal load calculations. *ASHRAE Transactions* 103(2): 137-148.

Fujii, T., and M. Fujii. 1976. The Dependence Of Local Nusselt Number On Prandtl Number In The Case Of Free Convection Along A Vertical Surface With Uniform Heat Flux. *International Journal of Heat and Mass Transfer* 19: 121-122.

Glauert, M.B. 1956. The Wall Jet. *Journal of Fluid Mechanics* 1: 625-643.

Glushko, G.S. 1965. Turbulent boundary layer on a flat plate in an incompressible fluid, Bulletin of Academic Sciences USSR, Mechanical Series 4:13.

Govindan, A. P., and K. Subba Raju. 1974, Hydrodynamics of A Radial Wall Jet. Journal of Applied Mechanics. *Transactions ASME* 41(E)(2): 518-519

Grimitlin, M. 1970. Zuluftverteilung in raumen (Supply air distribution in rooms). *Luft und Kaltetechnik* 5: 247-256

Holland, J.T., and J.A. Liburdy. 1990. Measurements of the Thermal Characteristics of Heated Offset Jets. *International Journal of Heat and Mass Transfer* 33(1): 69-78.

Iacovides, H., and B.E. Launder. 1984. The computation of momentum and heat transfer in turbulent flow around pipe bends. *Institution of Chemical Engineers Symposium Series* 86: 1097-1114.

Inard, C., and D. Buty. 1991. Simulation of Thermal Coupling between a Radiator and a Room with Zonal Models. *Proceeding of 12th AIVC Conference* 2: 125-131.

Irving, S.J. 1982. Energy Program Validation: Conclusions of IEA Annex 1. *Computer Aided Design* 14 (1): 33-38.

Jones, W.P., and B.E. Launder. 1972. The Prediction of Laminarization with a 2-Equation Model of Turbulence. *International Journal of Heat and Mass Transfer* 15: 301-314.

Jones, W.P., and B.E. Launder. 1973. The calculation of low-Reynolds-number phenomena with a two-equation model of turbulence. *International Journal of Heat and Mass Transfer* 16: 1119-1130.

Kakac, S., and Y. Yener. 1995. *Convective Heat Transfer, 2nd Edition*. CRC Press, Inc.

Kapoor, K. and Y. Jaluria. 1991. Mixed convection flow due to a buoyant wall jet turning downwards at a corner. *HTD 163, Mixed convection heat transfer*: 119-128.

Kays, W.M. and M.E. Crawford. *Convective Heat and Mass Transfer*. McGraw-Hill, Inc.

Khalifa, A.J.N. and R.H. Marshall. 1990. Validation of Heat Transfer Coefficients on Interior Building Surfaces Using a Real-Sized Indoor Test Cell. *International Journal of Heat and Mass Transfer* 33(10): 2219-2236.

Kim, S., and D. Choudhury. 1995. Computations of Complex Turbulent Flows and Heat Transfer using Two-layer Based Wall Functions. *ASME HTD* 311(9): 169-177.

Kirkpatrick, A., T. Malmstrom, K. Knappmiller, and D. Hittle. 1991. Use of Low Temperature Air for Cooling Of Buildings. *Proceedings of Building Simulation*: 62-66.

Kline, S. J., and F.A. McClintock. 1953. Describing Uncertainties in Single-Sample Experiments. *ASME* 75: 3-12.

Krarti, M., and S. Choi. 1997. A Simulation Method for Fluctuating Temperature in Crawlspace Foundations. *Energy and buildings* 26: 183-188.

Kumada, M., I. Mabuchi, and K. Oyakawa. 1973. Studies on Heat Transfer to Turbulent Jets with Adjacent Boundaries. *Bulletin of the JSME* 16(101): 1712-1722

Kurnitski, J. 2000. Crawl Space Air Change, Heat and Moisture Behavior. *Energy and buildings* 32: 19-39.

Kurnitski, J., and M. Matilainen. 2000. Moisture Conditions of Outdoor Air-Ventilated Crawl Spaces in Apartment Buildings in a Cold Climate. *Energy and buildings* 33: 15-29.

Lam, C.K.G., and K. Bremhorst. 1981. Modified Form of the k-ε Model for Predicting Wall Turbulence. *Journal of Fluids Engineering* 103: 456-460.

Launder, B. E. and W. Rodi. 1981. Turbulent Wall Jet. *Progress in Aerospace Sciences* 19(2-4): 81-128.

Launder, B.E., and D.B. Spalding. 1974. The Numerical Computation of Turbulent Flows. *Computer Methods in Applied Mechanics and Engineering* 3(2): 269-289.

Libby, P. A. 1996. *Introduction to Turbulence*. Taylor Francis.

Lomas, K.J. 1996. U.K. Applicability Study: an Evaluation of Thermal Simulation Programs for Passive Solar House Design. *Building and Environment* 31(3): 197-206.

Lucas, J., K. Benes, W. Oldfield, and W. Siemens. 2002. Computer Controlled Bulk Air Measurement Trolley (Final Report).

Monteith, J. L. 1973. *Principles of Environmental Physics*. New York: Edward Arnold.

Nagano, Y., and M. Tagawa. 1990. An Improved k-ε model for Boundary Layer Flows. *Journal of Fluids Engieering* 112: 33-39.

Neiswanger, L., G.A. Johnson, and V.P. Carey. 1987. An Experimental Study of High Rayleigh Number Mixed Convection in a Rectangular Enclosure with Restricted Inlet and Outlet Openings. *ASME Transactions* 109: 446-453

Nielson, P.V. 1974. Flow in Air-Conditioned Rooms. Ph.D. thesis. Technical University of Denmark, Copenhagen.

Niu, J. 1990. Numerical Simulation and Experimental Investigation of Natural Convection in an Enclosure Room. Delft University of Technology.

Parameswaran, V., and S.A. Alpay. 1975. Studies on Re-Attaching Wall Jets. *Transactions of the Canadian Society for Mechanical Engineers* 3(2): 83-89.

Patankar, S.V., and D.B. Spalding. 1970. *Heat and Mass Transfer in Boundary Layers: 2nd Edition*. London: Intertext Books.

Patel, V.C., W. Rodi, and G. Scheuerer. 1984. Turbulence Models for Near-wall and Low Reynolds Number Flows: a Review. *AIAA Journal* 23(9): 1308-1318.

Pedersen, C.O. 2001. Toolkit for Building Load Calculations. Atlanta: American Society of Heating, Refrigerating, and Air-Conditioning Engineers, Inc.

Pedersen, C.O., D.E. Fisher, and B. Mansfield. 1994. Energy Estimating Methods for Predicting Ventilative Cooling Performance for Mixed Convection. ASHRAE 664 RP Final Report. Atlanta: American Society of Heating, Refrigerating, and Air-Conditioning Engineers, Inc.

Pelfrey, J.R.R., and J.A. Liburdy. 1986. Mean Flow Characteristics of Turbulent Offset Jet. *Journal of Fluid Engineering* 108: 82-88.

Perry, C.C. 1967. Advances in Fluidics. *ASME*: 142-162.

Rautaheimo, P., and T. Siikonen. Improved Solid-wall Boundary Treatment in Low-Reynolds Number Turbulence Models. *AIAA Journal* 39(5): 824-830.

Rødahl, E. 1977. The Point of a Separation for Cold Jets Flowing Along the Ceiling. Clima 2000. Belgrade, Yugoslavia.

Roy, J. C., T. Boulard, C. Kittas, and S. Wang. 2002. Convective and Ventilation Transfers in Greenhouses Part 1: The Greenhouse Considered As a Perfectly Stirred Tank. *Biosystems Engineering* 83(1): 1-20.

Sanders, S. 1995. An Experimental Facility for Studying Convective Heat Transfer in Buildings. M.S. Thesis. Oklahoma State University.

Song, H., S. Yoon, and D. Lee. 2000. Flow And Heat Transfer Characteristics Of A Two-Dimensional Oblique Wall Attaching Offset Jet. *International Journal of Heat and Mass Transfer* 43(13): 2395-2404.

Spalding, D.B. 1967. Monograph on Turbulent Boundary Layers. Imperical College: Mechanical Engineering Department Report TWF/TN 33.

Sparrow, E.M., and J.L. Gregg. 1959. Buoyancy Effects in Forced-Convection Flow and Heat Transfer. Journal of Applied Mechanics 1959: 133-134.

Spitler, J.D. 1990. An Experimental Investigation of Air Flow and Convective Heat Transfer in Enclosures Having Large Ventilative Flow Rates. Ph.D. thesis. University of Illinois –Urbana Champaign.

Spitler, J.D., C.O. Pedersen, and D.E. Fisher. 1991. Interior Convective Heat Transfer in Buildings with Large Ventilative Flow Rates. *ASHRAE Transactions* 1991(1): 505-515.

Spitler, J.D., C.O. Pedersen, D.E. Fisher, P.F. Menne, and J. Cantillo. 1991. An Experimental Facility for Investigation of Interior Convective Heat Transfer. *ASHRAE Transactions* 1991(1): 497-504.

Tanaka, T., and E. Tanaka. 1978. Experimental Studies of a Radial Turbulent Jet Em Dash 4. Flow at and after an Attaching Point of Attaching Jet Flow. *Bulletin of the JSME* 21(159): 1349-1356.

Tavakkol, S., M.H. Hosni, P.L. Miller, and H.E. Straub. 1994. A Study Of Isothermal Throw Of Air Jets With Various Room Sizes And Outlet Configurations. *ASHRAE Transactions* 100(1): 1679-1686.

Taylor, J.R. 1982. An Introduction to Error Analysis – The Study of Uncertainties in Physical Measurements. University of Science Books, Mill Valley, California

Togari, S., Y. Arai, and K. Miura. 1993. A Simplified Model for Predicting Vertical Temperature Distribution in a Large Space. *ASHRAE Transactions* 99(1): 84-99.

Waters, J.R. 1980. The Experimental Verification of a Computerized Thermal Model for Buildings. *Building Services Engineering Research and Technology* 1: 76-82.

Wolfshtein, M.W. 1969. The Velocity and Temperature Distribution in One Dimensional Flow with Turbulence Augmentation and Pressure Gradient. *International Journal of Heat and Mass Transfer* 12: 301-318.

Yuan, X. 1995. Wall Functions for Numerical Simulation of Natural Convection along Vertical Surfaces.

Appendix A: Thermocouple Calibration Curves

Table A.1 Thermocouple Calibration Curves of Wireless Data Logger

Channel No.	Calibration Curve
11	y = 1.0003x - 0.0461
12	y = 1.0009x - 0.0888
13	y = 1.0004x - 0.0966
14	y = 1.0005x - 0.1002
15	y = 1.0001x - 0.1016
16	y = 0.9997x - 0.1072
17	y = 0.9999x - 0.1171
18	y = 0.9993x - 0.1135
19	y = 0.9998x - 0.1175
20	y = 0.9992x - 0.0806

Table A.2 Thermocouple Calibration Curves of Helios Data Logger

Channel No.	Calibration Curve	Channel No.	Calibration Curve
0	y = 0.9983x + 0.0951	**50**	y = 1.0004x + 0.0342
1	y = 0.9985x + 0.0957	**51**	y = 1.0021x + 0.0192
2	y = 0.9977x + 0.0978	**52**	y = 1.0028x + 0.0234
3	y = 0.9977x + 0.0851	**53**	y = 1.0026x + 0.039
4	y = 0.9971x + 0.0973	**54**	y = 0.9959x + 0.0995
5	y = 0.9964x + 0.0917	**55**	y = 1.0031x + 0.0237
6	y = 0.9965x + 0.0887	**56**	y = 1.005x - 0.0037
7	y = 0.9966x + 0.0848	**57**	y = 1.0029x + 0.0641
8	y = 0.9982x + 0.0512	**58**	y = 1.005x + 0.0301
9	y = 0.9956x + 0.0888	**59**	y = 1.0022x + 0.0819
10	y = 0.996x + 0.0809	**60**	y = 0.9985x + 0.03
11	y = 0.9961x + 0.0932	**61**	y = 0.9971x + 0.059
12	y = 0.9972x + 0.0909	**62**	y = 0.996x + 0.0795
13	y = 0.9973x + 0.089	**63**	y = 0.9963x + 0.0652
14	y = 0.9976x + 0.085	**64**	y = 0.9972x + 0.0565
15	y = 0.9979x + 0.0806	**65**	y = 0.9977x + 0.0441
16	y = 0.998x + 0.0882	**66**	y = 0.9983x + 0.0352
17	y = 0.9983x + 0.1152	**67**	y = 0.998x + 0.0533
18	y = 0.9987x + 0.1289	**68**	y = 0.9973x + 0.0649
19	y = 0.9985x + 0.1173	**69**	y = 0.9964x + 0.0691
20	y = 0.997x + 0.1134	**70**	y = 0.9994x + 0.0274
21	y = 0.9968x + 0.1119	**71**	y = 1.0003x + 0.029
22	y = 0.9965x + 0.1121	**72**	y = 1.0009x + 0.0418
23	y = 0.9966x + 0.0928	**73**	y = 1.0025x + 0.021
24	y = 0.9964x + 0.1009	**74**	y = 0.9995x + 0.0862
25	y = 0.9958x + 0.1039	**75**	y = 1.0021x + 0.0213
26	y = 0.9957x + 0.1018	**76**	y = 1.0022x + 0.0228
27	y = 0.9953x + 0.108	**77**	y = x + 0.09
28	y = 0.9959x + 0.0995	**78**	y = 1.0015x + 0.0708
29	y = 0.9953x + 0.0958	**79**	y = 1.0018x + 0.0561
30	y = 0.9957x + 0.102	**80**	y = 1.0018x + 0.0561
31	y = 0.9963x + 0.0997	**81**	y = 1.0032x + 0.0451
32	y = 0.9988x + 0.0692	**82**	y = 1.0035x + 0.0309
33	y = 0.9992x + 0.0715	**83**	y = 1.0031x + 0.0322
34	y = 0.9998x + 0.0644	**84**	y = 1.0036x + 0.0214
35	y = 1.0005x + 0.0485	**85**	y = 1.0022x + 0.0423
36	y = 1.0002x + 0.0574	**86**	y = 1.0089x - 0.0186
37	y = 1.0011x + 0.0842	**87**	y = 1.0005x + 0.0711
38	y = 0.9994x + 0.1324	**88**	y = 1.0018x + 0.0376
39	y = 1.0009x + 0.0998	**89**	y = 1.0003x + 0.0233
40	y = 0.9984x + 0.1243	**90**	y = 1.0014x + 0.0512
41	y = x + 0.0713	**91**	y = x
42	y = 0.9983x + 0.1055	**92**	y = 0.9992x + 0.0334
43	y = 0.9985x + 0.09	**93**	y = 0.9989x + 0.0372
44	y = 0.9997x + 0.065	**94**	y = 1.0023x - 0.0315

45	y = 0.9963x + 0.1342	**95**	y = 1.0025x - 0.0425
46	y = 0.9988x + 0.0758	**96**	y = 1.0026x - 0.0212
47	y = 0.9963x + 0.134	**97**	y = 1.0021x - 0.0017
48	y = 0.9979x + 0.0903	**98**	y = 1.0011x - 0.0449
49	y = 0.9979x + 0.0761	**99**	y = 1.0058x - 0.0848

Appendix B: OSU Experimental Parameters

Table B.1 Forced Convection Data Sets on Hot Walls

Exp. Code	ACH	T_hotwall (ºC)	T_inlet (ºC)	T_outlet (ºC)	VFR (m^3/s)	Dis_air (mm)
706041	9.5	37.73	15.12	24.89	0.143	128
706042	9.55	37.78	15.09	24.92	0.144	55
706043	9.68	37.76	15.15	24.93	0.146	79
706044	9.68	43.28	15.58	26.81	0.146	107
706045	9.61	43.29	15.66	26.92	0.145	30
707041	9.65	40.56	15.37	25.91	0.146	107
707042	9.63	40.55	15.51	26	0.145	55
707043	9.36	32.36	15.17	23.63	0.141	107
707044	9.31	32.28	15.28	23.45	0.141	152
707045	9.43	32.3	15.25	23.42	0.142	226
707046	9.6	32.28	15.35	23.42	0.145	55
708041	9.46	37.77	15.4	24.9	0.143	107
708042	9.51	37.8	15.46	24.97	0.144	55
708043	9.42	37.77	15.43	24.99	0.142	152
708044	9.24	43.34	15.75	26.94	0.14	107
708045	9.33	43.28	15.79	27.03	0.141	55
708046	9.27	43.36	15.73	27.05	0.14	152
709041	9.38	32.34	15.07	23.4	0.142	55
709042	9.41	32.31	15.09	23.41	0.142	107
710041	10.25	32.31	14.69	22.67	0.155	107
710042	10.26	32.33	14.71	22.73	0.155	152
710043	10.19	46.04	15.3	26.95	0.154	107
714041	4.94	37.83	17.84	27.94	0.075	128
714042	4.96	37.8	17.9	28.22	0.075	79
714043	4.93	37.81	17.89	28.23	0.075	177
715041	4.92	32.27	17.47	25.76	0.074	128
715042	4.95	32.15	17.45	25.88	0.075	177
715043	4.95	32.2	17.46	25.92	0.075	55
715044	4.96	32.21	17.56	25.94	0.075	30
716041	9.13	46.12	15.39	27.9	0.138	128
716042	9.06	46.12	15.53	28.06	0.137	177
716043	9.17	46.09	15.53	28.06	0.138	79
716044	9.09	46.05	15.57	28.17	0.137	30
716045	9.18	46.02	15.58	28.2	0.139	107
716046	9.07	45.96	15.62	28.26	0.137	55
717041	4.94	40.5	17.33	29.13	0.075	107
717042	4.96	40.52	17.36	29.28	0.075	128

718041	4.95	36.11	17	27.25	0.075	128
718042	4.96	36.07	17.1	27.36	0.075	107
718043	4.95	36.23	17.15	27.4	0.075	79
719041	4.96	37.81	17.1	27.91	0.075	30
719042	4.95	37.89	17.14	28.01	0.075	55
719043	4.93	37.76	17.18	27.93	0.074	152
826041	22.55	32.25	16.55	21.34	0.341	128
916041	22.87	34.82	15.08	21.1	0.345	30
916042	22.61	34.99	14.91	21.02	0.341	128
917041	22.91	37.75	15.21	21.69	0.346	128
917042	22.9	37.76	15.35	21.86	0.346	177
917043	22.9	37.63	15.5	21.98	0.346	226
918041	22.94	37.55	15.48	21.94	0.347	128
918042	22.95	37.8	15.37	21.9	0.347	79
919041	22.92	40.39	15.41	22.43	0.346	128
919042	22.49	40.35	15.31	22.43	0.34	177
919043	22.98	40.36	15.37	22.44	0.347	79
920041	21.67	37.58	15.12	21.72	0.327	128
920042	22.11	37.5	15.15	21.77	0.334	177
921041	22.11	37.72	15.22	21.74	0.334	226
923041	23.28	43.05	16	23.46	0.352	128
923042	23.29	42.78	15.88	23.4	0.352	226
1006041	32.66	37.74	20.39	24.5	0.493	128
1006042	32.7	37.74	20.35	24.54	0.494	177
1007041	32.42	37.73	20.39	24.48	0.49	226
1007042	32.46	37.68	20.40	24.56	0.49	274
1008041	32.46	43.26	20.83	25.84	0.49	128
1008042	32.36	43.24	20.85	25.87	0.489	177
1008043	32.43	43.06	20.99	25.97	0.49	226

Table B.2 Forced Convection Data Sets on Cold Walls

Exp. Code	ACH	T_coldwall (ºC)	T_inlet (ºC)	T_outlet (ºC)	VFR (m^3/s)	Dis_air (mm)
317051	17.00	18.76	19.23	23.61	0.26	128
318051	22.17	18.35	21.04	23.55	0.21	128
322051	21.93	18.25	18.91	23.18	0.21	128
419051	11.30	15.68	20.91	24.35	0.17	128
422051	10.61	18.33	22.09	24.94	0.16	128

Table B.3 Natural Convection Data Sets

Exp. Code	T_hotwall (ºC)	T_Coldwall (ºC)	Dis_air (mm)	Panel Data
1014041	40.56	16.18	128	Hot
1014042	40.56	16.18	79	Hot
1018041	35.03	14.96	79	Hot
1018042	35.03	14.96	55	Hot
1019041	32.28	15.84	79	Hot
1019042	32.28	15.84	55	Hot
1019043	32.35	17.43	79	Hot
1019044	32.35	17.43	55	Hot
1020041	32.31	21.00	79	Hot
1020042	32.31	21.00	55	Hot
1021041	29.57	20.55	79	Hot
1024041	29.50	20.45	79	Hot
1024042	29.50	20.45	55	Hot
1025041	29.54	20.61	79	Cold
1026041	35.08	17.75	55	Cold
1027041	35.08	18.43	55	Cold
1028041	32.27	17.71	55	Cold
1028042	32.27	17.71	128	Cold
1029041	23.97	11.04	128	Cold
1207041	37.8	13.55	79	Cold
1207042	37.8	13.55	128	Cold
1210041	43.3	13.16	79	Cold
1211041	43.27	11.47	79	Cold
1212041	32.29	15.64	79	Cold
1213041	32.31	17.49	79	Cold

Appendix C: UIUC Experimental Parameters

Table C.1 UIUC Experimental Data Sets

Exp. Code	ACH	Tinlet (˚C)	VFR (CFM)	MFR (kg/s)	Toutlet (˚C)	Area (m^2)
112933	3.00	10.00	60.81	0.0348	25.00	0.022379
624921	14.92	19.97	302.19	0.1693	27.91	0.022379
428895	70.10	16.72	1419.58	0.7914	24.59	0.093
505891	94.09	16.87	1905.37	1.0628	24.31	0.093
1015892	30.27	20.95	612.90	0.3459	27.02	0.093
1016891	50.21	20.99	1016.74	0.5736	26.63	0.093

VITA

Weixiu Kong

Candidate for the Degree of

Doctor of Philosophy

Thesis: A CONVECTIVE HEAT TRANSFER MODEL FOR SIMULATION OF ROOMS WITH ATTACHED WALL JETS

Major Field: Mechanical Engineering

Biographical:

Education: Received Bachelor of Science Degree in Thermal Engineering from Shenyang Architectural and Civil Engineering Institute, Shenyang, P. R. China, in July, 1994. Received Master of Science Degree in Thermal Engineering from Tianjin University, Tianjin, P. R. China, in March, 1997. Completed the requirements for Doctor of Philosophy with a major in Mechanical Engineering from Oklahoma State University, Stillwater, Oklahoma in May 2006.

Experience: Employed as an assistant professor Dalian University between April 1997 and July 2000. Employed as Research Assistant at the School of Mechanical & Aerospace Engineering, Oklahoma State University, Stillwater, Oklahoma from August 2000 to present.

Professional Memberships: American Society of Heating, Refrigerating and Air-Conditioning Engineers (ASHRAE), American Society of Mechanical Engineers (ASME), International Building Performance Simulation Association (IBPSA).